ON THE PRODUCTION OF DEFECT

FREE HONEYCOMB EXTRUDATE

by

THOMAS W. AVERY

A thesis submitted to the University of Birmingham for the degree of

DOCTOR OF ENGINEERING

Department of Chemical Engineering

University of Birmingham

February 2016

Abstract

MAST Carbon are scaling up production of activated carbon honeycomb monoliths made from an extruded particulate phenolic resin paste. There are two major barriers to scaling up which this work addresses.

Firstly the extrusion process suffered from an unacceptably high rejection rate (around 50%) of monoliths due to malformation of channels and tearing at the surface and interior of the structure. Pastes were characterised using the Benbow Bridgwater paste flow model and it was shown that the parameters of this model could be controlled by the careful addition of various extrusion aids to the formulation. It has also been shown that the extrusion profile can be predicted from the extrusion die geometry and the Benbow Bridgwater parameters. A previously unreported link between the viscoelasticity of the liquid component of the paste and the rate of phase migration was demonstrated. These discoveries led to a new paste formulation, specifically designed to produce defect free monoliths with MAST Carbon's extrusion dies. Since the introduction of this new formulation, the rate of monolith rejection has reduced to zero.

Secondly, the monoliths required 10 days to dry at ambient conditions; a serious bottleneck in the production process. A forced drying regime was introduced which reduced the drying time to less than 24 hours without causing any internal cracks. A model describing the drying and shrinkage behaviour of the monoliths was developed. The model was used to predict the shape of the stress field in the monolith and to investigate the mechanism of internal fracture.

Acknowledgments

TABLE OF CONTENTS

TABLE OF FIGURES

NOMENCLATURE

A	m^2	area of extrusion die
A_0	m^2	area of extrusion barrel
D	m	diameter of extrusion die
		diameter of sample after compression in Norton test
D_0	m	diameter of extrusion barrel
	m	diameter of sample before compression in Norton test
$\overline{D_0}$	m^2.s^{-1}	maximum effective diffusion constant
E	Pa	Young's modulus
E_a	J.mol^{-1}	activation energy for diffusion
G	Pa	rigidity modulus
G'	Pa	storage modulus
G''	Pa	loss modulus
h	m	distance between marks on sample after compression in Norton test
h_0	m	distance between marks on sample before compression in Norton test
h_c	m	cone penetration depth
kh	m	Rough's modification term
k	Pa.s	shear consistency index
k_u	Pa.s	uniaxial consistency index
L	m	die length
M	m	perimeter of extrusion die
M_T	kg	total mass of monolith
m	-	bulk nonlinear velocity dependence term
n	-	nonlinear velocity dependence term at wall
n_f	-	behaviour/flow index for power law or Hershel Bulkley equation
P	Pa	total extrusion pressure
P_1	Pa	extrusion pressure attributed to convergence of paste

P_2	Pa	extrusion pressure attributed to die wall friction
R	m	monolith radius
R_{gc}	J.mol^{-1}.K^{-1}	universal gas constant
T	K	temperature
$T_{chamber}$	K	temperature of drying chamber
t	s	time
V_i	m^3	volume of phase i
W	kg	mass of cone penetrometer
α	Pa.m.s-1	bulk linear velocity dependence term
α_H	m^2.s^{-1}	thermal diffusivity
β	Pa.m.s-1	linear velocity dependence term at wall
γ	-	deformation angle
$\dot{\gamma}$	s^{-1}	shear strain rate
δ	-	phase angle
ϵ	-	strain
$\dot{\epsilon}$	s^{-1}	strain rate
η	Pa.s^{-1}	viscosity
θ	-	half angle of convergence
θ_c	-	angle of cone penetrometer
μ_{dr}	-	Sherwood drying rate
ρ_i	kg.m^{-3}	density of phase i
σ	Pa	normal stress
σ_0	Pa	bulk yield stress
τ	Pa	shear stress
τ_0	Pa	yield stress at die wall in Benbow Bridgwater equation
		Hershel Bulkley yield stress
ϕ_i	-	volume fraction of phase i
ω	-	shrinkage

1   INTRODUCTION

1.1   Project Objectives

MAST Carbon produced activated carbon honeycomb monoliths via the extrusion of a phenolic resin particulate paste. As demand for this material increases, MAST plan to scale up production. There are two major barriers to scale up. First, there is an unacceptable rejection rate due to a number of different failure modes during extrusion. It is not uncommon for half of the monolith extruded to be rejected due to either surface tearing or malformation of the channels. Secondly, the monoliths currently require 10 days to fully dry after extrusion before they can be further processed. This presents an unacceptable bottleneck in the production process.

It is the aim of objective of this project to reduce the number of defects in the extrudate by reformulation of the paste or changes to the processing conditions and also to reduce the monolith drying time to less than 24 hours without introducing interior cracks.

1.2   Background

1.2.1   Activated Carbon

Activated carbon is a form of amorphous carbon with an extremely high specific surface area, in the region of 1200 $m^2.g^{-1}$ of material [1]. By varying the processing conditions, (in particular the extent of activation) and raw materials, it is possible to vary the specific surface area significantly from around 500 to 2000 $m^2.g^{-1}$. It is the high surface area that distinguishes it from standard carbon. Activated carbons find use in many industrial areas. They are commonly used as catalyst supports in the gas and liquid processing industries [2], for the removal of VOC's from air, in the water purification and energy storage devices such as

supercapacitors [3, 4]. Naturally derived carbons produced from a wide range of precursors including wood, coal, coconut shell etc., suffer from a number of limitations. These include the high levels of impurities, a very limited range of physical forms, relatively low strength of extruded materials and seasonal variation in the raw material. Synthetic activated carbons, such as those manufactured by MAST Carbon, can overcome these problems, largely due to the reliable reproducibility of the precursor and ability to produce complex structures [2, 5-7].

Granular carbon is the most common form found in adsorption applications [2, 8]. Granular carbons work well in most cases, but packed beds can suffer from high pressure drop and attrition of the granules. Monolithic honeycomb filters, pictured in Figure 1.1, are able to offer a lower flow resistance and reduced turbulence due to straight and narrow flow channels. It is also possible to manufacture filters with various open flow areas and surface area by modification of the extrusion die. Monolithic structures may be resistively heated allowing thermal regeneration of the bed [2, 9].

10 mm
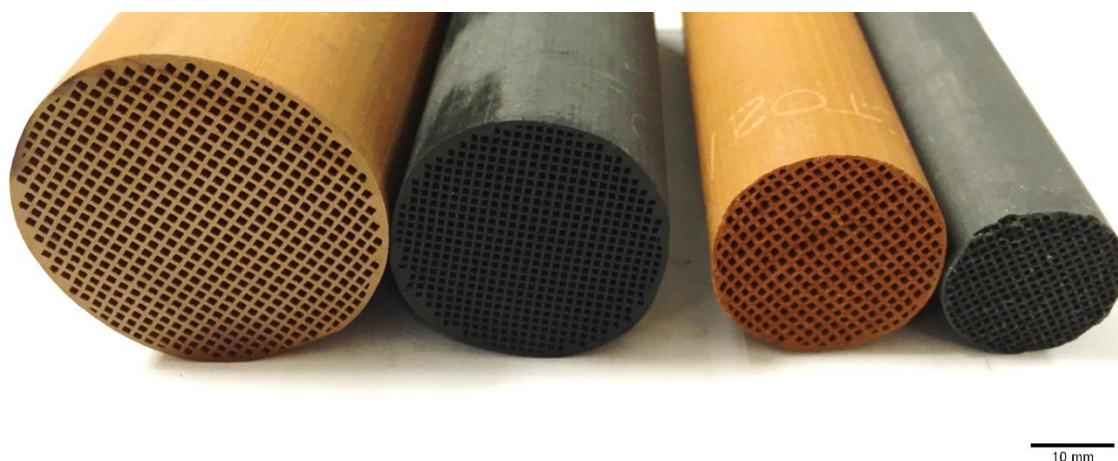
Figure 1.1 - Honeycomb Monoliths before and after activation

Phenolic resins have been used in the manufacture of activated carbon monoliths since at least 1995 [8]. Cornin, N.Y., used phenolic resin powder in the production of carbon monoliths but

not as the primary carbon yielding species. Instead, the phenolic resin acted as a binder in an aqueous solution of carbon particles also containing organic binders such as celluloses.

MAST Carbon uses a cured phenolic resin (hereafter simply referred to as phenolic resin) as the primary carbon yielding material. An 'extrusion package' (often also referred to as a 'binder package') containing a number of rheology modifiers (discussed in section 3.3) and water is mixed with powdered phenolic resin to form a paste which may be more easily extruded. The extrusion packages aids extrusion by modifying the rheology of the paste and then lends green strength to the finished extrudate [10, 11]. The extrusion aids are removed completely upon carbonisation, leaving a pure carbon honeycomb structure.

1.2.2   MAST Carbon Manufacturing Process

The process by which MAST Carbon's activated carbon monoliths are produced is illustrated in Figure 1.2.
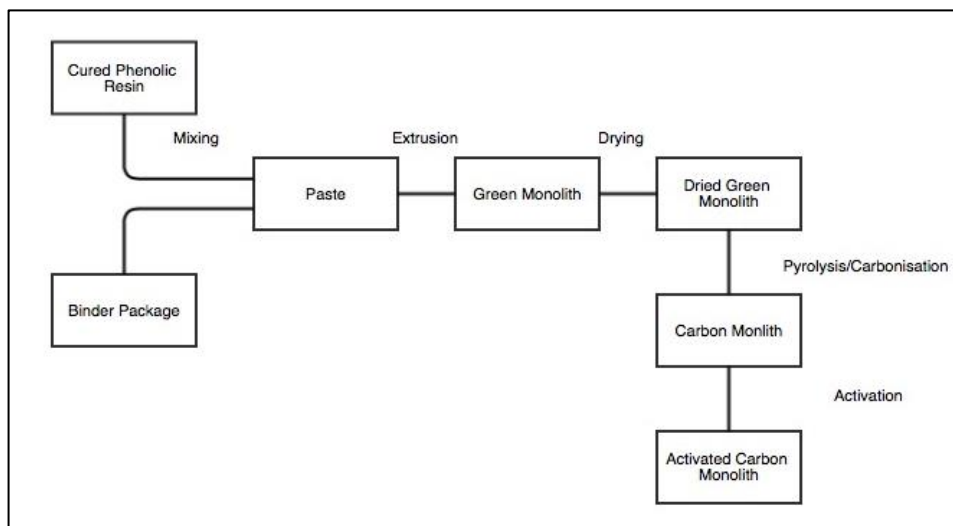
Figure 1.2 - MAST Carbon's current manufacturing process

1.2.2.1 **Phenolic Resin**

The phenolic resin, which makes up the bulk of the paste and is the sole carbon yielding substance, is cured in-house by MAST Carbon. The uncured phenolic resin is co-milled with hexamine and heated to promote cross-linking. The cured phenolic resin was milled by an external company to a mean particle diameter of roughly 45 µm. At some point in the development of the production process, variation in the content of fine particles (around 6 µm) between batches was identified. Batches with higher fines content would extrude well but would fail at the firing stages and the opposite was observed for low fines batches. From that point forward, it has been standard practice to classify the resin to 'coarse' and 'fine' particle sizes (around 45 and 6 µm respectively). The resin is typically added in a weight ratio of 8 parts fine material to 92 parts coarse, a greater large particle fraction than required for maximum packing fraction.

1.2.2.2 **Binder Formulation**

The binder package has been added to and refined over the course of several years. Modifications have been made to its formulation in response to changes in downstream processing, environmental conditions and unknowingly to the particle sized distribution of the phenolic resin.

At this stage, the binder formulation has become fairly standardised and tweaked slightly depending on the die being used or changes in the weather.

The components that make up the binder package are discussed in further detail in Chapter 3.

1.2.2.3 **Mixing**

Solid components, i.e. phenolic resin and dry binders are added to a twin z-blade mixer and dry mixed for approximately 5 minutes before the liquid components are added. Once the

liquid phase has been added, the mixture is blended for a few hours. Without any objective measure of the extent mixing, it is the operator's role to judge when mixing is complete. No environmental controls are in place; therefore the mix is subject to the prevailing weather conditions, resulting in different mixing times from summer to winter.

1.2.2.4 **Extrusion**

Small-scale extrusion (up to roughly 27 mm in diameter) is carried out on a table mounted Instron load frame run in compression mode. MAST Carbon has access to two barrels which can be fitted with a number of extrusion nozzles, or dies, of various design. Extrusion is carried out vertically and the extrudate is cut by hand and carried to a bench top rolling table to dry. Monoliths produced on this scale can be up to approximately 40 cm in length and rods are limited by available space on the roller table. This equipment is connected to a PC and the load profile can be examined during extrusion and downloaded for later analysis. This makes it ideal for not only small-scale production but for paste characterisation and experimental work.

Larger scale extrusion is carried out on a dedicated Sulby ram extruder. The Sulby barrel can hold up to 7 litres of paste. This equipment is able to accommodate larger extrusion nozzles, up to 100 mm, and may produce monoliths of much greater length. The product is extruded horizontally onto a V-shaped airlift tray to reduce damage from friction.

MAST Carbon has many extrusion dies with various geometries, but they are made to the same design. The fundamental design is relatively unchanged from the original patent owned by Corning [12] and subsequent patents[13, 14].

The extrusion dies at MAST are made in two pieces; the first is a baseplate featuring a series of feed holes on one side and a series of narrow slots on the other. The second is a washer

which fits over the baseplate and forms the outer wall of the monolith. The major features of the honeycomb die are illustrated in Figures 1.3 and 1.4. The extrusion dies are discussed in more detail in section 3.2.1.
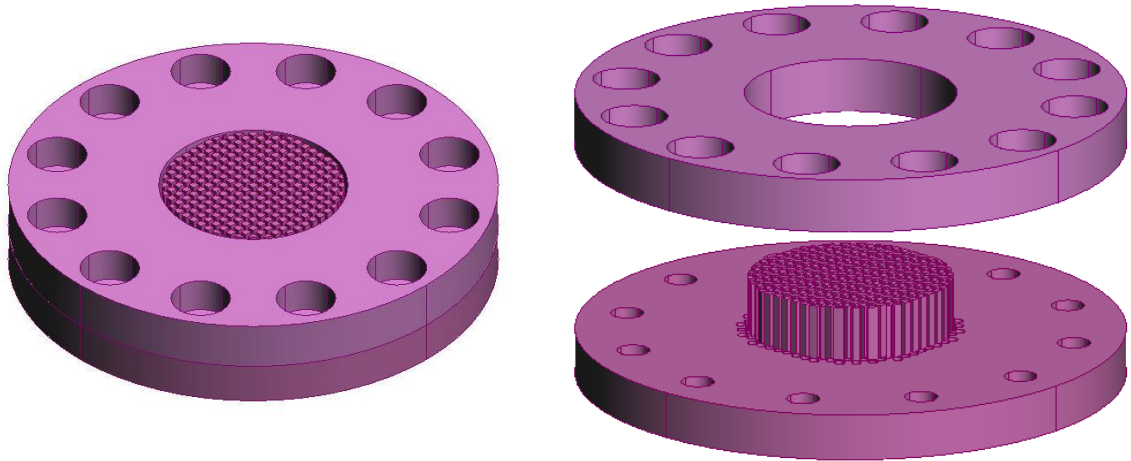
Figure 1.3 - 'Bath 2' extrusion die isometric and exploded views
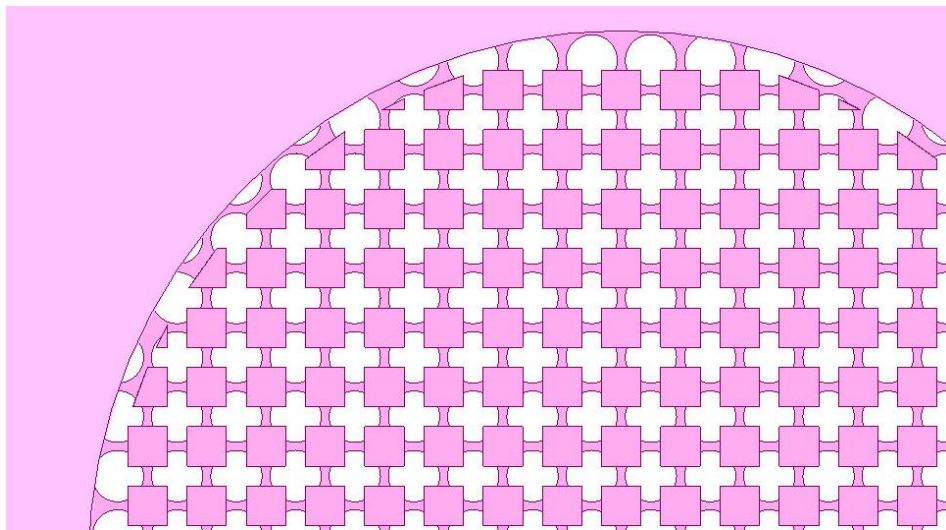
Figure 1.4 - 'Bath 2' extrusion die detail

1.2.2.5 **Drying**

As already alluded to, monoliths are air-dried at ambient condition on a rolling table to prevent bending. As no environmental controls are in place, monoliths are again subject to the prevailing weather conditions. Differences in temperature and relative humidity have a

pronounced effect on drying behaviour (discussed in more detail in Chapter 7). As historically the time between extrusion and carbonisation has been variable, it is certain that monoliths have been fired with very different moisture contents. It is likely that this has had an effect on rejection rate and final product performance but the extent to which remains unknown.

1.2.2.6 Carbonisation and Activation

Once dried, monoliths are heated gradually to 700 °C and held for around 1 hr. This stage is carried out under CO_2. In this stage, the phenolic resin is reduced to amorphous carbon. Approximately 45% of the mass of the phenolic resin is lost, largely as phenol derivatives and whilst this may seem high it is a considerably higher yield that would be achieved with cellulosic precursors where it is typically around 80% loss [1, 15-17].

The organic binders and water phase are removed completely, leaving only pure carbon. At this stage, the carbon only has a surface are of around 500 $m^2.g^{-1}$. The monoliths lose approximately 50% of their weight, a significant amount of strength and undergo shrinkage of roughly 30% in both linear and radial dimensions.

A second firing stage is required to increase the surface area to around 1200 $m^2.g^{-1}$; the activation stage. This stage is carried out under CO_2 and the temperature is raised to around 900 °C for around up to around 5 hours, depending on the level of activation required. The monoliths will lose approximately a further 20% weight and a reduction in size of around 5%.

In small-scale production, both these stages may be performed at the same time in bench top tube furnaces. During large-scale production, these stages are carried out separately in dedicated batch furnaces. Up to 30 monoliths can be processed in the activation furnace, but only around 10 in the pyrolysis furnace where it is limited by the capacity to treat the off-gases.

1.2.2.7 **Summary**

The development of the paste formulation until now has been done on largely an *ad hoc* basis. Changes in weather, die geometry, mixing regimes and raw materials have all required modification to the formulation to produce a satisfactory product. It is the nature of this kind of development that once a component has been added to the formulation, one is reluctant to remove it. MAST Carbon now finds itself in a position where the paste formulation, mixing and extrusion stages are well understood on a qualitative basis by an experienced operator, but the specific interactions of paste formulation and processing conditions are not well understood. These stages are very much regarded as a 'black art' in contrast with the better understood carbonisation and activation stages.

1.2.3   Description of Problem

The rejection rate during the extrusion and drying stages is high; around 50% of monoliths must be discarded by the end of the process. While this is acceptable when the batch size is no more than a dozen, it will become increasingly more pressing to reduce rejection as batch sizes increase. Some of the reasons for monolith rejection are outlined below

1.2.3.1 **Surface Defects**

Surface defects form as the paste exits the die. They may take the form of a roughened surface, 'sharks teeth' type tearing or a slight rippling effect. This type of defect has a significant impact on the aesthetic properties of the product in addition to detrimental effects on performance. Ragged tears have a greater impact on performance, causing disturbance to internal flow patterns at the site of the defect.

1.2.3.2 **Delamination**

Paste elements extruding perpendicular to one another must bind together upon exiting the die in order for the monolith to properly form. In some cases, the paste streams will either not contact or the bond between them will be weak and split along the interface. In order to perform correctly, the monoliths must be in one piece and channels must remain discrete.

1.2.3.3 **Preferential Flow at Core or Walls**

It is extremely important that the flow profile across the face of the die remain even, i.e. paste at the edges, or walls, flow at the same rate as paste in the bulk, or core. Depending on the severity, in cases where the paste will flow faster at either the wall or core, the monolith may become unusable. Misalignment of the exterior washer of the die may lead to bent or 'banana' shaped monoliths. Depending on the application of the piece, bent monoliths may be entirely unusable, particularly where more than one monolith is to be used in parallel.

1.2.3.4 **Phase Migration**

Phase migration occurs when the liquid phase of the paste flows preferentially to the solid matrix. The effect of this phenomenon is the paste becomes progressively drier during extrusion, resulting in non-uniform product and damage to equipment as the paste becomes more difficult to form.

1.2.3.5 **Cracking upon Drying**

The monoliths are dried at ambient conditions and constantly rolled to prevent bending. Monoliths sometimes form cracks along the central cell walls and may even split in half. More often, the cracks are a few millimetres in length and are always observed in or about the very centre of the monolith.

1.2.3.6 **Cracking upon Carbonisation/Activation**

Similar crack failures are more frequently observed at the final two stages of processing. While the carbonisation and activation stages are beyond the scope of this work it is likely that formulation and upstream processing and not solely the firing stages that influence the failure rate at this stage. It is, therefore, important to be aware of this failure mode and to consider it when working to optimise the formulation and forming processes.

1.2.4 **Project Approach Outline**

In order to allow the scale up of monolith production, it was clear that there were two steps in the production process which needed to be addressed. First, the development of defects during extrusion. The favoured approach was to determine whether there is a method for predicting the development of defects from the paste rheology and therefore whether paste could be formulated to have rheological behaviour most suitable for defect formation. In other words, to design out the possibility of defects before extrusion begins. If the rheological properties could be measured simply by a shop floor test, this would be extremely useful.

Secondly, the drying time presented a serious production bottleneck and should be minimised. The possibility of a forced drying regime without introducing internal cracks should be addressed. To achieve this, a forced drying trial was conducted and a model for predicting the stress profile during drying was developed.

2 LITERATURE REVIEW

2.1 Paste Formulation

A paste is a complex system comprising a solid and liquid phase [18-20]. The solid phase is highly concentrated, the liquid phase (usually aqueous) only being present to fill the voids between particles and provide lubrication, making it possible to form industrially useful shapes.

There are many factors which influence the properties of a paste, including the ratio of solids to liquid; the particle shape, size and distribution of the solid phase [10] and the rheology of the liquid phase [20, 21]. The latter of these is usually modified by the addition of one or more binders or extrusion aids.

Extrusion requires that a paste is formulated such that it exhibits a high yield stress, is shear thinning and that the liquid phase is sufficiently viscous. A yield stress ensures that the paste will only deform during processing and will retain its shape once extruded [22]. Shear thinning behaviour is desirable so that the paste becomes easier to deform when greater force is applied and will not deform during handling. Finally, a highly viscous binder system is required so that the liquid phase will remain well distributed in the paste and not dewater.

These terms are described more fully below, beginning with a basic overview of some rheological models.

2.2 Rheology

2.2.1 Stress Tensor

The stress tensor describes the stress state of an element of a material. It is a 3 x 3 matrix containing terms resolving all acting stresses on the element into 3 terms for each face of the element, shown in Equation 2.1. The element and the planes are shown in Figure 2.1.

$$\boldsymbol{\sigma} = \begin{bmatrix} \sigma_{11} & \sigma_{12} & \sigma_{13} \\ \sigma_{21} & \sigma_{22} & \sigma_{23} \\ \sigma_{31} & \sigma_{32} & \sigma_{33} \end{bmatrix} \qquad \textbf{Equation 2.1}$$
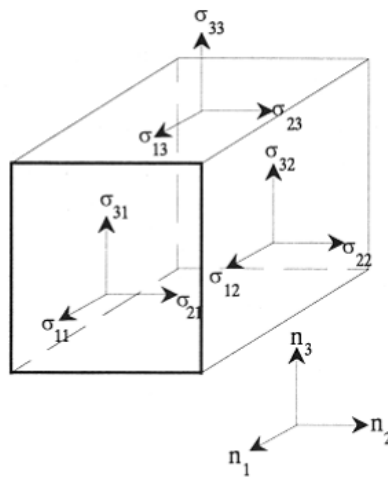
Figure 2.1 - Forces acting upon element of material [23]

2.2.2 Simple Shear Rheology

Simple rheology describes the deformation behaviour of materials when placed under stress. The two simplest models apply to the deformation of simple liquids and solids [23-25].

In 1678, Robert Hooke proposed what has now become known as Hooke's Law. He said in his "True Theory of Elasticity" that the relationship between the extension of a spring (ε) and

the tension (σ) is proportional. The proportionality constant, E, is known as Young's modulus. Equations 2.2 - 2.3 describe this relationship.

$$\sigma_{ii} = \frac{\text{Force applied normal to i plane}}{\text{Area}}$$

Equation 2.2

$$\sigma_{ii} = E\varepsilon_i$$

Equation 2.3

When a shear stress is applied to a Hookean solid, the deformation is in the direction of the application of the force as shown in Figure 2.2.
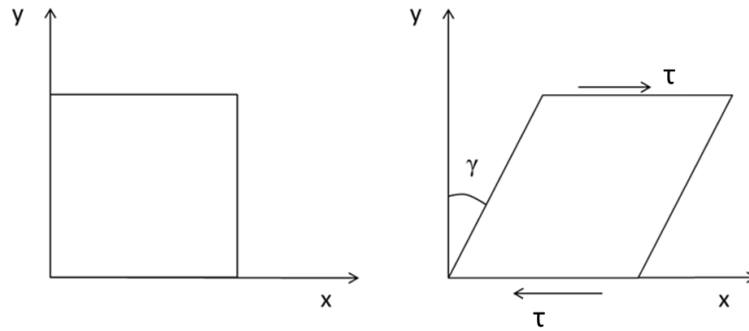
Figure 2.2 - Deformation of a Hookean solid under application of shear stress

The deformation angle, γ, is related to the shear stress by the rigidity modulus, G (Equation 2.4).

$$\tau_{ij} = G\gamma$$

Equation 2.4

A few years later, in 1687, Isaac Newton proposed in his "Principia" that the *rate* at which a liquid deforms is directly proportional to the shear force [24]. Navier and Stokes have since further developed Newton's ideas into the Navier-Stokes equations.

$$\tau = \eta\dot{\gamma}$$

<div align="right">**Equation 2.5**</div>

These two simple models describing the responses of solids and liquids to stress were sufficient for many years until Wilhelm Weber observed that when threads of silk were stretched, they continued to deform even after the initial response [24]. This may be thought of as the beginning of the study of rheology.

2.2.3 Extensional Viscosity

Extensional viscosity is distinct from shear viscosity. During convergent flow, extensional strain plays a large part in the deformation, [26]. The relationship between the elongational strain rate ($\dot{\epsilon}$) and the shear rate at the wall depends on the type of convergence. The two types of convergence that are of interest are forced and free convergence (shown in Figure 2.3). Figures 2.3a and b show forced convergence with wall slip and parabolic flow profile respectively.
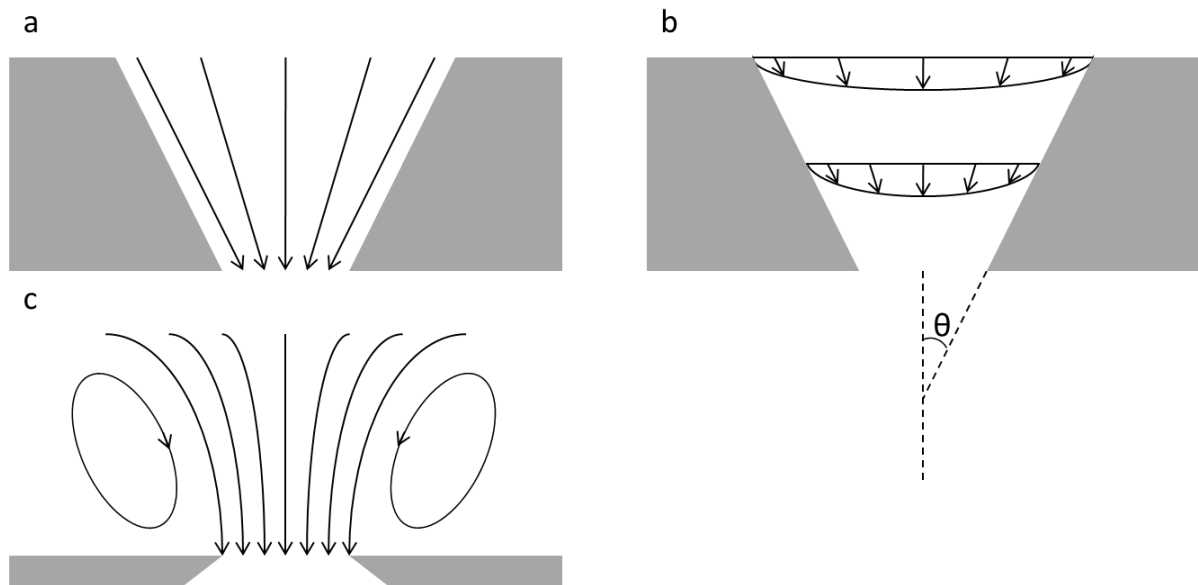
Figure 2.3 - Types of convergent flow (a) forces convergence with lubrication at wall (b) forced convergence with no slip at wall (c) free convergence with static zones adjacent to orifice

During free convergence (Figure 2.3c), the fluid forms curved streamlines with either static regions of fluid or vortexes at the peripheral edges. Cogswell [27] gives the rate of elongational strain as

$$\dot{\epsilon} = \frac{\dot{\gamma}}{2} \tan \theta$$

<div align="right">**Equation 2.6**</div>

where $\dot{\gamma}$ is the shear rate at the wall given by Equation 2.5 and θ is the half angle of convergence. At least 2 other authors suggest different but similar relationships between the elongational strain rate and shear strain rate, all of which are almost identical at half cone angles less than 30 degrees [26].

During constrained convergence when the walls are lubricated, the fluid will flow through the entrance as a plug (Figure 2.3a). In this case, the relationship between the elongation strain rate at the die exit and the shear strain rate is given by Cogswell by the same relationship as for the free convergence case (Equation 2.6).

For the unlubricated forced convergence case (Figure 2.3b), telescopic flow is observed and the elongational strain rate is given by

$$\dot{\epsilon} = \dot{\gamma} \tan \theta$$

<div align="right">**Equation 2.7**</div>

2.2.4 Viscoelasticity

While many simple fluids and classic solids fit into the Hookean and Newtonian models of stress response, a far greater number of fluids lie somewhere in between the spectrum from simple solid to simple fluid. Almost all of the fluids discussed in this work are more accurately described as a colloidal suspension of more than one pure substance whose

behaviour lies somewhere on this spectrum. Fluids of this type are described as 'viscoelastic' as they exhibit both viscous and elastic properties. In an overwhelming number of cases, the fluid is considered to be a single continuous fluid, rather than accounting for particle/particle interactions and the complex behaviour of the dissolved polymer network in the liquid phase.

A number of models attempt to define the relationship between stress and deformation of viscoelastic systems, which are made up of two primary components: a spring (Figure a) and a dashpot (Figure b).
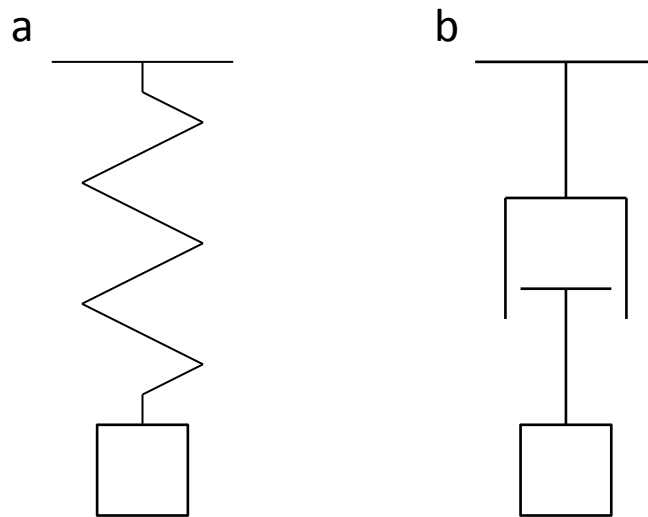
Figure 2.4 - (a) Spring element (b) Dashpot element

The spring element represents a perfect Hookean solid; it responds immediately to stress and the extension is directly proportional to the stress. The dashpot element represents a perfect viscous fluid; it responds gradually to an applied stress and the rate of extension is directly proportional to the stress. These elements may be combined to model a viscoelastic material. Three popular models are the Kelvin (or Voigt) model and the Maxwell model.

2.2.4.1 **Kelvin**

The Kelvin model (also known as the Voigt model) is the simplest of all the viscoelastic models. This model assumes that the shear stress is equal to the sum of a linear function of the strain and a linear function of the shear rate.

$$\sigma = G\gamma + \eta\dot{\gamma}$$

The Kelvin-Voigt model may be considered as a spring and dashpot element working in parallel, as shown in Figure 2.5.
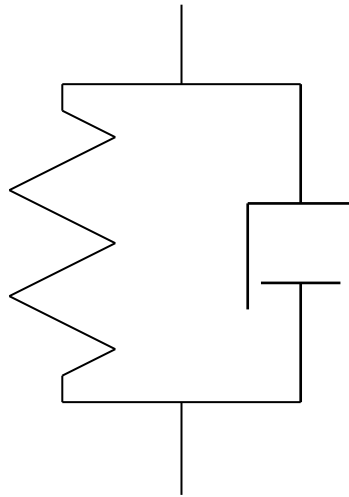
Figure 2.5 - Kelvin model represented by a spring and dashpot element in parallel

The response of this model to a sudden stress, $\bar{\tau}$, over time can be shown to be:

$$\sigma = \frac{\bar{\tau}}{G}\left[1 - \exp\left(-\frac{t}{\tau_K}\right)\right]$$

Equation 2.9

where $\tau_K = \eta/G$. This response differs from that of a Hookean or Newtonian material. With a Hookean material, the response is immediate and constant and with a Newtonian material, the response is continual and unlimited. With the Kelvin model, the response is limited to the maximum strain defined by the parameter G and is retarded by the rate of extension defined by η.

2.2.4.2 **Maxwell**

The Maxwell model is made up of a spring and dashpot element working in series, as shown in Figure 2.6.
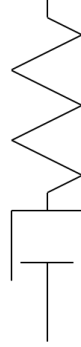
Figure 2.6 - Maxwell model represented by a spring and dashpot element in series

The strain rate of the Maxwell system is assumed to be the sum of the strain rates of the viscous and elastic components.

$$\dot{\gamma}_M = \dot{\gamma}_E + \dot{\gamma}_V$$

<div align="right">

Equation 2.10

</div>

This leads to:

$$\sigma + \tau_M \dot{\sigma} = \eta \dot{\gamma}_M$$

<div align="right">

Equation 2.11

</div>

It can be shown from Equation 2.11 that upon application of a sudden strain rate, $\bar{\gamma}$, the strain response at time t is:

$$\sigma = \eta \bar{\gamma} \left[1 - \exp\left(-\frac{t}{\tau_M} \right) \right]$$

<div align="right">

Equation 2.12

</div>

where τ_M is the time constant.

2.2.5 Complex rheometry measurement

It is possible to quantify the viscoelastic properties of the sample using oscillatory rheometry. An oscillatory force is applied by the geometry and the response is measured by a torque transducer. If the sample is a perfect Hookean solid, then the input/response curve will match and they are said to be in phase. At the other end of the scale, if the sample is a perfect viscous fluid, then the input/response curves will be one half phase (90°) out of sync. If the phase angle (δ) is between 0 and 90°, then the material is viscoelastic and exhibits both liquid and solid-like behaviour.

The storage and loss moduli are calculated from the phase difference. The storage modulus, G', is a measure of the 'solidness' or elastic behaviour of a material and the loss modulus, G'', can be described as a measure of the 'liquidity' or viscous behaviour of a material. A phase angle of 45° is often considered the gel point, or when G' and G'' are equal.

$$G' = \frac{\text{stress}}{\text{strain}} \times cos\delta \qquad \textbf{Equation 2.13}$$

$$G'' = \frac{\text{stress}}{\text{strain}} \times sin\delta \qquad \textbf{Equation 2.14}$$

More accurately, the storage modulus is a measure of the energy stored by the sample during deformation. Once the shear force has been removed, the energy is available to the body and acts as the driving force for the sample to return to its original shape before the deformation [28]. Similarly, the loss modulus is a measure of the deformation energy lost by the sample. Energy is lost as molecules or particles are rearranged and the body changes its shape. The energy may also be lost as heat during deformation. A body which loses all of the deformation energy experiences irreversible deformation i.e. behaves entirely viscously.

Oscillatory rheometry may be conducted by varying the shear force applied (shear sweep), the magnitude of deformation (strain sweep) or the frequency of oscillation (frequency sweep). A shear stress sweep of a material yields curves similar to those shown in Figure 2.7. Stress or strain sweeps are commonly used to identify the 'Linear Viscoelastic Region' (LVR) where the relationship between stress and strain is linear and G'/G'' are constant. Frequency sweeps are conducted at a constant strain or stress located within the LVR.
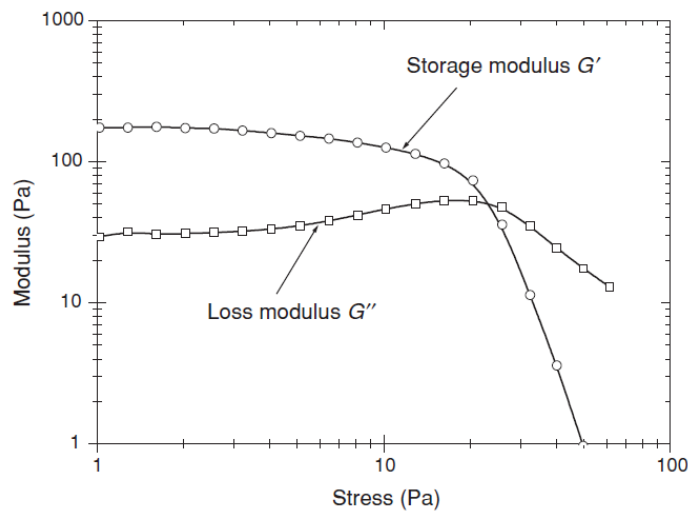
Figure 2.7 - Shear Stress Sweep of a viscoelastic material [29]

Oscillatory rheometry can be used to determine a number of things about a material such as its stability over a range of stresses and the strength of the dispersion. This can lead to conclusions about the properties of the suspension and its response to process relevant conditions.

2.3   Paste Models and Formulation

A number of attempts have been made to model the behaviour of pastes, particularly during extrusion. The simplest approach is to apply a power law or, commonly, a Herschel-Bulkley model (Equation 2.15) to describe flow [30-32]. This approach is effective for describing

pastes in capillary flow [22] and useful for performing computational fluid dynamics or finite element modelling.

$$\tau = \tau_0 + k\dot{\gamma}^{n_f}$$

A very well-known and widely used paste model proposed by Benbow and Bridgwater [33-35]. Their work focused on the relationship between extrusion pressure and die geometry as a function of some semi-empirical properties of the paste. Ram extrusion was considered by them to have 2 major resistances to flow. The first being the energy required to deform the paste from the barrel cross section to the smaller cross section of the extrusion die. The second is the friction at the walls in the die land. There is also wall friction found in the extruder barrel, but this is, generally speaking, negligible compared to the other two pressure drops and is usually not considered unless extrusion data shows a reduction in load as the piston travels along the barrel.
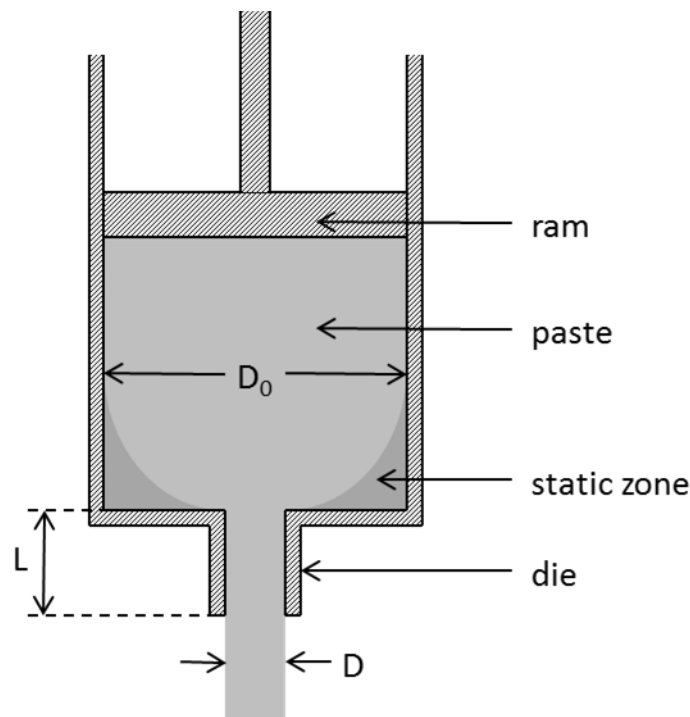
Figure 2.8 - Simple ram extrusion

The pressure drop related to the reduction in extrusion cross-sectional area is linked to the extrusion velocity in the die land by three 'paste parameters' as shown in Equation 2.21. This relationship was adapted from a similar expression given to describe the extrusion of metals.[34]

$$P_1 = (\sigma_0 + \alpha V^m) \ln\left(\frac{A_0}{A}\right)$$

Equation 2.16

The pressure drop associated with the wall friction is expressed in a similar way, relating pressure drop to extrusion velocity by another three 'paste parameters'. Beginning with the assumption that a paste in plug flow and applying a force balance, the pressure drop in the die land is given by Equation 2.17.

$$P_2 = (\tau_0 + \beta V^n)\frac{M}{A}$$

Equation 2.17

The overall pressure drop can, therefore, be given in its generalised 6 parameter form as

$$P = P_1 + P_2 = (\sigma + \alpha V^m) \ln\left(\frac{A_0}{A}\right) + (\tau + \beta V^n)\frac{M}{A}$$

Equation 2.18

The model was originally published without the exponents m and n and they were added later to account for the non linear extrusion profiles found in most pastes [33].

The Benbow Bridgwater model (hereafter referred to as the BB model) is a semi-empirical model and as such the six paste parameters, while they may be used to describe the pressure drop in ram extrusion, are not tied to any real, measurable property of the paste outside of the specific conditions under which the model is valid. Indeed, the 6 parameter model has been recently been criticized as recently as 2015 by Stitt *et al.* [36] for containing exponential terms purely to make the model fit data without consideration of their physical relevance.

 These concerns have prompted some authors to develop constitutive paste models.

One such attempt was made by Basterfield *et.al.* in 2005 [37], building on earlier work that showed that paste flow behaviour is closely approximated by an elasto-viscoplastic model in finite element analysis [38, 39]. The model is in some ways an evolution of the BB model in that the paste is assumed to undergo a period of convergent flow, followed by plug flow at the die exit. The most significant improvement the Basterfield model offers over the BB model is that it describes a constitutive relationship between the pressure drop and the extrusion velocity. The model is shown in Equation 2.19.

$$P = 2\sigma_0 \ln\left(\frac{D_0}{D}\right) + Ak_u \left(\frac{2V}{D}\right)^{n_f} \left(1 - \left(\frac{D}{D_0}\right)^{3n_f}\right)$$

Equation 2.19

where
$$A = \frac{2}{3n_f}\left(\sin\theta_{max}\left(1 + \cos\theta_{max}\right)\right)^{n_f}$$

This approach, however, is limited in its utility as it only considers the convergent flow region of the extrusion process and does not deal with the pressure drop in the die land. This is also the case with other models which have been proposed by other authors such as Horrobin [40]

These models, while described as constitutive, could also be considered to be semi-empirical. It has been shown that the flow of pastes in orifice extrusion can be accurately modelled with a Herschel-Bulkley type rheology, this approach assumes that paste exists as a single continuous fluid, rather than a complex system of more than one phases. If thought of in this way, it could be argued that the Basterfield model and others are no more constitutive than the original BB model. Even so, the constitutive models, as they are, can be used successfully in finite element modelling as the assumptions made by the model do not only apply to ram extrusion, as is the case with the BB model.

While there are many methods for accurately predicting the extrusion pressure through a die, very little work has been done which successfully uses these models to improve extrusion processes. Rather, they are typically used to characterise pastes and aid in the design of

extrusion tools. Work done by Blackburn and Wilson in 2008 [10] has shown that the reciprocal of the yield stress of a paste, σ_0, can be used as a measure of 'extrudability'. It was shown that this term can be used to aid paste formulation when considering moisture content and ratio of coarse and fine particle sizes. This relationship is shown in Figure 2.9.
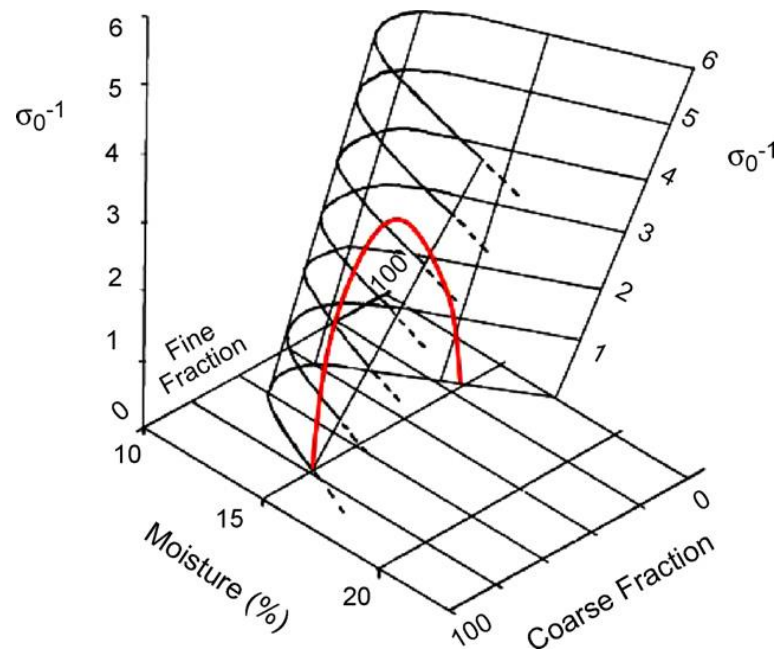
Figure 2.9 - 'Plane of Extrudability' developed by Blackburn and Wilson [10]

There still exists a gap in the literature for a quantitative measure which can be directly linked to the 'quality' or 'ease' of extrusion through a given die geometry. Such a measurement would allow extrusion processes and pastes to be designed so as to minimise or even eliminate the formation of defects in the extrudate. This would be of particular power for more complex honeycomb extrusion.

2.4 Extrudability Tests

2.4.1 Definition of Extrudability

One of the major objectives of this work is to establish a simple shop floor test which could give an operator an immediate indication of the 'extrudability', or 'workability' of the paste. This would help avoid wasting time and material on processing poor quality pastes.

Despite a number of attempts to define a measure of extrudability, there exists no generally accepted specific definition. The term is typically used to describe the ability or propensity of a paste to form a consistent defect free monolith. A number of attempts have been made to develop tests to quickly assess the viability of a paste.

2.4.2 Atterburg Test

The Atterburg test was developed by Albert Atterburg in 1911 as a test to define the range of moisture content within which a clay body could be moulded. The test defines the plastic and liquid limits of the material (otherwise known as the Atterburg Limits).

The plastic limit is the lowest moisture content at which a clay may be formed into rods by rolling it against the palm of the hand and a hard surface, as depicted in Figure 2.10. The liquid limit is the lowest moisture content at which the clay begins to flow, determined with a Casagrande apparatus (named for Arthur Casagrande (1902-1980)) shown in Figure 2.11a. The material is placed in the brass bowl and a groove is cut through to the metal, as shown in Figure 2.11b. The handle on the apparatus is turned 25 times which will cause the two halves of the clay to flow together. The moisture content at which the clay forms a ½" 'bridge' across the groove is defined as the liquid limit. The difference between the liquid and plastic limits is known as the "plasticity index".

Figure 2.10- Rolling a clay body to measure plastic limit [4]
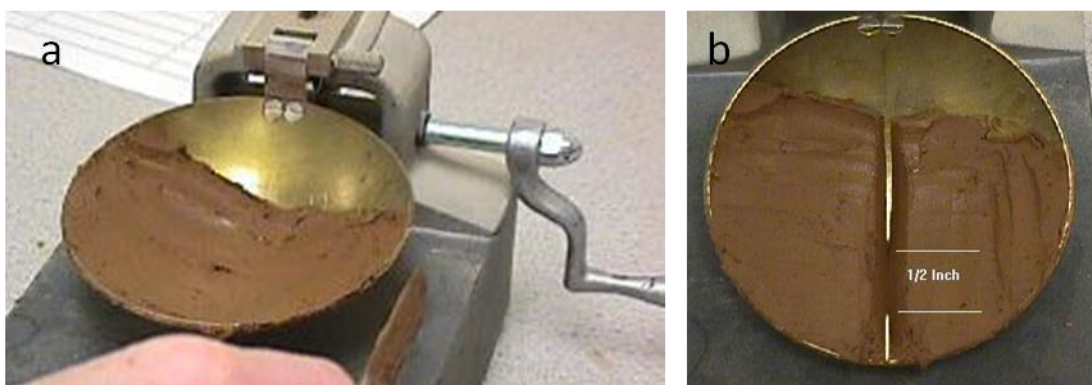
Figure 2.11 a & b - Casagrande apparatus [41]

The Atterburg test is an indirect workability method. A disadvantage of this technique is that it is heavily dependent on the technique of the user and as such the repeatability of the test is very low. While an experienced experimenter may be able to use this test with a high degree of self-consistency, it is likely not of any value to compare results from two different sources. Additionally, measuring the moisture content of paste after it has been prepared is difficult to do accurately and can be a source of error when determining the plasticity index. However, the test is cheap and easy to perform.

While this method may be used to see if a paste falls between the Atterburg limits, this method is of very limited use as a quality control test. An operator would need to perform parts of the test on the paste after it had been mixed. All that would be learned is whether the

paste falls within the Atterburg limits, not where in the spectrum the paste lies. This gives the operator very little information to determine whether a paste will work or not.

If a large enough body of empirical data was collected, it might be possible in principle to measure where the paste should fall between the Atterburg limits to give the best extrusion possible. However, the test was only designed to account for the difference in rheology caused by changing the moisture content. It may not properly account for the changes in rheology due to modification to the binder package.

As a quality control test, it should only be used as a very rough "go/no go" test for assessing raw materials, where it does see some use in the brick making industry [10]. This test would be more useful as an aid to formulation development, for which it was originally designed.

2.4.3   Pfefferkorn Test

In the Pfefferkorn test, a cylindrical sample of 40 mm in height and 33 mm in diameter is prepared (either manually or by extrusion) and deformed by dropping a mass of 1.192 kg on it [42]. The measured deformation at varying moisture contents gives an indirect indication of the workability. The reported "Pfefferkorn moisture content" refers to the moisture content which leads to a 30% contraction.

The results are displayed in a graph of the ratio of initial to final height versus the moisture content (see Figure 2.12). The steeper the curve, the more significantly the body will react to changes in moisture (referred to as shortness).
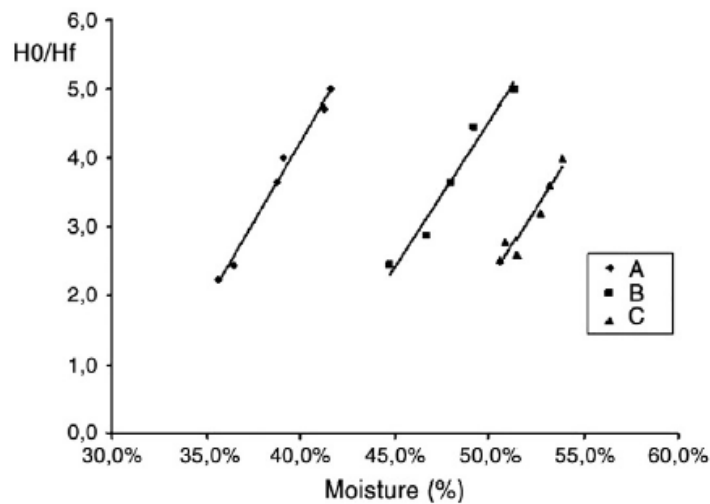
Figure 2.12 - Typical Pfefferkorn test results [6]

The accepted limits for extrusion are roughly 37% reduction for soft extrusion and roughly 8% reduction for stiff extrusion [11].

This method is the most commonly used test to determine the plasticity of a material [43]. As with the Atterburg tests, correctly measuring the moisture content is very difficult and can result in imprecise data. The action of dropping the weight on the sample is highly repeatable, although the forming of the sample itself is less so (particularly if the sample is prepared by hand).

Unlike the Atterburg test, this test will give the user some idea of where the paste lies in relation to the lower and upper deformation limits. If a large body of empirical data was collected, deformation could be correlated with defect formation or extrusion quality. If there is a satisfactory correlation between the two, then this test might be used as a method of determining how well an extrusion is going to go.

Like the Atterburg test, it was developed to account for the differences in deformation based on changes in moisture content and may not be suitable for characterising the differences in rheology caused by changing the binder package. Deformation of a cylinder is quite a coarse

method for characterising paste rheology. While a more sophisticated characterisation method will likely be necessary to predict extrusion quality, the fact remains that this test may prove to be a useful shop floor quality control test.

2.4.4 Indentation Test

An indentation test is performed by dropping a cone into a sample over a known time delay and measuring the depth of penetration. A typical setup is shown in Figure 2.13.
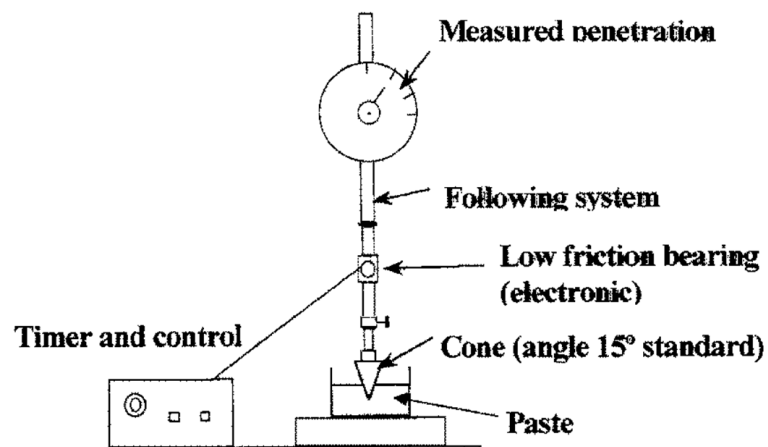
Figure 2.13 - Cone Penetrometer [44]

Indentation as a method of measuring the Atterburg limits is another indirect way of measuring the workability of a sample. In the standard method, a sample is prepared and penetrated with a cylindrical 30° cone with a mass of 50g. The cone must be suspended above and just in contact with a flat area of the sample. An inclined light is shone on the side of the apparatus so that the cone can be positioned correctly from the shadow. The cone is allowed to fall for 5 seconds and the penetration distance is measured. The moisture content which corresponds to a penetration depth of 20 mm is the plastic limit. The liquid limit is determined with the same test using a cone with a total mass of 240 g [42].

An alternative method is suggested by Modesto and Bernardin (2008)[43] in which the Atterburg limits are determined by observing the type of mark left in the sample (see Figure 2.15a). The presence of cracks suggests that the plastic limit has been reached. No cracks or a lack of consistency left by the cone corresponds to the liquid limit (see Figure 2.15b).

This method is considered by Modesto and Bernardin (2008) to be a faster and more practical method than the Pfefferkorn test. While the standard indentation method is highly repeatable, the method proposed by Modesto and Bernardin (2008) is highly dependent on the examiner's technique as the end points are more open to interpretation. Measuring the Atterburg limits by observing the behaviour of the walls may only be, as with the Atterburg tests themselves, internally consistent even when performed by an experienced operator.
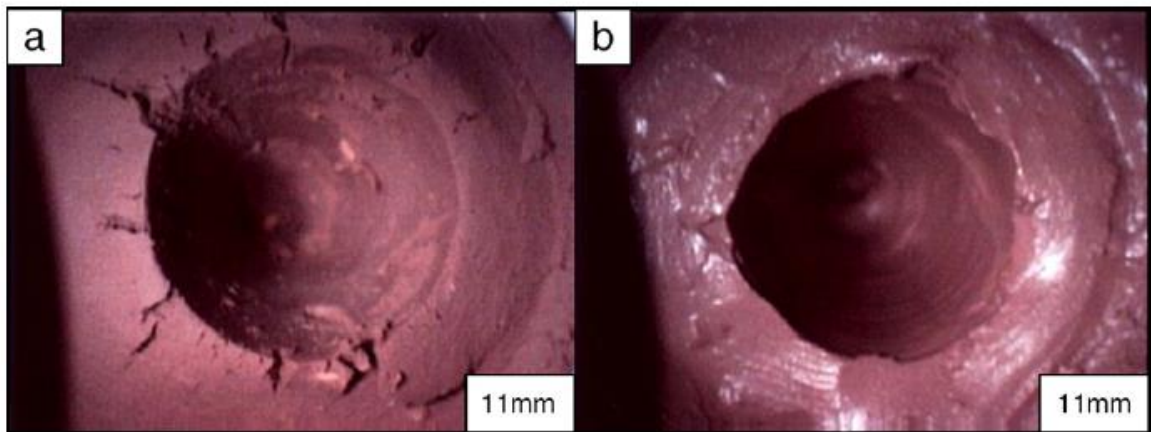
Figure 2.14 - Clay indentation (a) Plastic Limit (b) Liquid Limit [8]

The depth of penetration may be used to calculate the yield stress, σ_c, [44, 45].

$$\sigma_c = \frac{W}{\pi h_c{}^2 tan^2(\theta_c)}$$ **Equation 2.20**

Where W is the mass of the cone assembly, h_c is the penetration depth and θ_c is the cone angle.

The indentation test is cheap and quick to perform. If the material is mostly viscous, not plastic, the penetration will depend on the time for penetration. Additionally, forces due to deceleration are not considered [33].

If used to measure the yield stress, the indentation may be of use as a quality control test in some circumstances, particularly as it is very quick and easy to perform and is highly repeatable. It may also be possible to determine where the sample lies between the Atterburg limits, if they are known, which may be of additional use. However, only a limited amount of information can be gathered, so another test may be required.

As a method for determining the Atterburg limits, the standard method is highly repeatable and quick to perform. The endpoints proposed by Modesto and Bernardin (2008) may correspond more closely to the limits proposed by Atterburg but this method suffers from sensitivity to operator technique and the associated inaccuracies. As with the Pfefferkorn and Atterburg tests, numerous samples must be prepared which is time-consuming and may lead to inaccuracies.

As a shop floor test, this method allows the operator to potentially measure where the paste lies between the Atterburg limits. Determining this objectively using this method is not possible. Like the Atterburg test, this should only be used as an aid to formulation development.

2.4.5   Norton Test

The Norton test was proposed by F.H. Norton in 1974. Norton wrote that a workable clay would "have a yield value high enough to prevent accidental deforming and an extension large enough to allow forming without fracture" [46]. Extension, in this case, refers to the maximum length by which a body can be extended before it fractures. The yield value and

maximum extension are not independent of each other. Typically, the yield value will decrease and the maximum extension will increase as moisture content is increased. The Norton workability may be expressed as the product of the yield value and the maximum extension.

Baran *et al.* (2001) calculated the workability of two clays using the Norton workability test. Measuring the maximum extension of a clay or paste is difficult [47]. In fact, Norton did not discuss any of the detail on how to measure either parameter. Baran *et al.*, used the tensile strain limit value, measured with an upset test (discussed below).
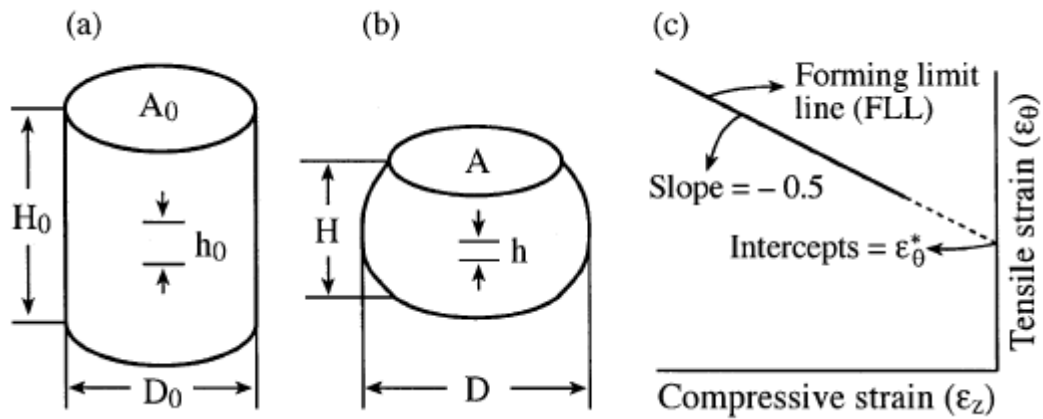
Figure 2.15- (a) initial sample (b) sample after deformation (c) forming limit line (FLL) [12]

In the upset test, a cylindrical sample of the clay is prepared and two lines scored along the side, separated by a distance h_0 (see Figure 2.15a). The sample is placed in a hand vice and compressed until fractures appeared on the sides of the clay. The ratios of h/h_0 and D/D_0 are used to calculate the compressive and tensile strains,

$$\varepsilon_z = \ln \frac{h}{h_0}$$

Equation 2.21

$$\varepsilon_\theta = \ln \frac{D}{D_0}$$

Equation 2.22

The results were repeated for samples with different H_0/D_0 ratios and the results were plotted on a graph, called the Forming Limit Line (see Figure 2.15c). The intercept of the line ε_θ^* is the maximum tensile strain.

The yield stress can be found using a cone penetrometer (see section 2.4.4).
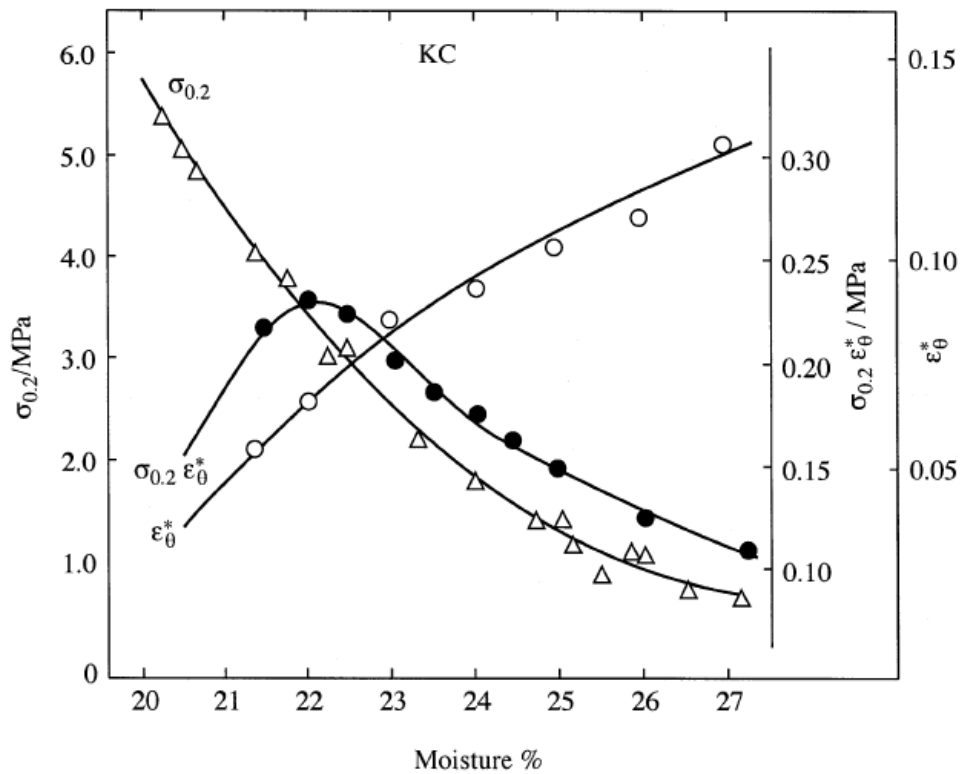
Figure 2.16 - Graph showing the Norton workability index [12]

Figure 2.16 shows the Norton workability index ($\bullet$) for a clay sample "KC" as a function of moisture content. The Norton workability index is a direct method for measuring the workability. As can be seen in Figure 2.16, unlike in the previous workability test, the optimum conditions for extrusion or moulding can be clearly seen. This may make the test particularly useful for determining paste formulation.

As a method determining the working moisture content limits for a given clay or paste, the Norton test is time-consuming and tedious. Multiple samples of different dimensions must be prepared for each level of moisture content.

As a quality control test, it is also much more time consuming than the tests already discussed. However, with the greater time cost comes a much more valuable measure of workability. The Norton workability index combines two important parameters, giving the operator a better indication of how workable the clay is. It remains to be seen whether the yield stress and

2.4.6   Summary of Workability Tests

The various workability tests reported in the literature vary in their suitability as a quick determination of the viability of a paste. None were developed with the application in mind. The tests such as the Atterburg or cone penetrometer tests are quick to perform but their subjectivity limits their utility. They also give the user only a crude measure of workability, only useful if backed up with a large body of correlative data.

The more time-consuming test, the Norton test, is more promising. It gives the operator more information upon which to base a prediction of extrudate quality but is still a crude method of paste characterisation when compared to paste model such as the Benbow Bridgwater model. The time required to perform these test is very problematic. From years of extrusion experience at MAST Carbon, it is known that once a paste has been mixed, its rheological properties can change quite quickly. The paste that has been tested and passed may not be the same rheologically speaking as the paste which is extruded, rendering this test unusable.

The complicated geometry of the honeycomb die makes predicting defect formation based on paste rheology a difficult question. It has not been demonstrated in the literature that any of

the workability tests discussed here are accurate predictors of extrusion quality through a honeycomb die, nor is it likely to. These tests could potentially be used as a very simple quality control to detect any major differences in paste consistency from batch to batch. This would not guarantee extrusion quality and it is possible that a change in paste rheology, important to defect formation, would remain undetected by such a test.

2.5   Defect Formation

Defect formation during extrusion may manifest itself in a number of ways, outlined in section 1.2.3. The majority of the work done in this field focusses on the tearing of paste at the walls. These are often referred to as "Sharks Teeth" or "Feathering". Surface fractures reduce the strength of the ceramic body and affect its aesthetic appeal. In some applications, such as electronic ceramics, the aesthetics of the product is very important to the customer. According to Benbow & Bridgwater [33], there are four criteria which, when met, will cause surface fracture:

- A drag force parallel to the surface of the extrudate

- The flowing paste tearing in response to the drag

- The tearing must be caused to cease by some mechanism

- Repetition of this process

Domanti *et al.* have done a great deal of work on predicting the formation of surface defects in the die land [39, 48, 49]. Domanti and Bridgwater found that the paste formulation was a heavy influence on the nature of the crack formation.
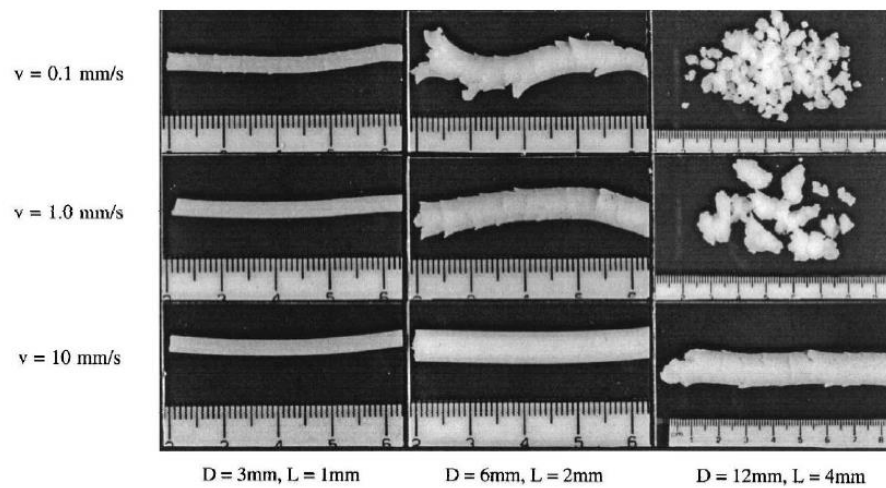
Figure 2.17 - Effect of extrusion velocity on surface fracture in a soap sample [48]

The paste formulation is a big influence on the formation of surface fracture. Almost every variable in a paste's formulation may affect the surface characteristics of the extrudate, including the particle size distribution and liquid content. Benbow & Bridgwater found that increasing the liquid content of the paste decreased the amount of surface fracture [33]. This was matched by a decrease in the bulk yield stress, σ_0, and τ_0.

Their later work involved finite element analysis of the paste in the die land and predicted fracture according to the tensile yield stress of the paste (ductile yield stresses could not predict the formation of cracks) [49]. They found through observation of paste extruding through a transparent die and by the predicted stress field that crack formation occurs at the die exit and in the case of some starch pastes, propagated backwards into the die land. Domanti and Bridgwater [48] also found that the rate of extrusion influenced the amount of surface cracking although the effect differed for each paste. In pastes with a glucose additive, an increase in extrusion velocity resulted in deeper cracks whereas for a soap preparation, the opposite was found. The reason for this discrepancy is thought to be because of the presence of a lubricating layer at the wall in glucose pastes which is absent in the soap.
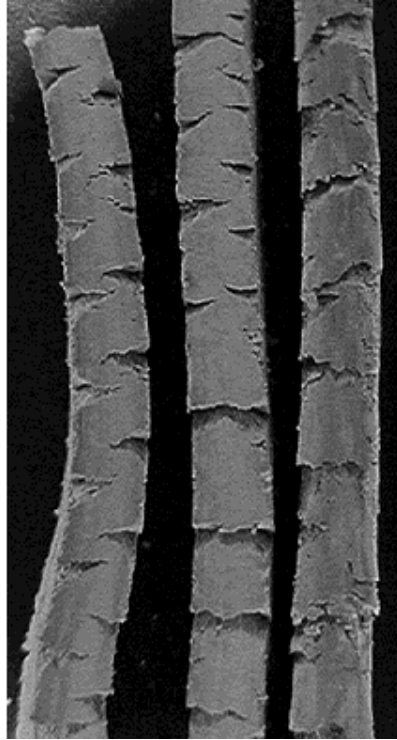
Figure 2.18 - Surface defects on ceramic paste extrudates (no scale given) [49]

Kulikov and Hornung [50] extruded various pastes through transparent dies of various length to diameter ratios. Using high-speed photography, the observed that some pastes became detached from the wall, leaving voids which grew into cracks. The frequency of the defects was highly influenced by extrudate speed. While the authors did not fully explain what causes this phenomenon, it is an interesting observation. It is not known to what extent this phenomenon could occur in the very small geometry of the honeycomb extrusion dies, but it is likely to be very little.

The approaches to defect formation appear to accurately predict the formation of surface fracture in simple cylindrical or slot-shaped dies. The majority of the defects encountered during production at mast appear to be caused to be large differences in flow rate between paste elements flowing from adjacent feed holes. That is to say, the effect appears to be slightly larger in 'scale' than the localised effects reported in the literature.

2.6   Phase Migration

Phase migration is a common and undesirable phenomenon in extrusion processes. Also known as dewatering, phase migration occurs when the liquid phase in a paste flows preferentially to the solid phase. This leads to an increase in extrusion pressure as the paste begins to dry in the barrel of the extruder. Phase migration has also been linked to the formation of defects such as 'shark's teeth'[49]. In extreme cases, an overpressure of the paste can lead to damage of the extruder [51].

The tendency for a paste to experience phase migration has been found to be affected by a number of factors, mainly the permeability of the solid matrix, water content, binder viscosity and the paste flow velocity. It was reported by Bayfield *et al* [52] that phase migration is greater when the paste velocity approaches the percolation rate through the solid matrix.

The most commonly applied paste extrusion model is the BB model. This model approximates a paste system as a viscoplastic undergoing plastic deformation [37] and plug-flow through the die land [33]. Resistance to flow comes from the energy required to compress the fluid in the convergent zone and to overcome friction at the die walls. The model is usually used in a form where there are six parameters relating to the paste flow independent of geometry, shown in Equation 2.23. While this model is successful at predicting the pressure drop of stable systems, it is unable to deal well with unstable pastes.

$$P = 2(\sigma_0 + \alpha V^m)\ln\left(\frac{D_0}{D}\right) + 4(\tau_0 + \beta V^n)\left(\frac{L}{D}\right) \qquad \textbf{Equation 2.23}$$

A number of attempts to model phase migration have been made, both using a modified form of the Benbow Bridgwater model. Bayfield *et al.* [52] observed that the length of static zones increased during extrusion and that this could be correlated with the increase in extrusion pressure. The static zones may be imagined to act as an 'extension' of the die, effectively

increasing the length to diameter ratio included in the second part of Equation 2.23. Equation 2.23 was then modified to include a term, *kh*, describing the height of the static zone and a proportionality constant in the second part of the equation dealing with pressure drop over the die. The modified form is shown in Equation 2.24

$$P = 2(\sigma_0 + \alpha V^m)\ln\left(\frac{D_0}{D}\right) + 4(\tau_0 + \beta V^n)\left(\frac{L + kh}{D}\right)$$ **Equation 2.24**

Rough *et al.* [53] have taken a combination of a soil mechanics approach with a modified Benbow Bridgwater model. The paste in the barrel was divided into discrete 10 mm high elements which were treated independently. At the beginning of each time step, the pressure gradient in the barrel was calculated. Using a Darcy's law approach, the liquid phase percolation rate through the solid matrix was calculated resulting in a moisture content profile. During each time step, the element closest to the die was considered to have been extruded through the die and the next element up was considered to undergo compression and replace the element below it. It was shown that if the relationship between the BB parameters and the moisture content of the paste is known, it is possible to use parameters specific to each paste element in Equation 2.23 to calculate the anticipated extrusion pressure for that time step.

Both models have limitations. The Rough *et al.* model does not include the effect of the growing static zone and does not estimate the moisture content well close to the die. The Bayfield model, on the other hand, includes terms for the growth of the static zones but doesn't take account of the drying out of the bulk paste and its effect on the Benbow Bridgwater model parameters.

Ceramic paste binders are typically composed of a blend of polymers suspended in water. The binders act to lubricate the particles so that they may flow over one another and to also bind

them together so that the paste flows as though it were an apparently continuous fluid. The rheological characteristics of the binder are very important for it to function properly.

The literature has shown that there are a number of factors, such as binder viscosity, solid matrix permeability, moisture content and ram speed which will affect the rate of dewatering in a ceramic paste. In this work, these variables will be kept constant and the polymer chain length of the binder will be varied and its effect on the rate of phase migration will be measured.

2.7   Drying

The drying stage is a critical step in the monolith production process. Once a defect free monolith has been produced, it must be fully dried before it can be carbonised. Controlled, or forced, drying is placing the sample in a heated chamber and controlling the relative humidity (RH) [54].

Work done by Misra *et al.* [55] on the controlled drying of lead zirconate titanate (PZT) showed that the drying rate could affect the mechanical properties of the ceramic. Drying a sample of material under controlled conditions (50°C and various levels of relative humidity) increased both the density and tensile stress, with higher drying rates being associated with stronger materials.

In the field of honeycomb ceramics, Aranzabal *et al.* [56] investigated the optimisation of several aspects of HZSM5 monolith production, including the drying regime. The authors encountered defects such as those shown in Figure 2.19. It was found that by gradually increasing the heating rate, defect free monoliths could be produced. This was attributed to the slow initial drying ramp causing less migration of the binder phase from the core of the monolith leading to a higher tensile strength a crack resistance.
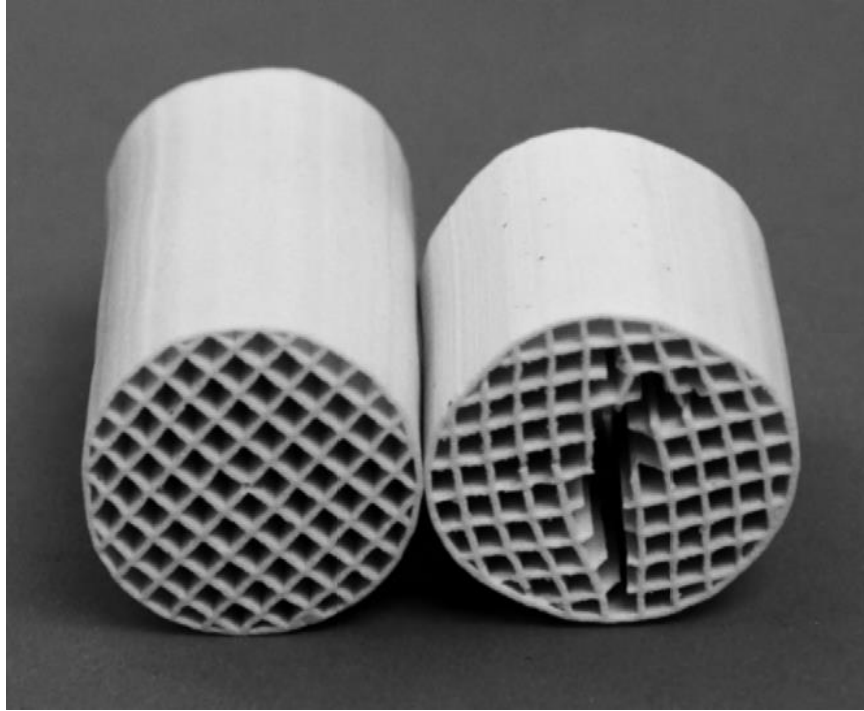
Figure 2.19 - Internal cracks caused during drying.

Some authors have used a 'reaction engineering' approach (REA) to modelling the drying stage of various products [57-59]. Specifically, this is an approach to modelling which shares some similarity with the types of equations typically used when modelling reaction dynamics. Some models are empirical in nature and combine the many different transport routes of the liquid phase out of the solid matrix together in a single effective mass transfer coefficient [57, 60] . Other, more complex, models consider each of these mass transfer mechanisms separately [61].

Sherwood's models on the drying of solids are based on a two-part drying mechanism where drying is rate limited by evaporation at the surface, followed by a rate limited period of diffusion through the solid matrix [62]. Puyate and Lawrence [63] have argued that the model is valid for high and low drying rates, denoted by μ, but not for moderate drying rates.

$$\mu_{dr} = \frac{\text{time for diffusion}}{\text{time for evaporation}}$$ **Equation 2.25**

Puyate and Lawrence did note however that the model for the diffusion limited step, 'falling rate', the equations well represented the drying curve.

All of these approaches have been used to accurately predict moisture content profiles of different materials, showing that REA to the drying stage is a viable route for modelling the drying stage of the monoliths.

2.8   Summary

There is much work been done in the field of the processing of ceramic pastes. There are a variety of approaches to paste modelling, the most well known a widely used of which is the Benbow Bridgwater model. Additionally, there are some paste models which are based on a Herschel-Bulkley approximation of paste flow. The application of the latter models to extrusion through a die is more complex than the Benbow Bridgwater model which was originally applied to that system. While approaches such as the Basterfield model may be applied more widely, this project was concerned with the ram extrusion of pastes through a honeycomb die. For this reason, it was decided that the paste model which was used exclusively in this work is the Benbow Bridgwater model. The methods for determining the model parameters are simple, well established and can be performed on equipment found at MAST Carbon's facilities.

There is enough information in the literature and in industry expertise to design a stable paste that will extrude, but missing from the literature is an explanation for the formation of defects during extrusion which can be directly informed by the paste rheology. Without this, it is not possible to use rheology to design a paste which will produce a high-quality extrudate. While it has been shown that the various paste models are sufficient for predicting pressure drop

during extrusion, outside of this, they are of very little use. It would be extremely valuable if the paste models could be applied to a theory of defect formation in honeycomb extrusion.

There are many tests described in the literature which attempt to predict 'extrudability' in a simple way. From these, only a small fraction of a paste's complex flow behaviour can be measured. None of the results tests have been shown to correlate with the quality of the extrudate using a honeycomb die.

3   METHODS AND MATERIALS

3.1   Paste Preparation

Two z-blade mixers were available during this project with capacities of ~ 250 ml and ~ 2 l.

Ingredients, both dry and wet, were weighed on a Mettler PC 4400 balance individually before being added to the mixer. Pastes were prepared by first blending the dry components for 1 minute to ensure proper distribution before the addition of the liquid components. Once the liquid phase had been added, the paste was allowed to mix for 20 minutes, at which point, mixing was paused. The paste which had become stuck to the walls of the mixer and was not being mixed into the bulk of the paste were removed and returned to the bulk. Mixing then continued for a further 10 minutes before being placed into a marked polyethylene bag and stored overnight in a refrigerator.

3.1.1   Formulation

As the solid particle size distribution and coarse to fine ratio was fixed by MAST (see section 3.3.1), the first step in paste formulation was to determine the correct ratio of solid to liquid. A 'pinch test', a fairly crude but effective method, was used to determine roughly the level of solid to liquid. A known mass of powder was placed on a glass surface and water is added dropwise until the paste can be formed into a self-supporting pyramid. At this point, the water has filled the voids and just begun to form a paste. The stages of the test are shown in Figure 3.1.
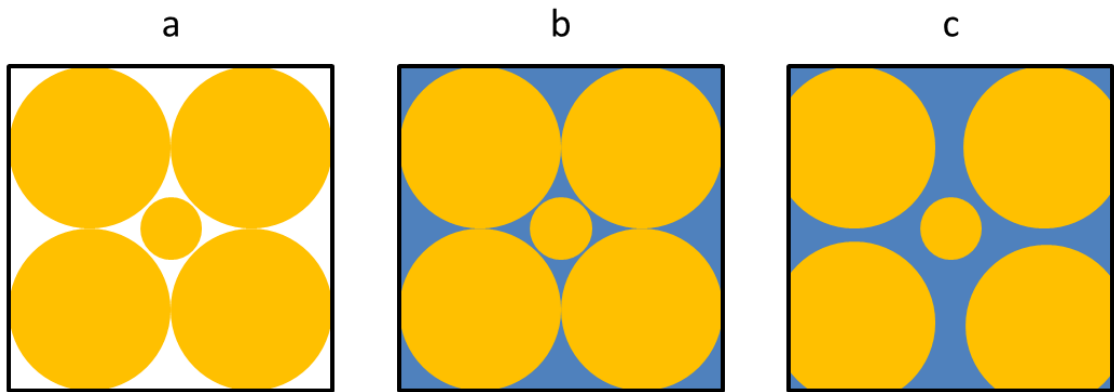
Figure 3.1 - (a) dry powder (b) voids filled with liquid (c) liquid lubricating particles

A paste is then made using a slightly higher liquid content than found using the pinch test, with the exact amount depending on the rheology of the liquid phase, size and shape of the solid phase and the desired stiffness of the paste. The liquid phase is added on a volume basis. The volume of the liquid phase is calculated including the mass of the binders added to the water. It was assumed that the density of the liquid phase is constant.

The concentration of the various binders could then be changed depending on the requirements of the experiment.

3.2 Extrusion

3.2.1 Extrusion Dies

A number of honeycomb extrusion dies were available during this work and are described in Table 3.1. Figures 3.2 and 3.3 show the extrusion dies in more detail.

Table 3.1 - Extrusion die geometry

Die Name	Cells	Washer Diameter	Open Area	Base Diameter	Pin Width	Slot Width
		mm	%	mm	mm	mm
Minilith 2	31	10.5	27.8	50	0.9	0.6
Bath 2	241	27	44.6	70	1.0	0.5
Bath 5	562	42	43.2	100	1.0	0.5
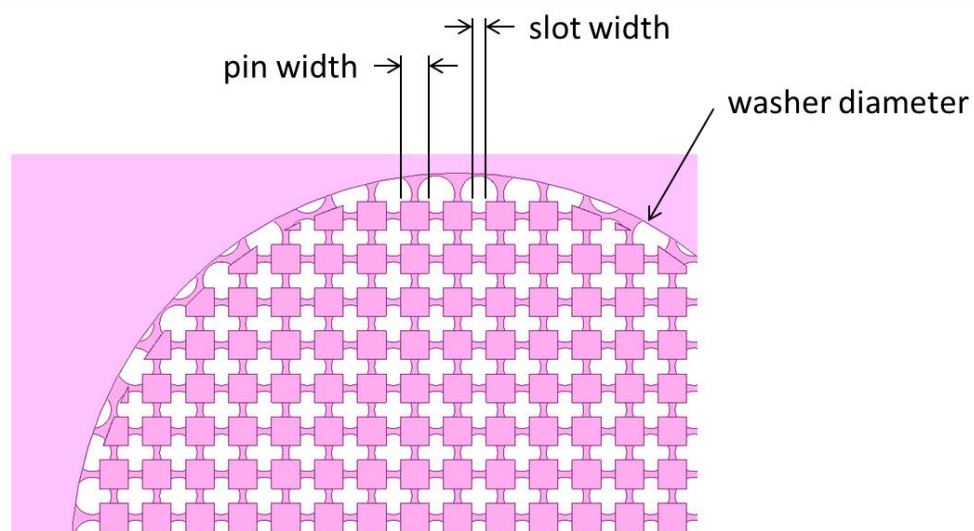
Figure 3.2 - Die dimensions
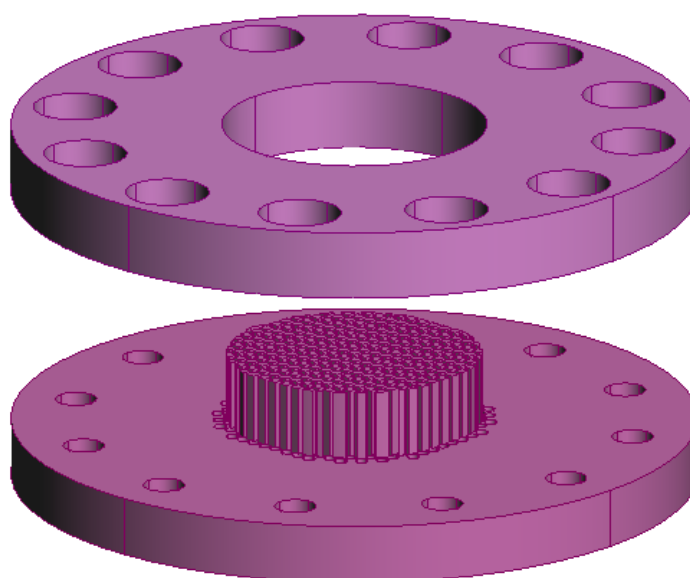
Figure 3.3 - Exploded view of extrusion die

Figure 3.3 shows both parts of the extrusion die. The base features both the round feed holes and the square pins. A separate washer gives the extrudate its round shape. It is removable for both ease of manufacture and to allow the possibility of changing the outer diameter of the extrudate.

3.2.2 Small Scale

Small scale extrusion was carried out using an Intron 4302 screw driven load frame fitted with a 10 kN load cell. The stainless steel barrel had an internal diameter of 35.4 mm. A stainless steel cap was secured over the extrusion die and fixed with four 0.25 inch bolts. Figure 3.4 shows the assembly. Gaps between components are exaggerated for clarity.
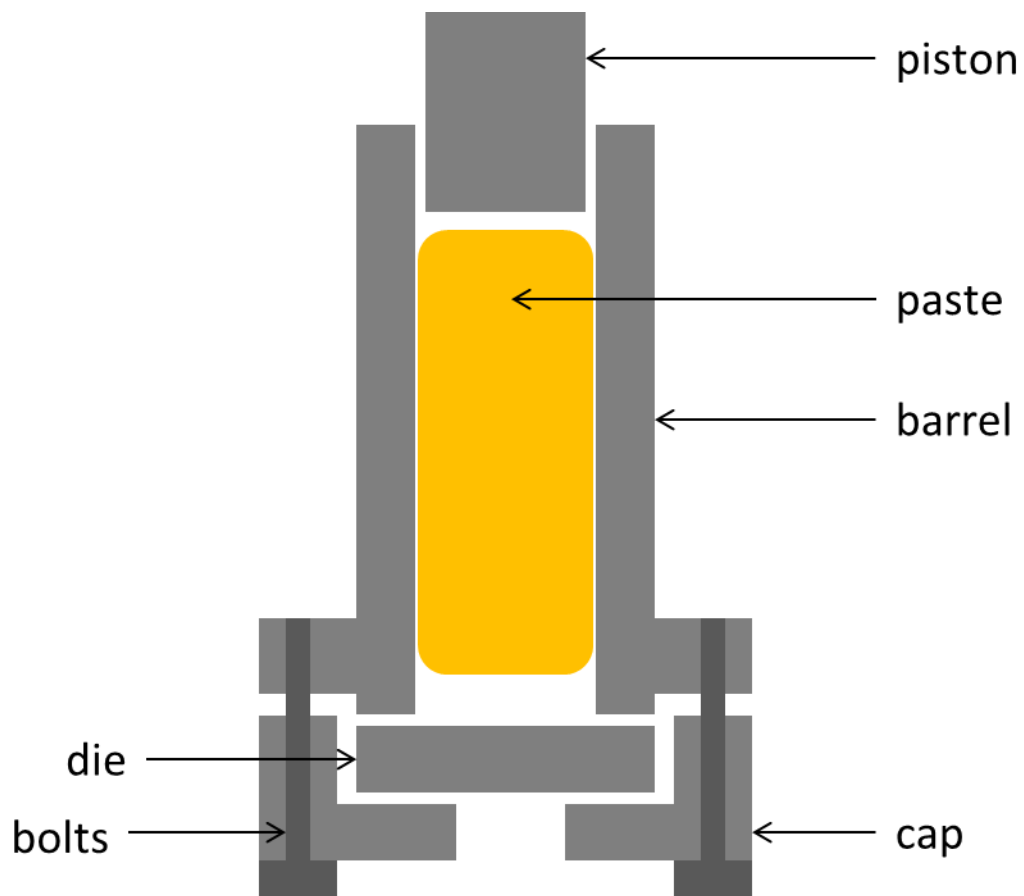
Figure 3.4 - Extrusion barrel assembly

The paste was loaded into the barrel and compacted with a wooden dowel before the piston was inserted. The barrel assembly was then placed on a stand in the load frame and the load cell is lowered into place. The load frame was then slowly lowered until the paste began to compact, indicated by a slight rise in the load, then retracted clear of the piston. The load reading was then set to zero. The extrusion setup is shown in Figure 3.5.
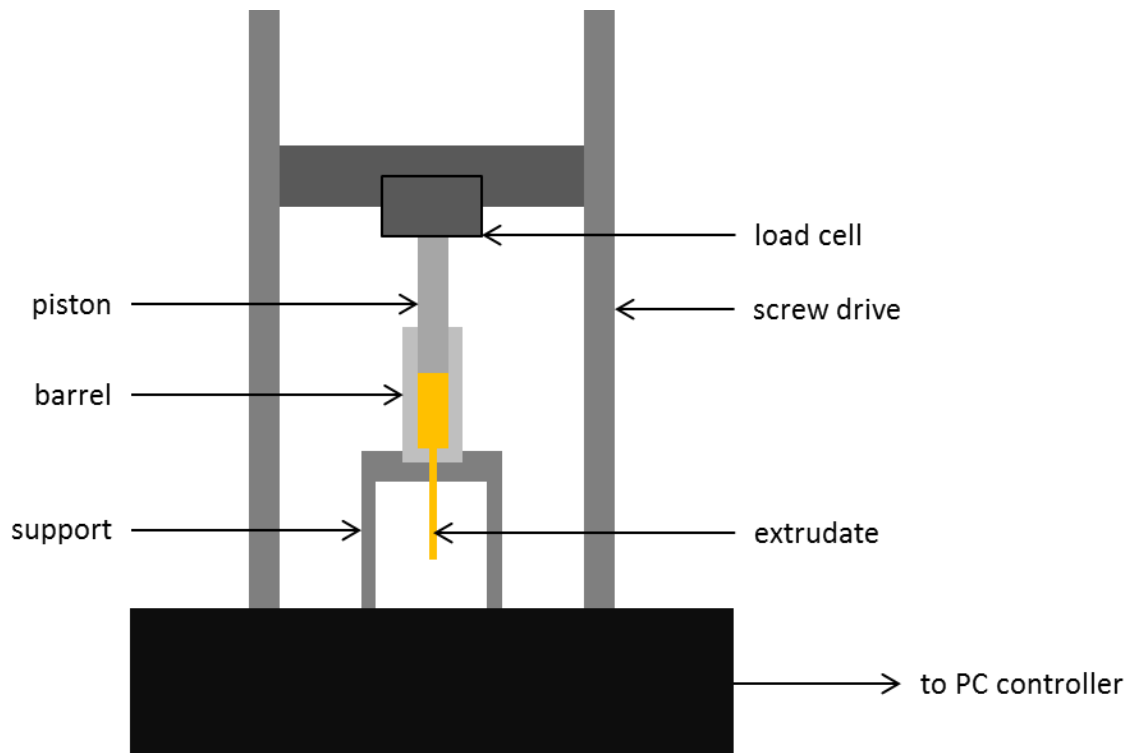
Figure 3.5 - Small scale extrusion equipment

The load frame was connected to a PC which was able to control the speed of extrusion and record extension and load data. Data was stored as a comma separated variable (.csv) file and analysed in Microsoft Excel.

3.2.3 Large Scale Extrusion

A large-scale hydraulic ram extruder, the 'Sulby' (shown in Figure 3.6) was used to extrude monoliths of ~ 40 mm in diameter. The barrel was positioned vertically to load paste. The extruder then rotated into a horizontal position before the ram was moved forwards into the

barrel. Once sealed, an integral vacuum pump evacuated the barrel to remove pockets of air from the paste. The paste was then compacted against a removable bung and the extrusion die fixed to the front of the extruder. An air slide received the extrudate and delivered the monoliths directly onto a rolling table.
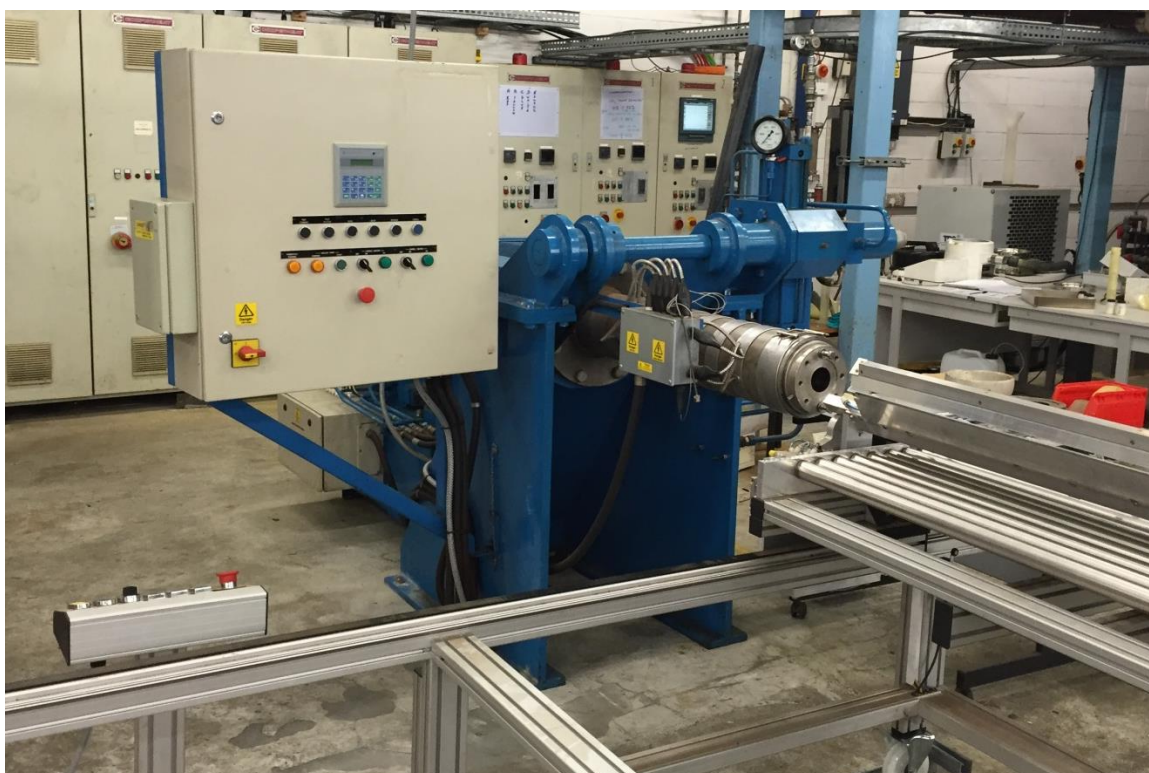
Figure 3.6 - 'Sulby' extruder in the horizontal position. The control panel is visible on the left. The air slide and roller table are visible on the bottom right.

The piston was controlled by ram speed rather than pressure. A ram speed of 20 mm/s was typically used. The pressure of the ram is displayed on the control panel but could not be recorded digitally.

3.2.4 Rheological Testing

The various extrusion additives described in this work were tested on an AR500 rheometer. The required mass of binder was weighed into a glass beaker to a precision of 0.0001 g, then distilled water was added on a mass basis to the same precision. The binders were then

worked with a spatula to mostly dissolve the solid phase. The glass beaker was then sealed with plastic wrap and left overnight to allow the binder to fully dissolve.

Prior to testing, the binder solutions were mixed with a spatula to ensure proper distribution as it was observed that for some binders, a small degree of separation occurred overnight. Binders were added to the plate of the rheometer using a syringe or a spread with a spatula if the binder was too stiff. In some cases, small air bubbles were noted inside the fluid. These could not be removed either by applying a vacuum or vibrating the sample. Bubbles could, however, be removed by lowering the top plate or cone of the rheometer. The instrument layout is shown in Figure 3.7
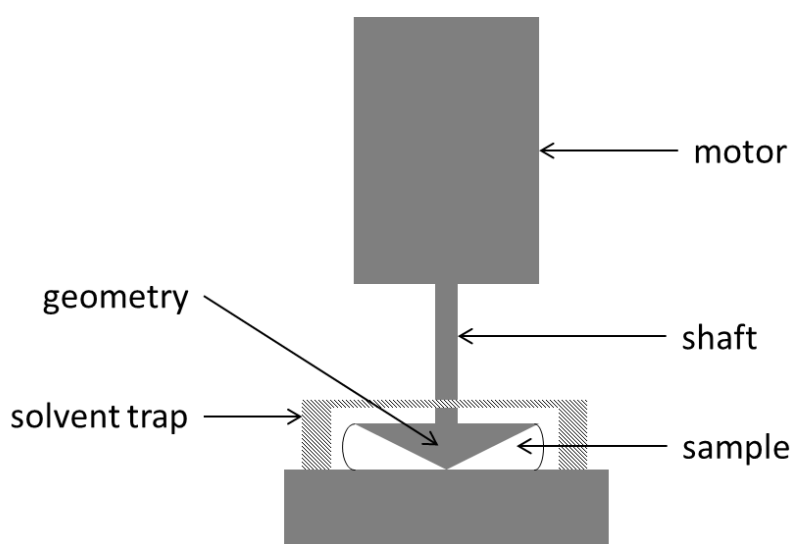
Figure 3.7 - Rheometer layout

The rheometer plate was lowered into position and excess binder was removed with a spatula and a plastic cover (solvent trap) was placed over the plates to mitigate evaporation during the test. A 40 mm diameter 2° steel cone was used for most tests. Cone and plate geometry is preferred as it allows the shear rate gradient to be constant over the surface of the cone. A very narrow gap between the tip of the cone and the plate is necessary to reduce the deviation of the shear rate gradient from linear. The literature accompanying the geometry specified a

gap of 40µm. Some of the very high concentration samples could only be tested with a 40 mm flat plate geometry. This is because the cone geometry could not be lowered to the required gap when testing the stiffest samples. Temperature was maintained at 20℃, controlled by chilled water circulation and a Peltier cooler build into the instrument.

Rheometry tests were carried out in triplicate, with the sample being removed and replaced by another sample from the bulk in between tests. In some cases, results from one test did not match the others. In these cases, tests were repeated until visual repeatability was achieved.

3.3   Materials

3.3.1   Phenolic Resin

Partially cured phenolic resin is used as the carbon precursor in MAST Carbon's products. Pastes are formed from a blend of two powder fractions with a d_{50} of ~ 45 µm and ~ 6 µm. Particle size analysis of both fractions, measured on a HELOS H2290 laser diffraction dry particle size analyser, are shown in Figures 3.8 and 3.9.

A high percentage of fine powder was found to inhibit the release of off gases during carbonisation which led to severe cracking due to a reduction in the permeability of the matrix. A blend of 8% fine powder has been used for many years at MAST to give the best compromise between ease of extrusion and ease of carbonisation.
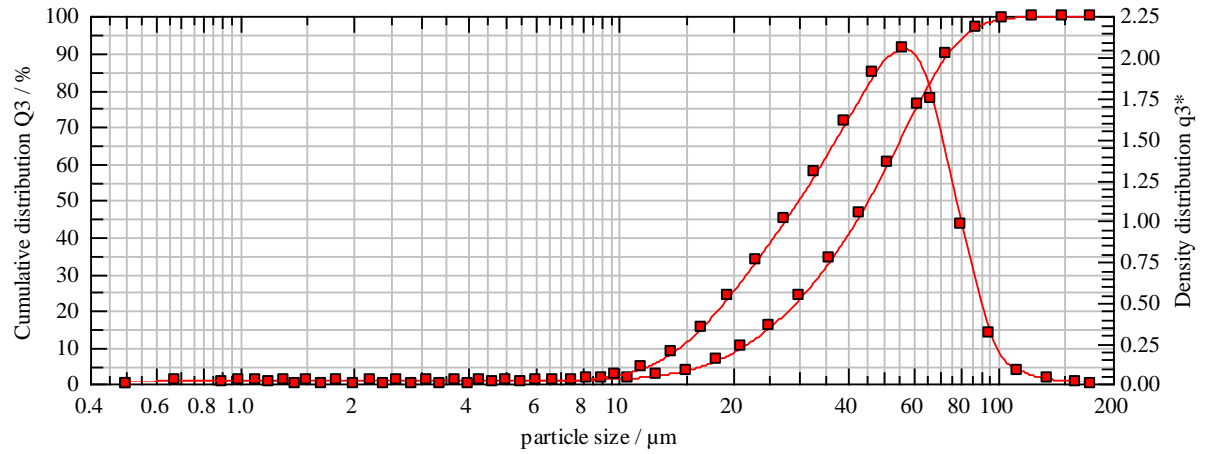
Figure 3.8 - Particle size distribution of coarse particle fraction
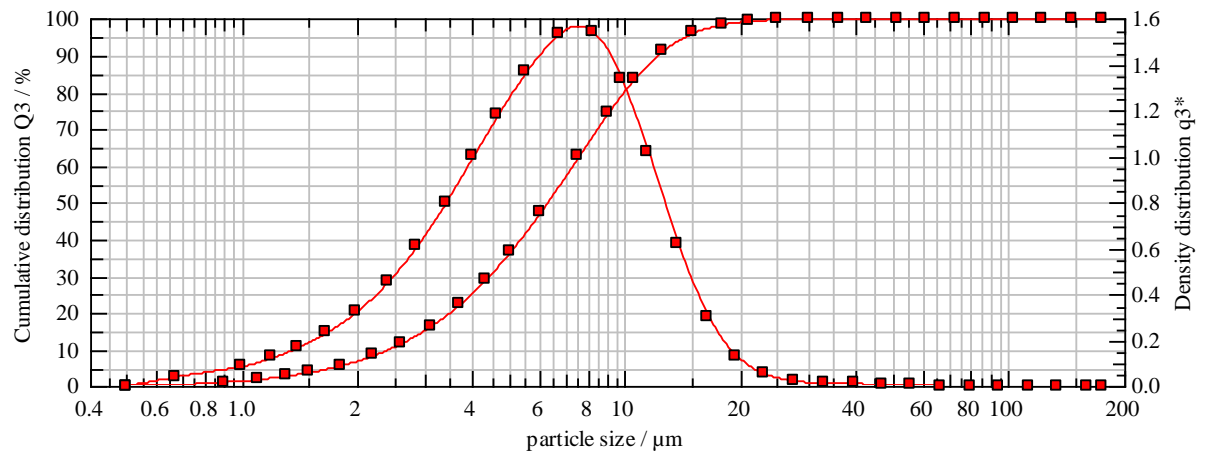
Figure 3.9 - Particle size distribution of fine particle fraction

The particles are quite irregular in shape, as shown in Figure 3.10.
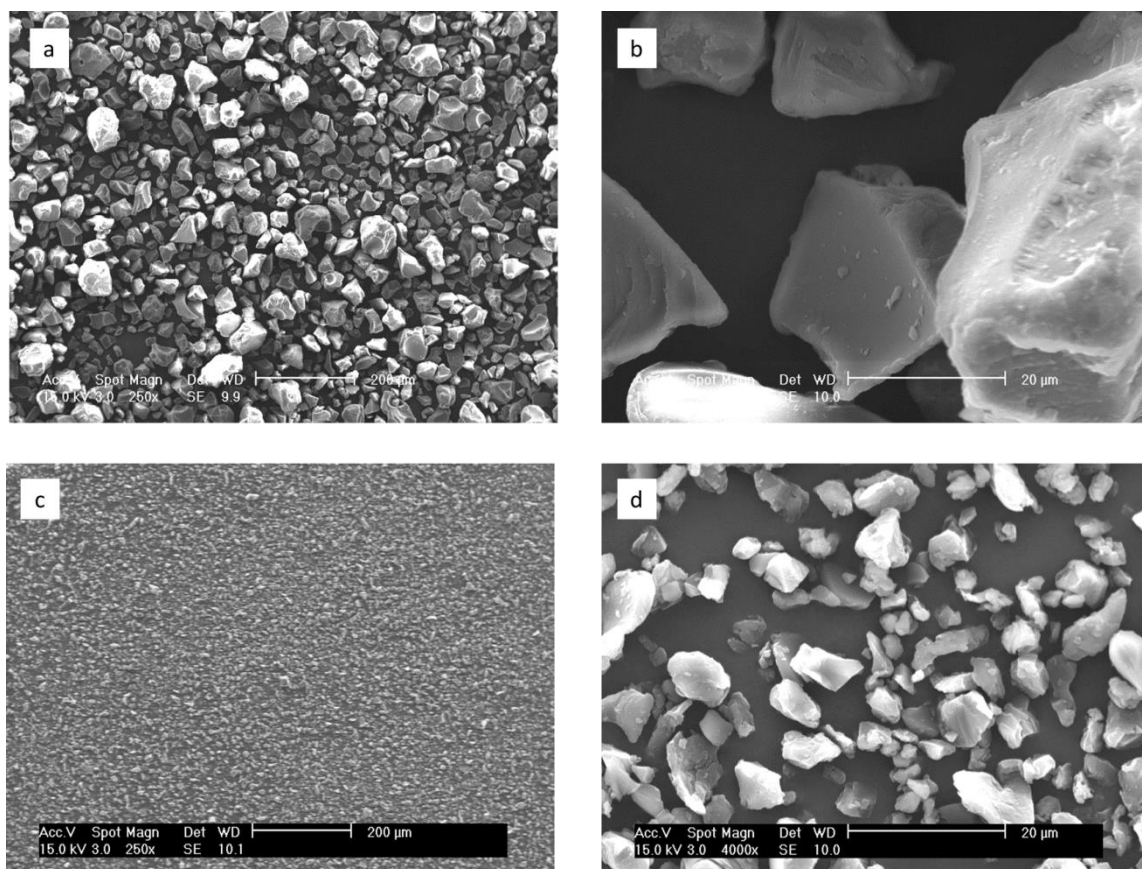
Figure 3.10 - SEM images of phenolic powder. (a) & (b) coarse fraction (c) & (d) fine fraction

3.3.2 Methocel (K15M)

Hydroxypropylmethyl Cellulose (HPMC) has been used as the main component of the extrusion formulation at MAST for many years. HPMC comes in many different grades, characterised by different molecular masses and ratios of side chain species. The specific grade used by MAST is marketed by Dow Chemicals as K15M Methocel.
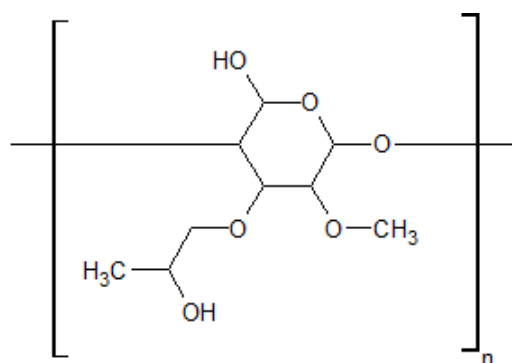
Figure 3.11 - Structure of HPMC

This component is used in the extrusion package as the primary viscosity modifier. K15M forms a strong gel-like structure when dissolved, which may break down when manipulated too much (this is observed as the formation of small balls of material when performing oscillatory rheometry, or a change in paste consistency when mixed for a prolonged period of time). Approximately 20 wt% is used in order to greatly increase the viscosity of the liquid phase and to bind the solid phase together during extrusion. A concentration of less than 10 wt% is more typical for HPMC [64]. At such high concentrations, K15M could be considered to form more a stable network in the liquid phase, rather than a true solution.

3.3.3   Polyethylene Glycol (Oxide)

Polyethylene glycol (PEG), also called Polyethylene Oxide (PEO) depending on molecular mass, is used by MAST to modify the rheology of the paste. PEO is available in a very wide range of molecular masses, 3 of which are used by MAST.
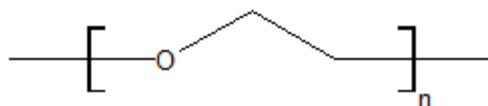
Figure 3.12 - Polyethylene Glycol structure

Each of the molecular masses, (6000 $g.mol^{-1}$ (PEG), 200,000 $g.mol^{-1}$ (PEOL) and 5,000,000 $g.mol^{-1}$ (PEOH)) were added for a specific reason. PEOH was added in order to even out the flow of the paste as it exits the die and to reduce tearing at the walls. PEOL was also added as a viscosity modifier. Over time, it was observed that PEOL seemed to increase the flow rate of the paste at the outer wall. PEG was originally added as a cheaper alternative to PEOH and PEOL. The function of PEG in paste formulation is to encourage the paste to mix properly without the addition of water. I was sometimes added during the mixing stage.

3.3.4 Polyvinyl Alcohol

Polyvinyl Alcohol (PVA), not to be confused with Polyvinyl Acetate, a popular wood glue, is a synthetic polymer additive. It is used in the construction industry as an additive to concrete. It is used to improve cohesion and 'fluidity' as well as drying time [65, 66]. PVA was added to the recipe by MAST in order to make the extrudate less brittle and more "waxy". The specific grade used by MAST is marketed by Nippon Gohsei as GOHSENOL KH17S.
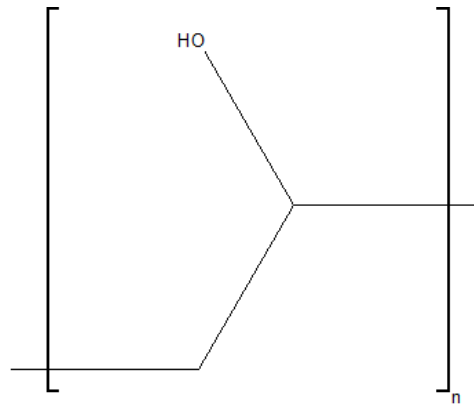
Figure 3.13 - structure of Polyvinyl Acrylate

4 PASTE CHARACTERISATION

4.1 Benbow Bridgwater Model

The various forms of the model proposed by Benbow and Bridgwater and their collaborators have been commonly used to characterise ceramic pastes since their popularisation in the late 1980s.

The two most common forms of the Benbow Bridgwater (BB) model are the so-called 4-parameter and 6-parameter equations, the only difference between them being the inclusion of two exponential terms in the 6-paramter form to account for apparent velocity dependent behaviour of the paste, something akin to the shear thinning properties of power law or Herschel-Bulkley fluids. The geometry of the extrusion process is shown in Figure 4.1.

$$P = 2ln\left(\frac{D_0}{D}\right)(\sigma_0 + \alpha V) + 4\left(\frac{L}{D}\right)(\tau_0 + \beta V) \qquad \textbf{Equation 4.1}$$

$$P = 2ln\left(\frac{D_0}{D}\right)(\sigma_0 + \alpha V^m) + 4\left(\frac{L}{D}\right)(\tau_0 + \beta V^n) \qquad \textbf{Equation 4.2}$$
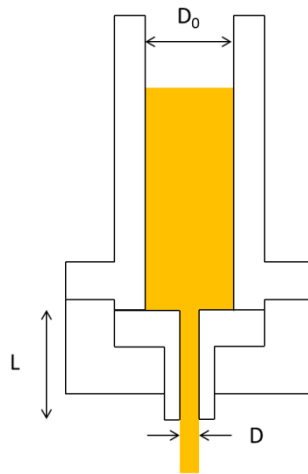
Figure 4.1 - Dimensions of barrel and die

4.2   Particulate Phenolic Resin Paste Characterisation

4.2.1   Experimental Design

The formulation of the paste used in this chapter is given in Table 4.1.

Table 4.1- Paste Formulation

Resin (g)	75.0
Water (g)	41.9
K15M (g)	6.28
PEOH (g)	0.42

Extrusion data was collected using an Instron Load frame fitted with a cylindrical barrel to act as a vertical ram extruder. Pastes were extruded through 3 square ended cylindrical dies of the same diameter, but of different lengths. The dies all had a diameter of 3 mm and lengths of 3, 24 and 48 mm, giving them a length to diameter ratio of 1, 8 and 16 respectively. These dies will be hereafter referred to as short, medium and long respectively.

The extrusion procedure was as follows: the first die (the long die) was fitted to the extrusion barrel and the barrel filled with paste. A ram was inserted into the open end and the paste was tamped down lightly by hand using a wooden dowel slightly narrower than the barrel. Once the barrel was secured to the load frame, the load cell was lowered until it began to move the ram into contact with the paste. At this point, the load cell was backed off slightly until it was no longer in contact with the ram and the load was then set to zero.

At this point, the extrusion procedure began. The ram speed was computer controlled via a LabView interface and followed a pre-set extrusion procedure shown in Table 4.2.

Table 4.2 – Benbow Bridgwater Extrusion Test Program

Ram Speed (mm.min^{-1})	Extension (mm)	Total extension at speed change (mm)
20.0	12.0	0.0
0.5	4.0	12.0
1.0	2.5	16.0
2.5	2.5	18.5
5.0	2.5	21.0
7.5	2.5	23.5
10.0	2.5	26.0
15.0	2.5	28.5
20.0	2.5	31.0

The initial extrusion step of 20 mm.min^{-1} proceeds for 12 mm of ram travel in order to compact the paste and allow extrusion to begin and reach a stable pressure. The ram speed decreased to 0.5 mm.min^{-1} for an extension of 4 mm of ram travel and then increased as shown in Table 4.2 every 2.5 mm of ram extension. It was observed that at the lowest ram speed (0.5 mm.min^{-1}) it took longer for the extrusion pressure to stabilise, so this stage was extended to 4 mm of ram travel.

Once the program had completed, the load cell was backed off to the initial gauge length and the barrel was removed from the load frame. The extrudate was discarded. Paste remained in the barrel while the die was changed over to the medium die. The load cell was reset, re-zeroed and the extrusion procedure was begun. The process was repeated for the short die.

The barrel was not refilled with fresh paste between extrusions through the long, medium and short dies. If batches of dough were prepared separately for each of the dies, variations in

procedure at any point could lead to differences in the properties of the paste. By preparing enough paste in one batch to extrude through all three dies immediately after one another, this concern is eliminated.

If phase migration was present, however, the paste in the barrel would steadily lose moisture, during extrusion, seriously affecting the results. All three extrusions through different dies would effectively be performed on a different paste. However, phase migration would manifest itself as a constant increase extrusion pressure at a constant ram speed, which was not observed in any of the extrusions performed for this work.

Data was sampled at a rate of 0.7 Hz and exported by the LabView interface to a data file which could be read in Microsoft Excel. A typical example of the raw extrusion profile data is shown in Figure 4.2, showing the results of an extrusion using the long die. An Excel program was developed using a combination of built-in formulas and custom macros written in Visual Basic which identifies regions of stable extrusion and reports the average ram speed and extrusion load.
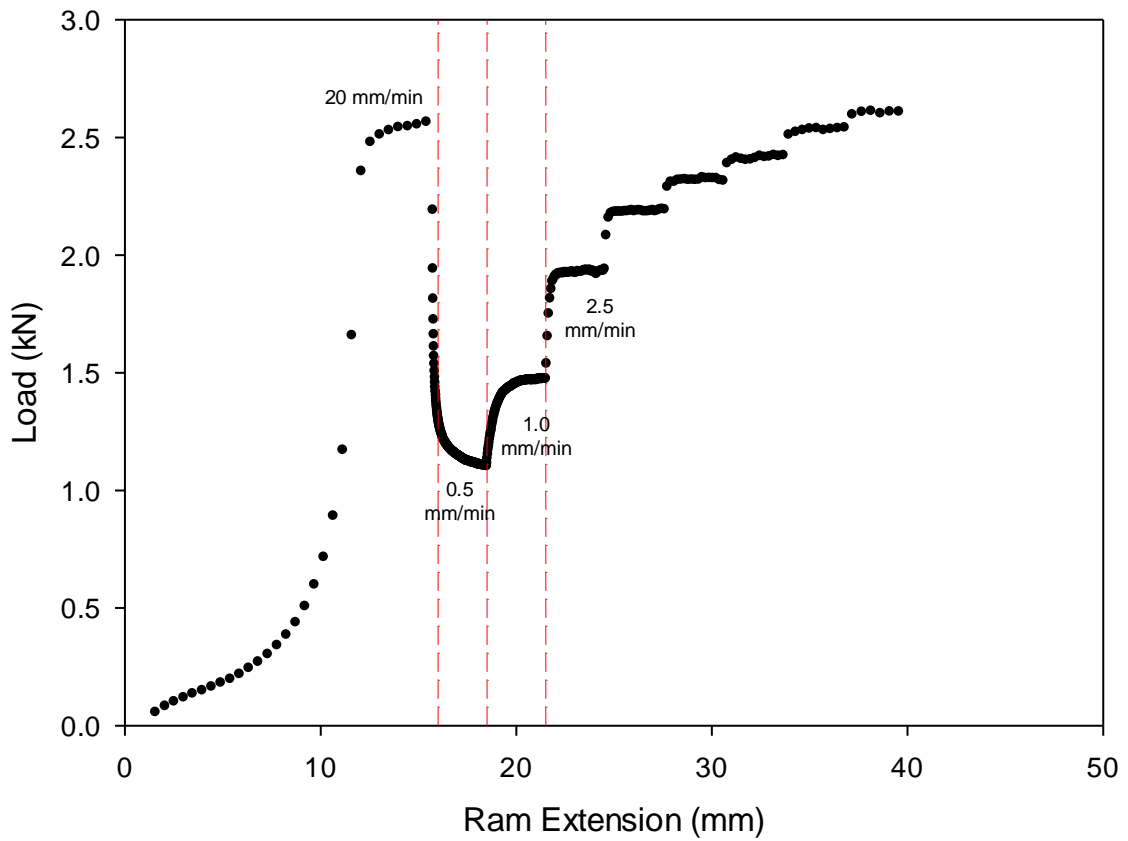
Figure 4.2 - an example of a raw extrusion profile. Note the clear step changes in extrusion load. Red vertical lines mark the initial 3 increases in extrusion speed.

The selection of the range of speeds is very important. The experimental range must include all conditions under which the paste is expected to operate and large enough to show any effects from velocity dependence.
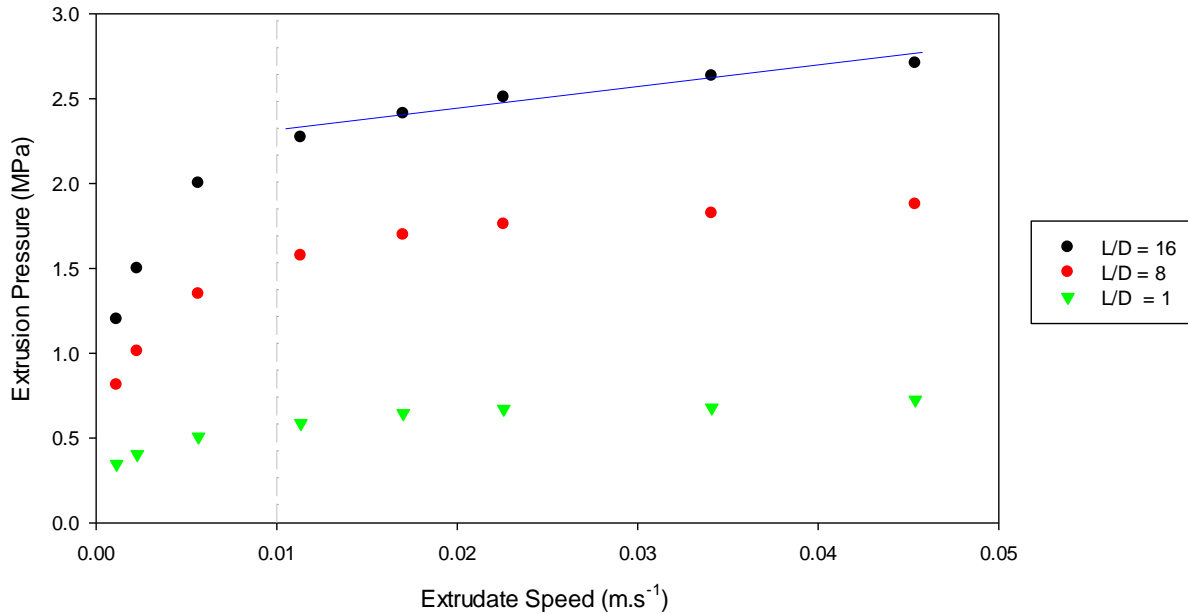
Figure 4.3 – extrusion pressure with respect to ram speed at various die length ratios. The blue reference line shows where the region where the results could be considered linear

In Figure 4.3, the non-linearity of the flow of this paste is evident. Above an extrudate speed of around 0.01 m/s the relationship between pressure and speed appears to be approximately linear, illustrated by the solid line in Figure 4.3. At lower extrudate speeds, however, the non-linear response of extrusion pressure to ram speed is in evidence. This non-linear behaviour was caused by the liquid phase forming a non-newtonian slip layer at the wall and potentially the orientation of the particles of the solid phase as ram speed increases. It was initially thought that the non-linear relationship below 0.01 m/s was an artefact caused by the domination of yield stresses or due to the paste taking longer to equilibrate at low ram speeds. Repeated extrusions using the same procedure showed that this was not the case and the paste indeed exhibits non-linearity. Figure 4.3 suggests that the most appropriate form of the BB model is the 6 parameter equation, including both yield stress terms (σ_0 and τ_0) and the two exponents (m and n).

The following sections, fitting various forms of the BB equation will all be performed on a single data set for consistency. This dataset is representative of all pastes used for this work. The discussion in this chapter is specific to this dataset, but may be applied generally to all pastes used in this work except where otherwise stated.

4.2.2 Full 6 Parameter Model Parameter Estimation

The 6 parameter BB model was initially fitted to the data shown in Figure 4.3 using the Dynamic Curve Fitting feature of SigmaPlot. This feature performs non-linear regression on the data set an arbitrary number of times (the default number of convergences is 200) and then selects the parameters which best fit the data, based on a suite of statistical results. Figure 4.4 shows the code used to define the 6 parameter form of the BB model. The ratio of die to barrel diameter, $\frac{D_0}{D}$, in for this geometry is $11.\dot{6}$.

```
Equation

f= 2*(sigma+alpha*V^m)*ln(11.66666667)+4*(tau+beta*V^n)*LD

fit f to P

Constraints

sigma>0          alpha > 0          0 < m <= 1

tau>0            beta > 0           0 < n <= 1
```
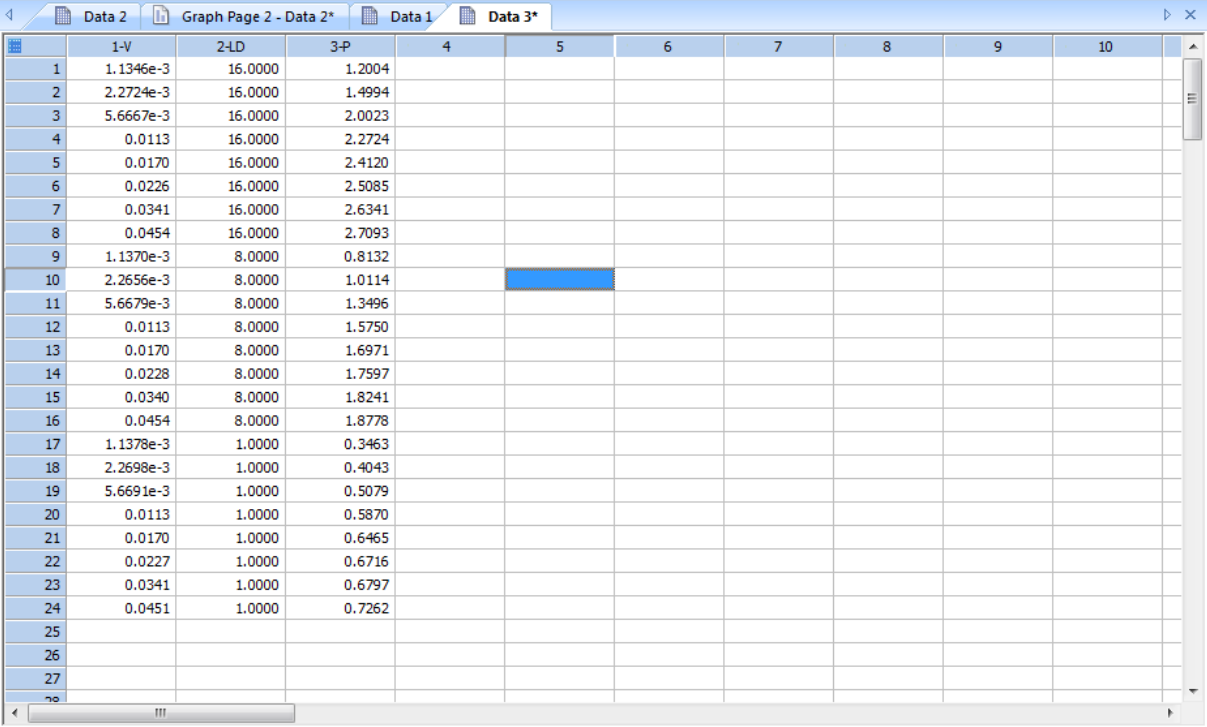
Figure 4.4 - SigmaPlot code for 6 parameter form of BB model

The extrusion data is entered into SigmaPlot in three columns, extrudate velocity, aspect ratio of die and extrusion pressure. Three variables (highlighted in red) in Figure 4.5, V, LD and P

(extrudate velocity, length to diameter ratio and extrusion pressure respectively) are drawn from columns in the spreadsheet in SigmaPlot, shown in Figure 4.5. SigmaPlot requires that the user defines an equation in terms of 'f'. SigmaPlot will then attempt to fit 'f' to the values of another column specified by the user.

	1-V	2-LD	3-P	4	5	6	7	8	9	10
1	1.1346e-3	16.0000	1.2004							
2	2.2724e-3	16.0000	1.4994							
3	5.6667e-3	16.0000	2.0023							
4	0.0113	16.0000	2.2724							
5	0.0170	16.0000	2.4120							
6	0.0226	16.0000	2.5085							
7	0.0341	16.0000	2.6341							
8	0.0454	16.0000	2.7093							
9	1.1370e-3	8.0000	0.8132							
10	2.2656e-3	8.0000	1.0114							
11	5.6679e-3	8.0000	1.3496							
12	0.0113	8.0000	1.5750							
13	0.0170	8.0000	1.6971							
14	0.0228	8.0000	1.7597							
15	0.0340	8.0000	1.8241							
16	0.0454	8.0000	1.8778							
17	1.1378e-3	1.0000	0.3463							
18	2.2698e-3	1.0000	0.4043							
19	5.6691e-3	1.0000	0.5079							
20	0.0113	1.0000	0.5870							
21	0.0170	1.0000	0.6465							
22	0.0227	1.0000	0.6716							
23	0.0341	1.0000	0.6797							
24	0.0451	1.0000	0.7262							
25										
26										
27										

Figure 4.5 - SigmaPlot spreadsheet containing extrusion data

Results for the initial estimation run for this example dataset are shown in Table 4.3. The R-squared for this solution is 0.9759. The results are shown in the table below and the fitted curve shown in Figure 4.6.

Table 4.3 - Initial SigmaPlot convergence results for 6 parameter BB model

Parameter	Result	t-score	95% Confidence Interval
σ_0 (MPa)	8.81×10^{-18}	2.360×10^{-17}	0.731
τ_0 (MPa)	5.79×10^{-19}	1.300×10^{-17}	0.087
α (MPa.s.m^{-1})	0.265	2.365	0.220
β (MPa.s.m^{-1})	0.064	4.771	0.026
m (dimensionless)	0.202	0.268	1.473
n (dimensionless)	0.201	0.548	0.718

The results for σ and τ are very small indeed. It may be assumed that the fitting algorithm has attempted to reduce the values as far as possible given the constraints in Figure 4.4. This is discussed in more detail below.
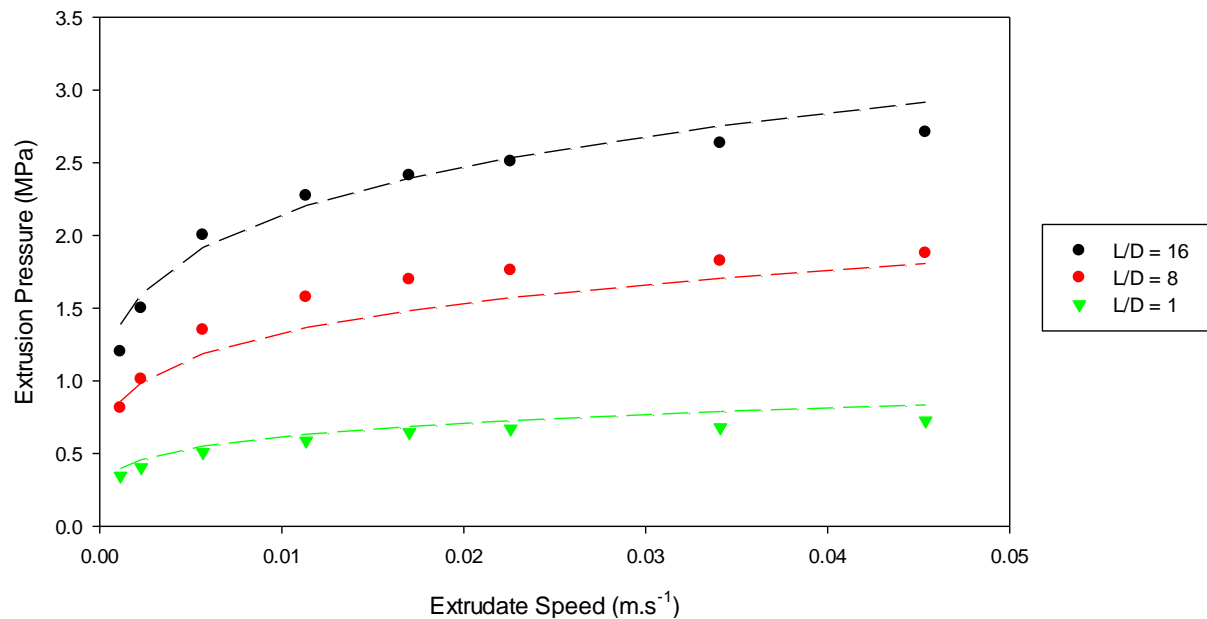
Figure 4.6 – Initial solution of 6 Parameter BB model

Although this solution has a high value of R squared and a visual assessment of Figure 4.6, shows the fit of the model as being reasonably good, there are a number of other methods for evaluating the suitability of this model and the initial solution for this dataset.

Table 4.4 - Covariance matrix for 6 Parameter BB model solution

	σ	τ	α	β	m	n
σ	0.1394					
τ	-0.0134	0.0020				
α	-0.0226	0.0022	0.0126			
β	0.0023	-0.0003	-0.0012	0.0002		
m	0.2789	-0.0269	-0.0375	0.0038	0.5651	
n	-0.1097	0.0162	0.0147	-0.0023	-0.2223	0.1344

SigmaPlot performs, by default, 200 unique non-linear regressions to solve for the given dataset. The software performs statistical analysis on the 200 sets of solutions allowing one to determine whether the equation is fit for the system being described. One of these analyses is the covariance matrix. Sigma plot looks for a pattern in the way pairs of parameters vary. A highly bound (or coupled) pair of parameters will have a covariance close to 1. This implies that as one parameter in the pair increases, the other will also increase. If this is the case, it may be possible for the system to be described using only one of these parameters. Parameters may also be inversely bound, i.e. as one increases, the other decreases. This would result in a covariance value close to -1. A very low or zero covariance suggests a pair of parameters which are unrelated and are both necessary to describe the system.

For the BB equation to be really useful characterising a paste, it is very important that each of the parameters be unrelated. This would mean that each parameter describes a different aspect of the paste rheology or response to the extrusion geometry.

Table 4.4 shows that all of the parameters are uncoupled. Each of the parameters has a very low covariance value. These results suggest that the 6 parameter form of the BB equation is fit for use in describing this paste undergoing ram extrusion.

The covariance matrix in Table 4.4 also includes a variance value for each parameter. The diagonal entries in the matrix are simply the variances of the parameters, i.e. a measure of how the parameter varied during the 200 non-linear regressions.

The third column in Table 4.3 shows the t-statistics (or t-values) for the 6 parameters. The t-score is defined as the ratio of the calculated value of the parameter to the estimated standard error. The standard error of a quantity is simply the standard deviation of the sample size of a quantity, in this case, the sample of calculated values for each coefficient produced during the 200 iterations.

$$\text{t-statistic} = \frac{\text{value of coefficient}}{\text{standard error of coefficient}}$$

Equation 4.3

These scores give the modeller an indication as to whether a parameter is statistically significant or otherwise necessary to include in the model. Large t-statistics, i.e. a parameter which is itself large compared to the error, are likely to be important to the model whereas coefficients with a low t-statistic are likely to be unrequired for the model, i.e. zero. A 'critical' t-value is used as a benchmark for determining significance and may be found from published tables using the degrees of freedom of the data set and the desired confidence level.

For this dataset, the degrees of freedom, df, is 18 (24 observations – 6 parameters in model). To ensure a 95% confidence level given 18 degrees of freedom, the critical t-value, t_{crit}, is 2.101. Parameters with a t-score below the critical value may be unnecessary to include in the model and their removal could lead to a better description of the system.

The t-statistics (or t-values) reported in t-values in Table 4.3 for the parameters σ, τ, m and n suggest that the 6 parameter form of the BB model is not applicable for this system. The t-values for m and n are well below the necessary value of t_{crit} for statistical significance. The t-values of σ and τ, the yield stress terms, are almost zero. Correspondingly, the 95% confidence intervals are largest for these 4 parameters.

It should be noted that the yield stress values of σ and τ are very small indeed. This is the reason for the very low t-statistics for these two parameters. It appears that the algorithm attempted to reduce the yield stress as close to zero as possible without violating the constraints in Figure 4.4. This is unexpected. It is widely considered that ceramic pastes require a minimum stress before motion can occur and it would be expected that phenolic resin pastes would behave in much the same way. It is important that all of the parameters in the model have physically meaningful values. If these parameters are to be included in the model, they must have non-zero values of significance.

These results lead one to the conclusion that while the model as it stands does produce a curve which well approximates the experimental data, it is not wholly mathematically robust; the weakness of the model likely being the inclusion of the yield stresses (sigma and tau) and the exponential terms (m and n). The next step to improve the robustness of the model is to perform one of the following actions:

- The first option is to leave the solution as it is. This course of action is clearly unacceptable as the 95% confidence intervals of the parameters are so large. It is clear that one or more of the parameters must be removed from this model or another paste characterisation method should be sought.

- To declare a true null yield stress for this system. It is a commonly held belief among the rheological community that there is a stress required to initiate motion and that particulate pastes in particular behave this way. If this step is to be taken forward, it is important that the statistical relevance of the parameters is very high in order to justify a departure from the commonly held notion of a yield stress.

- The next alternative is to remove the exponential terms from the model, reducing the 6 parameter model to the original 4 parameter solution proposed by Benbow and Bridgwater. This action would an effectively ignore the presence of shear thinning in this paste, which is clearly indicated by the shape of the curve of the extrusion profile shown in Figure 4.3.

- The final alternative is a combination of the above. It may not be necessary to remove both exponential or yield terms. If the above options fail to result in a model which adequately describes the system, then a combination of yield stress and exponential terms will be tried.

- If no form of the BB model can be found which describes the pastes in this work then another method of paste characterisation must be found.

4.2.3 Removal of Exponential Terms

First, the exponential terms, *m,* and *n*, have been removed from the model. The reason for this is that this 4-parameter form of the BB equation was the original form in which it was

proposed. Also, there is the general feeling amongst the ceramic extrusion community that yield stresses are an important paste characteristic.

The modified code is shown below in Figure 4.7. The solution is shown here in Figure 4.8. The R-squared value is still high at 0.9183, but as can be seen, the straight lines do not well describe the data set particularly at die to length ratios of 8 and 16.

```
Equation

f= 2*(sigma+alpha*V)*ln(11.66666667)+4*(tau+beta*V)*LD

fit f to P

Constraints

sigma>0          alpha > 0

tau>0            beta > 0
```

Figure 4.7 - SigmaPlot code for linear form of BB model
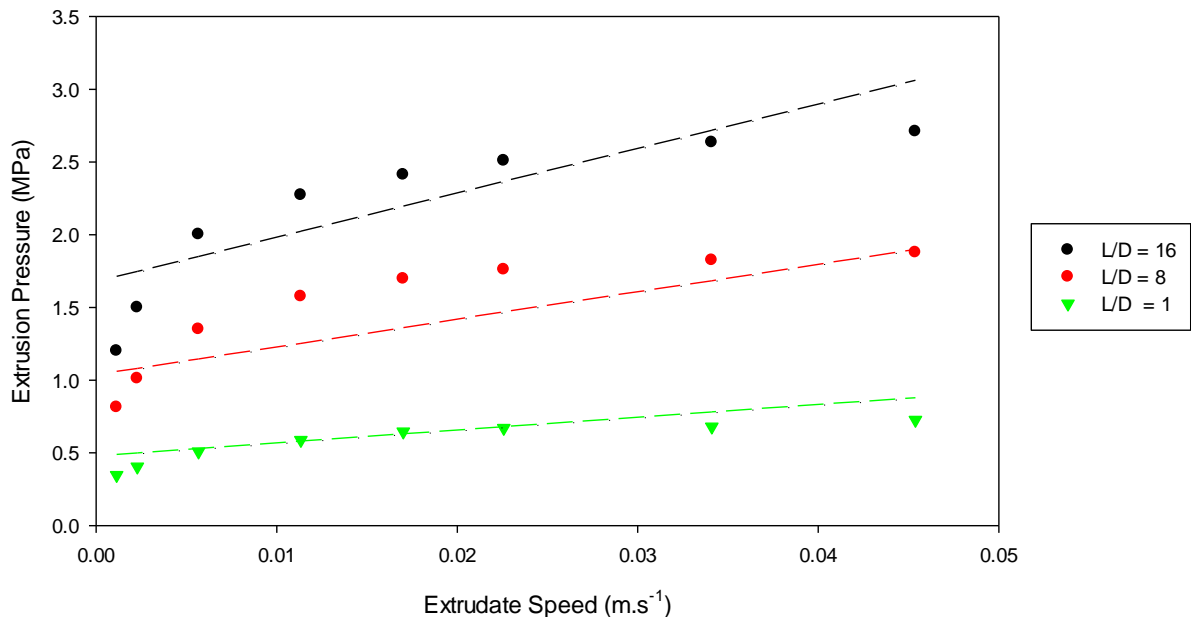
Figure 4.8 - Linear BB model solution

The report generated by SigmaPlot is shown in Tables 4.5 and 4.6. All of the parameters but α have t-values above the critical value, 2.086 (20 degrees of freedom at 95% confidence level). The t-statistic for α is, unsurprisingly given the size of the confidence interval, very low indeed. Confidence intervals for σ, τ and β are smaller but comparable to the values of the parameters.

Table 4.5 - SigmaPlot results for linear BB model solution

Parameter	Parameter	Result	t	95% Confidence Interval
σ_0 (MPa)	σ	0.081	3.200	0.050
τ_0 (MPa)	τ	0.020	6.627	0.006
α (MPa.s.m^{-1})	α	1.518	1.364	2.181
β (MPa.s.m^{-1})	β	0.360	2.726	0.259

The covariance matrix shown in Table 4.6 indicates that there is no cross correlation between the parameters. It should be noted that the only parameter which has a correlation value of 1 is α. This means that the value of α did not change during any of the 200 iterations. This is perhaps because the non-linear regression algorithm achieved a much better fit by manipulating the other variables. This, coupled with the very large confidence intervals, suggest that this variable is also unnecessary to include in the model.

Table 4.6 - Covariance matrix for solution to linear BB model

	σ	τ	α	β
σ	0.0010			
τ	0.0000	0.0000		
α	-0.0220	0.0020	1.0000	
β	0.0020	0.0000	-0.1190	0.0170

The removal of the exponential terms from the BB model has had mixed results. The model appears to be more mathematically rigorous than the full 6 parameter model, with only one parameter with a failing t-value. The R-squared value is high enough to inspire confidence in the result, however, it is paramount that the model is a reasonable reflection of the data, i.e. that the model be true to real life. Figure 4.8 clearly shows that the relationship between extrusion speed and pressure is non-linear.

Either the data points which do not fit the model are invalid or a linearized form of the BB model is not appropriate. Figure 4.2 shows the raw extrusion profile from which the data shown in subsequent plots was taken. Each of the extrusion stages was allowed to reach equilibrium and there was no observable difference in the mode of extrusion. If this region was dominated by yield stress effects, causing the extrusion pressure deviate from the linear

relationship, one might expect to see the 'stop-start' behaviour typical of yield stress dominated motion. This was not the case. Every indication is that the points below 0.01 m/s in Figure 4.8 are valid data points and should be well described by the model.

The next sensible course of action is applying a 4 parameter form of the BB model to the data, including exponential terms but with no yield stress terms.

4.2.4 BB model without yield stress

The SigmaPlot code was again modified to remove the yield stress. The solution given by the non-linear regression algorithm has an R-squared value of 0.9759. The solution is plotted over the data and given in Figure 4.8. The statistical reports are shown in Table 4.7 and Table 4.8.
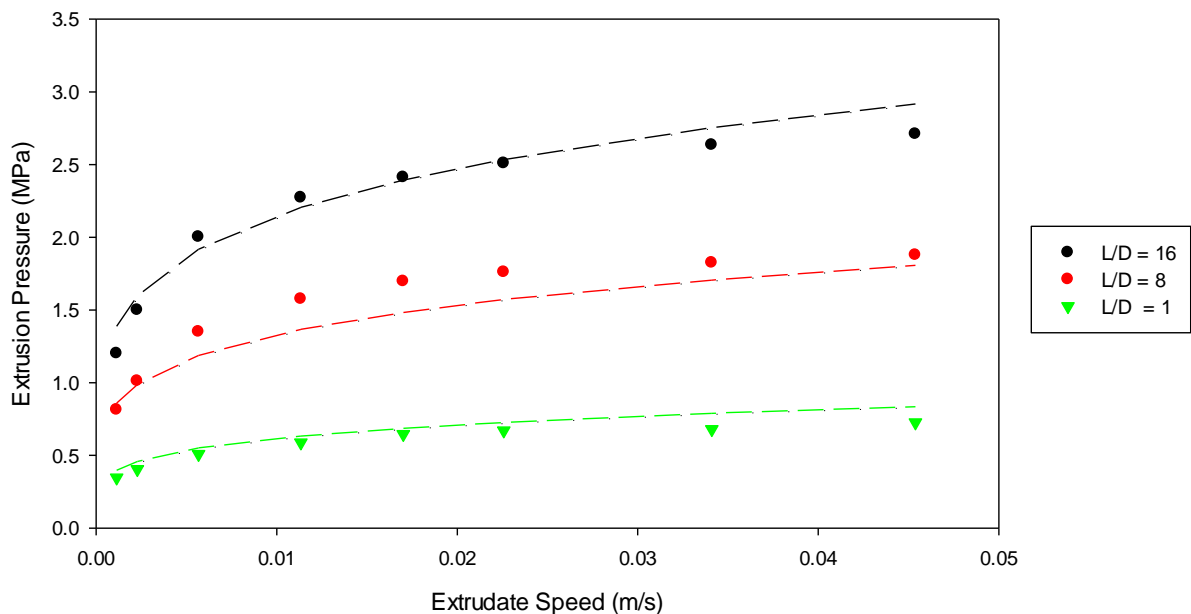
Figure 4.9- Solution for 4 parameter non-linear BB model

The critical t-value for this scenario is the same as for the linearized form of the BB model, 2.086. All of the parameters satisfy the t-test, which suggests that all 4 parameters are required for this form of the model. The 95% confidence intervals are all smaller than the

value of the parameter, but they are still quite large. The covariance matrix, shown in Table 4.8, indicates that all of the parameters are completely uncoupled. It is important to remember that this must be the case if the parameters are to be analysed individually.

Table 4.7 - Convergence results for 4 parameter non-linear BB model

Parameter	Result	t	95% Confidence Interval
α (MPa.s.m^{-1})	0.2656	2.9608	0.176
β (MPa.s.m^{-1})	0.0646	6.0850	0.021
m (dimensionless)	0.2020	2.5227	0.157
n (dimensionless)	0.2012	5.1666	0.076

Table 4.8 - Covariance matrix for 4 parameter non-linear BB model

	α	β	m	n
α	0.0080			
β	-0.0008	0.0001		
m	0.0070	-0.0007	0.0064	
n	-0.0027	0.0004	-0.0025	0.0015

This form of the model satisfies all 3 of the statistical tests heretofore applied (R-squared, t-score and covariance), suggesting that the model is mathematically valid. Whether the model is constitutive, i.e. whether the parameters have a physical meaning is less certain.

4.3 Discussion

The BB model is semi-empirical, meaning that it was not derived from first principles but was developed with consideration of the physical processes taking place. This is an acceptable compromise (particularly for the purposes of this work) as paste processing is a very complex

system and would require an enormous amount of computing power to model from first principles.

The BB model parameters have only an indirect connection to physical quantities. If the phenolic pastes do have a very low yield stress in truth and either the model or fitting technique is not sophisticated enough to account for them, the removal of these terms from the equation is problematic only inasmuch as it affects the values of the other parameters. That is to say, the value of m or α may increase slightly to compensate for the zero yield stress. The inclusion of the 95% confidence intervals will be sufficient to account for this. The utility of the model is, therefore, unaffected. This form of the model well describes the data collected, much better than the linear form of the model.

In light of the arguments made above, this last form of the BB model is the only one which is statistically robust while also accurately accounting for the non-linear relationship between extrusion speed and pressure. Pastes of this type are best modelled using a novel form of the BB model which includes exponential terms but does not include a yield stress term.

Removing the yield stress term form a paste model is a very unusual step. It is commonly held that pastes require a minimum load before they will start to move. Indeed, authors who have used very low ram speeds (0.2 mm.min^{-1}) [67, 68] have found that even at very low flow rates, pastes appear to exhibit a yield stress. It appears as though particulate phenolic resin pastes, at least, to do not exhibit this behaviour. Rather, motion will occur at any load but the extreme non-linearity of the extrusion profile means that at very small loads, the speed of extrusion is so low that it appears to be stationary. This behaviour would manifest itself when handled by an operator as a yield stress, where in reality there is none. To confirm this as the case would require further investigation, which is beyond the scope of this project. For the aims of this work, it is enough to satisfactorily describe the rheology of the paste through the

conditions that are likely to be present during processing. It is highly recommended that further work is done to establish whether phenolic resin pastes truly do not exhibit a yield stress.

It should be stressed again at this point that the 4 parameter non-linear form of the BB model found that all 4 parameters are uncoupled. These parameters, therefore, each describe a different aspect of the paste rheology and relationships between these parameters and extrusion phenomena may be considered independently of one another.

5   PASTE FORMULATION

In this chapter, an attempt is made to understand the causes of defect formation with respect to paste rheology and how they can be avoided through proper formulation. The current production methods and problems experienced at MAST are discussed. Pastes were characterised using a 4 parameter non-linear form of the Benbow Bridgwater model. It was first attempted to correlate the quality of a range of monoliths to their paste rheology. This would have both informed the selection of the binder package and given some insight into the mechanism of defect formation. However, the method of visually inspecting extrudate and rating the overall quality was not found to be robust enough for this purpose. In a second approach, a shared cause of the most commonly encountered defects was proposed. Application of the Benbow Bridgwater model to a honeycomb die showed which parameters are most influential in causing non-uniform flow. It was shown that the binder package can be selected to control each of the Benbow Bridgwater parameters. An optimal paste formulation was recommended and found to be effective in producing a defect-free extrudate with a 0% rejection rate.

5.1   Introduction

The current approach to formulation at MAST is very much a pragmatic one. Binder formulations and processing have been 'tweaked' and adjusted during process development based on the operator's experience and 'gut feeling'. At the commencement of this work, this approach was sufficient to allow MAST Carbon to produce reasonably small quantities of monolith; albeit with a rather high rejection rate (an exact number could not be determined but it was thought that a failure rate of 50% was not uncommon).

Many of the failure modes indicated that paste formulation was largely responsible. The defects shown in Figure 5.1 appear as soon as the paste exits the die. Figure 5.1a shows a monolith which suffered from a number of catastrophic defects which are hard to categorise. It can be seen that the wall of the monolith has become detached from the bulk of the paste and rippled. Figure 5.1b shows tearing on the interior of the monolith. Figure 5.1c shows a wall tear, sometimes called a 'sharks teeth' defect . It was thought that the defects are formed inside the die. The influence of the geometry of the extrusion die on monolith quality was not well understood. The specifics of the production dies at MAST such as the diameter of the feed holes and the dimensions of the pins were defined such that the open area of the feed holes was larger than the open area of the front of the die. It was possible that die design may have been improved to allow failure-free paste flow but the financial and time cost of manufacturing a new extrusion die was prohibitive. For this reason, it was decided that the paste could be formulated such that it could be tailored for the existing extrusion tools at MAST.

Figure 5.1 - Green monoliths showing different types of extrusion defect

As demand for MAST Carbon's material has increased, this approach to paste formulation and production was no longer sufficient to meet the company's needs. It was, therefore, necessary that the relationship between formulation and 'extrudability' be better understood. Extrudability is, unfortunately, a rather vague term. It has been defined in this work in a number of ways in an attempt to set benchmarks for rheological characteristics. This is discussed in detail later in this chapter. At this point, extrudability is taken to mean the general tendency of a paste to form defect-free and well-formed monoliths at commercially attainable pressures.

MAST Carbon also had need of a test which may be carried out on the shop floor by an operator which would, within at most a few minutes, indicate whether a given paste would be suitable to extrude or whether further mixing or binder addition is necessary.

5.1.1 Effect of Scale Up on Defect Formation

In late 2012, MAST Carbon was involved in a project during which 20 'full length' (approximately 2 m) green monoliths were produced per day over a period of months. For the purposes of that project, a large-scale mixer was obtained from Winkworth Mixers which was capable of mixing paste sufficient to fill the Sulby extruder completely. The Sulby when fully loaded will contain enough material to extrude approximately 15 m of 'Bath 5' monolith. The formulation used during the length of this project was MAST Carbon's then 'standard' formulation.

It was found that as soon as operations began at this scale and at a frequency of twice a day, the repeatability of the process was noticeably better, with the rejection rate being reduced to perhaps 25%. It was determined that the less frequent and smaller extrusions were more susceptible to variations in resin make-up, changes in ratios of additives, weather variations and changes in other processing conditions. This ultimately led to unpredictable levels of defect formation in small run manufacture. When working with exactly the same formulation and processing conditions (such as mixing time), the rate of defects decreased.

There is also something to be said for the operator in essence 'learning' how the process works. That is to say, at least some of this improvement in rejection rate can be attributed to increased operator skill and familiarity with the process.

Despite the increase in reliability of the process, the need still exists to form a theoretical understanding of the relationship between formulation, processing, rheology and eventual monolith quality.

5.2   Approaches to Reformulation

Once pilot work was completed, two approaches were taken to paste reformulation. The objective of each was to determine the mechanism of defect formation and what steps could be taken at the formulation level to prevent or reduce the failure rate.

The first approach was to systematically vary the formulation and measure the rheology of the paste and quality of the resulting extrusion. By comparing the rheology to monolith quality, it was hoped that conclusions may be drawn about the formation of defects from the relationship between quality and rheology. For instance, if any Benbow Bridgwater parameter was highly correlated with the formation of a particular defect, this could grant insight into the mechanism of formation of the defect based on the effect that that parameter might have on paste flow through the die and subsequently on defect formation.

The second approach involved studying the effect of varying formulation on rheology and separately predicting extrusion quality as a means of linking rheology to quality. This method relied on being able to apply a rheological model in such a way as to predict the formation of defects, which in turn required an understanding of that mechanism.

5.3   Primary Approach – Observational Study

This approach could be broadly considered to comprise of two linked studies. Pastes were prepared and the binder systems systematically varied. Benbow Bridgwater parameters were determined for each paste. An identical paste was then extruded on a standard honeycomb die and its 'quality' was assessed using the method discussed below. A semi-quantitative assessment of extrusion quality could then be plotted against each of the measured BB parameters.

5.3.1 Assessing Monolith Quality

There is no work in the literature which deals with qualitatively or quantitatively assessing the quality of extruded monoliths.

Assigning a numerical value to, or even defining, extrusion quality is very challenging, but necessary in order to effectively compare it with rheology. It would have been possible to simply describe quality with descriptive terms such as 'satisfactory' and 'good' and attempt to correlate them with numerical values for BB parameters, however, this would have been difficult to achieve and the results would be far from ideal. Having a numerical value for quality allowed rheology and quality to be plotted against one another and making it possible to correlate the two quantities. While handling and analysing quantitative data may be much easier, it is not a simple task to assess monolith quality in such a way. As no methods of doing so exist in the literature, a method of subjective assessment was developed.

5.3.1.1 Problems with Subjective Assessment

An operator may be able to judge whether a finished piece is acceptable or not simply by a quick visual inspection and assign a score out of 5, but this method is prone to all of the problems attendant with a subjective evaluation of this kind. Problems likely to be encountered when taking this approach include the following:

- The judgment of one operator may not agree with that of another. For instance, one operator may place a high level of importance on one aspect of monolith quality and overlook the formation of certain other defects.

- A rating given by an operator will be subject to changes in the relative quality of the monoliths; a monolith that may have 'passed' on one day may 'fail' on another day if the other monoliths in that batch are of particularly high quality.

- Operator bias may affect the rating. The operator may *a priori* be convinced that an adjustment to either the formulation or process methodology will have a positive impact and rate the monoliths accordingly.

These problems may be overcome to a certain extent by introducing strict assessment criteria against which the monoliths are judged, e.g. "monoliths showing sharks teeth on more than 20% of their length are rated a 3". This approach will only partially improve the problems outlined above.

5.3.1.2 Aspects of Monolith Quality

In addition to the problems associated with the subjective nature of qualitative assessment given by different operators on different days, the very nature of defining monolith quality is itself problematic. The first method of objectively assessing monolith quality used in the work was to rate the monoliths on a single 5 point 'quality' scale, this being the simplest method. In this case, the quality scale was defined as shown in Figure 5.1.
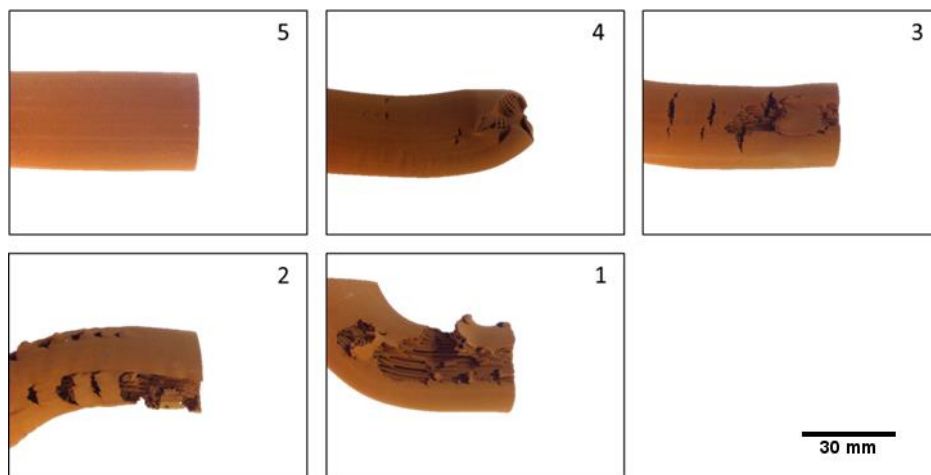
Figure 5.2 - 5 Point Rating Scale for Assessing Monolith Quality

Using the reference chart in Figure 5.2 was one step towards ensuring that the operator subjectivity does not colour the results of the assessment. The reference chart was developed

in conjunction with an experienced operator. A score of 5 was given to a monolith which had no visible defects of any kind. The surface was smooth and the channels were well formed. A score of 4 or 3 was given to monoliths which have surface tearing or missing channels. Scores of 2 and 1 were given to monoliths in which the surface was very poorly formed with large sections of missing wall and channels. These monoliths also typically were extremely bent.

The second method of monolith assessment was to separate several aspects of monolith quality and rate them separately. 'Monolith quality' is difficult to encapsulate in one single score, either qualitative or quantitative, as there are many types of defect that may arise. It was desirable to classify different defect modes and assess them each separately as distinct phenomena. This was to allow the comparison of each failure mode to rheology on an individual basis under the assumption that the mechanism of formation is different in each case.

The first attempt made to categorise defects formed during extrusion was to rate extrudate based on 3 criteria: straightness, surface quality, and channel formation. The five-point scale used is shown in Table 5.1.

Straightness may normally be characterised by the deflection from a straight monolith, but in the case of vertical extrusion, the monoliths often correct the direction of extrusion under the weight of the extrudate. This results in a 'hockey stick' shaped monolith which may not be easily characterised in this way.

A major drawback of this categorisation is that some failure modes may 'overlap' with others. For instance, monoliths will sometimes curve as they extrude. Depending on how severe the curvature is, this can lead to tearing on the trailing side of the monolith. In this circumstance, the monolith would score low on both 'straightness' and 'surface finish'.

Table 5.1- Five Point Rating Scale for Assessing Monolith Quality

	Score	Criteria
Surface Finish	1	rough with large holes and sharks teeth
	2	rough with sharks teeth
	3	rough surface with small tears or ribbing
	4	rough surface with some ribbing
	5	Shiny, smooth and no defects
Cell Formation	1	large sections of missing cells
	2	warped sections and intermittent gaps
	3	large cracks present
	4	small cracks or warped cells
	5	regular cells all walls intact
Straightness	1	completely one-sided extrusion
	2	continuous bend - large tears
	3	continuous bend - small tears
	4	starts bendy but corrects under its own weight
	5	straight extrusion

5.3.1.3 Verification

Single Point Rating Scale

A series of 7 monoliths were extruded for the purpose of validating the five-point rating scale. Each monolith was assessed twice by separate operators. The operators did not discuss the results with each other in order to prevent undue influence. This rating scale does not give the granularity of results that the multi-criteria rating scale as it encompasses all aspects of

monolith quality into one number. However, the results, shown in Figure 5.3, show that it may be relied on reasonably well to give an overall indication of general extrusion quality, suitable for comparison to the Benbow Bridgwater parameters.

Overall Quality
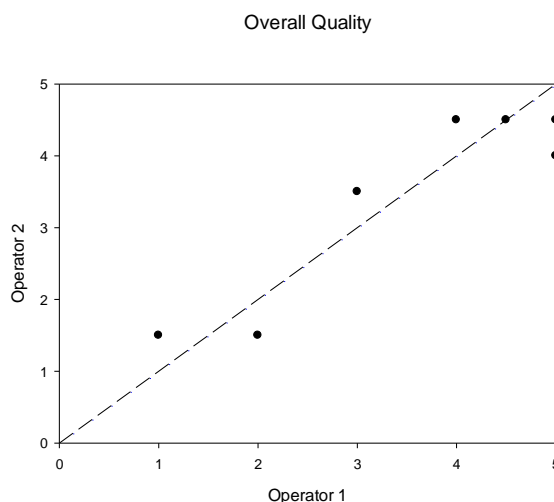
Figure 5.3 - Comparison of Results from two Operators using Simplified Rating Scale

Multi-Criteria Rating Scale

In the case of the multi-point rating scale, the results varied widely between the two sets of assessments. Separating the types of defects out allowed too much room for interpretation to useful as a reliable method of assessing quality. This is likely due to the way that each of the types of defect overlap as discussed in section 5.3.1.2. For this reason, this rating scale was not used to compare quality with paste rheology.
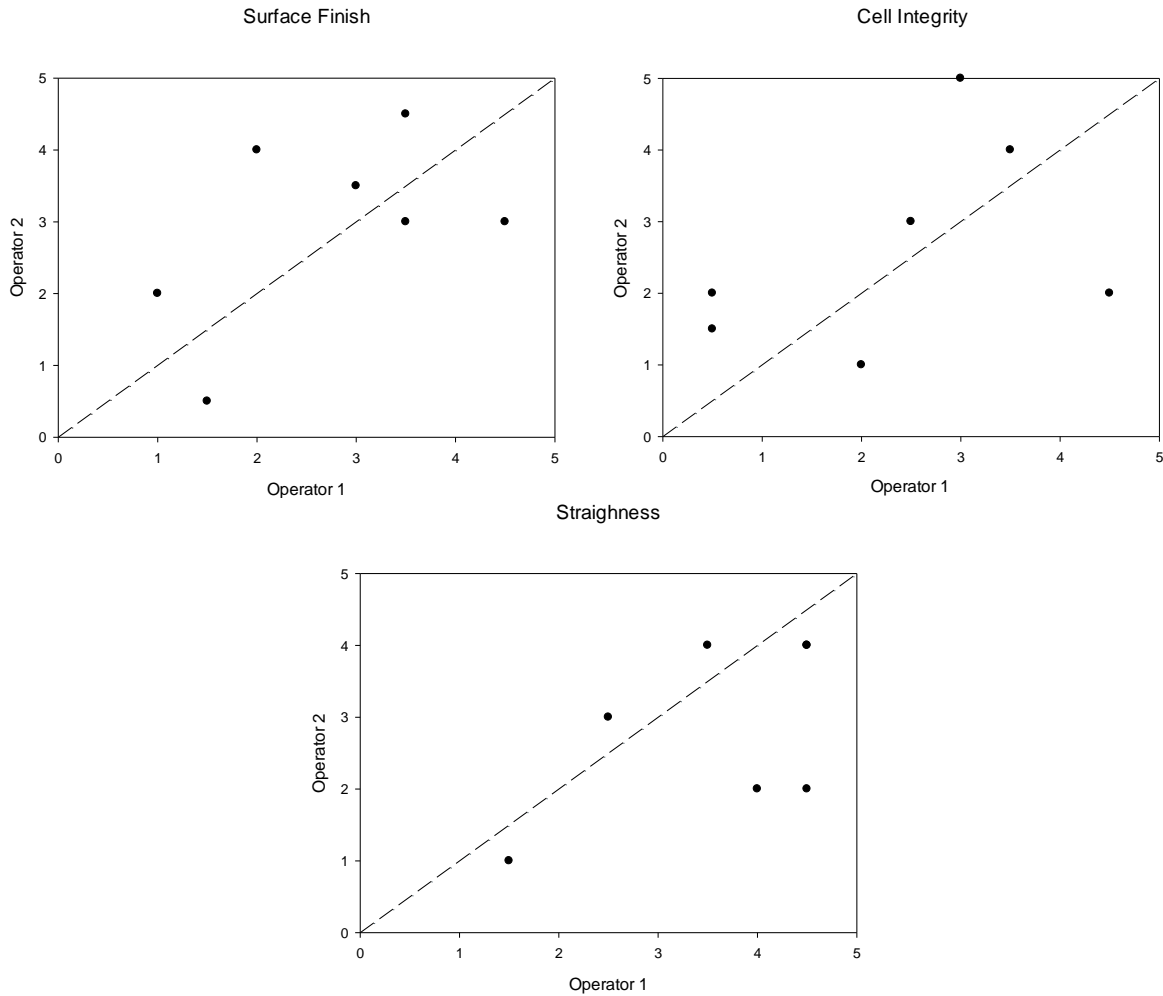
Figure 5.4 - Comparison of Results from Two Operators Using Multi-Criteria Rating Scale

5.3.2   Formulation Selection

There were two variables to be considered with respect to paste formulation. The solid phase must remain constant in terms of particle size and distribution due to downstream processing considerations, leaving only the solid to liquid ratio and the binder phase composition. Pastes selected here must be capable of extrusion through three dies of increasing length (in order to measure Benbow Bridgwater parameters) and to extrude through a 22 mm honeycomb die.

5.3.2.1   **Base Formulation Selection**

Initial pilot work on reformulation indicated that a 'base' level of K15M was required for an effective comparison of paste performance. Additive rheology was found to be far too diverse

to compare pastes to one another without the addition of some K15M to make the paste extrudable. A base loading of 15 wt% K15M was included in all pastes in this study. This ensured that all pastes were extrudable and the effect of the addition of the secondary binders could be assessed based on their effect on extrudability compared to the 'base' formulation.

Table 5.2 shows the four formulations from which the base formulation was selected. The weight percentage of K15M is with respect to the mass of water in the paste, calculated as shown in Equation 5.1.

$$\text{Weight percentage of additive} = \frac{\text{mass of additive}}{\text{mass of water}}$$

Equation 5.1

The solid to liquid ratio is the ratio of the volume of solids to the total volume of liquid, including the dissolved binders. A higher value indicates a 'wetter' paste.

Table 5.2 - Initial Paste Formulations

	AA	AB	AC	AD
Resin (g)	75.0	75.0	75.0	75.0
Water (g)	33.3	35.9	39.1	42.4
K15M (g)	4.2	5.4	5.9	6.4
K15M (wt%)	12.5	15.0	15.0	15.0
Solid/Liquid Ratio (vol)	0.50	0.55	0.60	0.65

- **Formulation AA**

The initial formulation, AA, was found to be extremely stiff and dry, making it difficult to mix using the available equipment. The paste was extruded through a square entry cylindrical

die, 3 mm in diameter and 48 mm long. This was the same die used for conducting Benbow Bridgwater extrusions as detailed in Chapter 4. The ram speed was set to a modest 10 mm.min^{-1}. The load cell had a range of $0 - 10$ kN. The ram came into contact with the paste and the extrusion load rose to the maximum limit within approximately 2 mm of ram displacement or 0.4 seconds, and the procedure was halted. This is shown in Figure 5.5. This formulation was unsuitable to use as a basis for further studies.
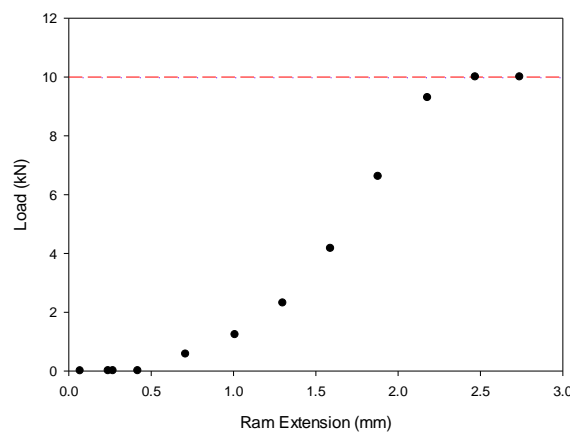
Figure 5.5 - Extrusion profile for paste AA at a ram speed of 10 mm.min^{-1}

- **Formulation AB**

Paste AB was similar to paste AA but reformulated to make a softer, more readily extrudable paste. The solid to liquid volume ratio was increased to 0.55, *i.e.* was made with a higher solids content. The weight percentage of K15M with respect to water was increased to 15% for fear that phase migration may occur if the binder was not sufficiently 'viscous'. Additionally, this paste was extruded through a shorter die (3 mm in length) to reduce die pressure drop. Ram speed for the initial extrusion was kept at 10 mm.min^{-1}.

The extrusion profile is shown in Figure 5.6. Paste AB also was unextrudable at the maximum allowable load on the Intron load frame. Encouragingly, paste AB did take slightly longer to

reach maximum load, suggesting that the combined effect of reducing the extrusion die length and increasing the liquid content was to produce a marginally more extrudable paste.
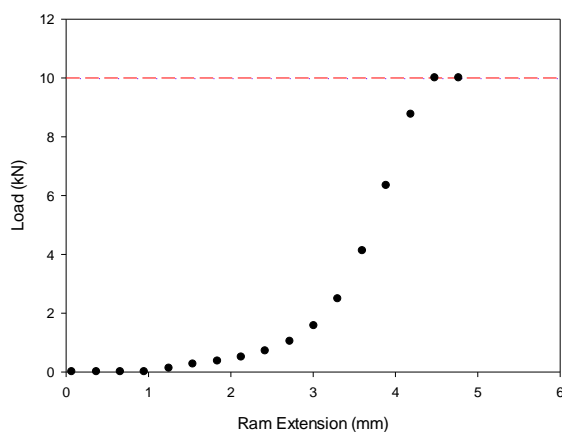
Figure 5.6 - Extrusion profile for paste AB at ram speed 10 mm.min^{-1}

- **Formulations AC and AD**

Pastes AC and AD had a solid to liquid ratio of 0.60 and 0.65 respectively and were otherwise identical.

Results for these pastes were much more encouraging. In both cases, at least some measurements were obtained for measuring Benbow Bridgwater parameters.
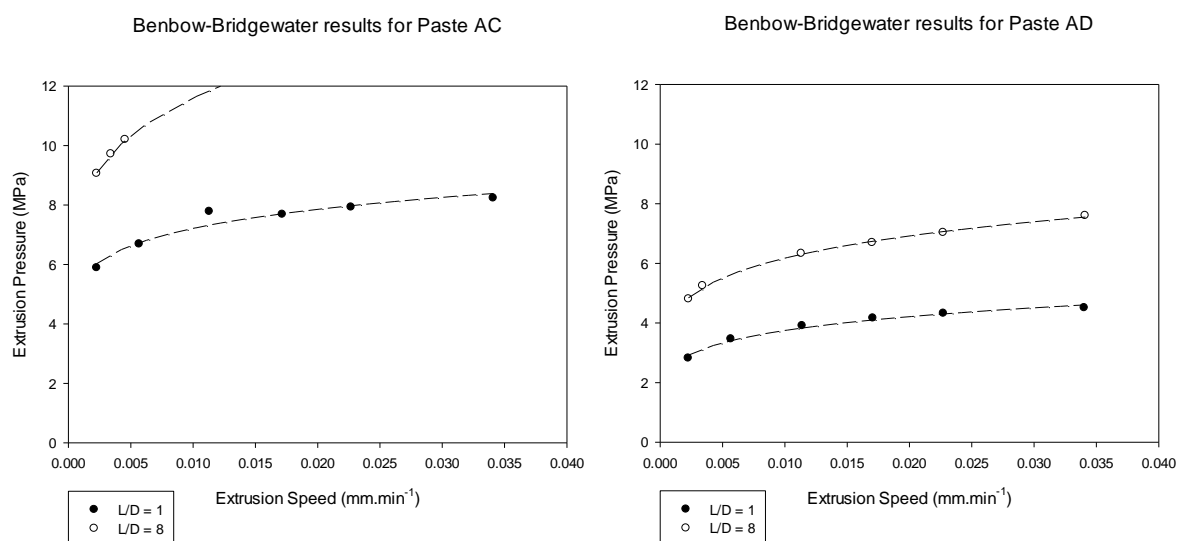
Figure 5.7 - Benbow Bridgwater extrusion profiles for pastes AC and AD

It was not possible to perform any tests on the longest die (L/D = 16) and in the case of paste AC, the medium length die (L/D = 8) could not be completed as the extrusion pressure was too high. Consequently, the Benbow Bridgwater parameters (for the 4 parameter non-linear form) for these pastes have been calculated using only a partial range of data and are therefore not as reliable as was desired.

Table 5.3 - Benbow Bridgwater parameters for pastes AC and AD

Paste	α MPa.s.m^{-1}	m -	β MPa.s.m^{-1}	n -
AC	2.23	0.11	0.48	0.24
AD	1.51	0.18	0.17	0.16

In neither case was it possible to produce any honeycomb monolith, even at very low ram speeds. The open area of the honeycomb die is much larger than the open area of the 3 mm cylindrical dies so it was expected that if the paste was extrudable through the narrow die, it would also be possible to produce monolith. However, the pastes have a reasonably large value of β indicating a resistance to flow at the wall. As there is considerably more wall surface in the honeycomb extrusion die than the cylindrical dies, extrusion pressure was subsequently high enough to prevent extrusion.
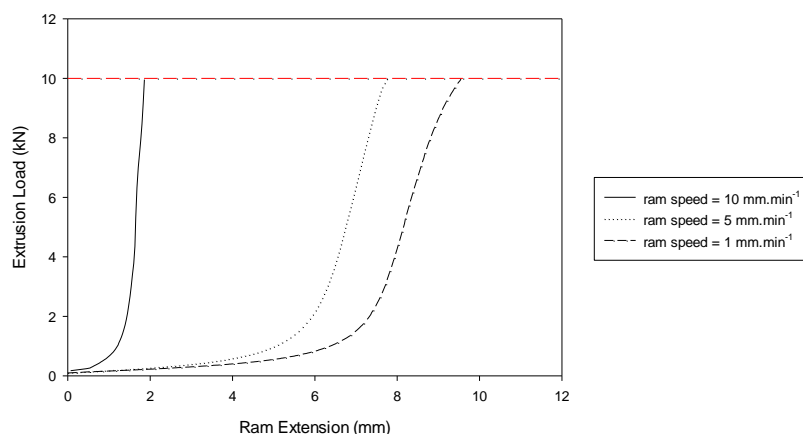
Figure 5.8 - Extrusion profiles for paste AC through Bath 2 honeycomb die

- **Formulations AE, AF, and AG**

Discussion at MAST with an experienced operator led to the addition of 1 wt% high molecular mass Polyethylene Oxide (nominal molar mass of 5,000,000 g.mol^{-1}), PEOH. This was again done to reduce the overall phase binder stiffness and increase the extrudability of the paste. It was still unknown at what solid to liquid ratio the pastes would be adequately extrudable, so pastes AE, AF and AG were produced with different solid to liquid ratios.

Table 5.4 - Formulations for pastes AE, AF, and AG

	AE	AF	AG
Resin (g)	75.0	75.0	75.0
Water (g)	38.8	42.0	45.3
K15M (g)	5.8	6.3	6.8
PEOH (g)	0.39	0.42	0.45
K15M (wt%)	15.0	15.0	15.0
PEOH (wt%)	1.0	1.0	1.0
Solid/Liquid Ratio (vol)	0.60	0.65	0.70

All three of these pastes were successfully extruded through all Benbow Bridgwater test dies and the Bath 2 honeycomb die at ram speeds of 5 and 10 mm.min^{-1}. As all three solid to liquid ratios were successful after the addition of 1 wt% PEOH, a solid to liquid ratio of 0.65 was selected for further pastes. The reason being that of the pastes which contained only K15M, this had been more successful and while a full dataset had not been obtained, paste AD was more suitable for comparison.

The remaining three additives of interest, PEOL, PEG and KH17S, were all added to a 'base' formulation, AF, at levels of 0.5 wt% and 2 wt%. A full table of pastes and their formulations is given in Table 5.5. Time constraints did not allow a greater range of concentrations, nor was it practical to investigate the binders in combination.

Table 5.5 - Formulations for pastes AH to AM

	AH	AI	AJ	AK	AL	AM
Resin (g)	75.0	75.0	75.0	75.0	75.0	75.0
Water (g)	41.9	41.9	41.9	41.3	41.3	41.3
K15M (g)	6.28	6.28	6.28	6.20	6.20	6.20
PEOH (g)	0.42	0.42	0.42	0.41	0.41	0.41
PEOL (g)	0.21	-	-	0.83	-	-
PEG (g)	-	0.21	-	-	0.83	-
KH17S (g)	-	-	0.21	-	-	0.83
K15M (wt%)	15.0	15.0	15.0	15.0	15.0	15.0
PEOH (wt%)	1.0	1.0	1.0	1.0	1.0	1.0
PEOL (wt%)	0.5	-	-	2.0	-	-
PEG (wt%)	-	0.5	-	-	2.0	-
KH17S (wt%)	-	-	0.5	-	-	2.0
Solid/Liquid Ratio (vol)	0.65	0.65	0.65	0.65	0.65	0.65

5.3.3 Benbow Bridgwater Results

All pastes AH to AM extruded through all three cylindrical dies at all of the test speeds. During every extrusion, the pastes reached a stable extrusion pressure at every ram speed meaning that all pastes were sufficiently stable. The pastes were all characterised using the 4 parameter non-linear form of the Benbow Bridgwater equation. The results are shown in Table 5.6.

Table 5.6 - Benbow Bridgwater Parameters for Pastes AC to AM

Paste Code	Paste Description	Solid/Liquid Ratio (vol)	α MPa.s.m^{-1}	m -	β MPa.s.m^{-1}	n -
AC	15% K15M	0.60	2.21	0.11	0.53	0.26
AD	15% K15M	0.65	1.51	0.17	0.18	0.16
AE	K15M + 1% PEOH	0.60	1.61	0.08	0.43	0.40
AF	K15M + 1% PEOH	0.65	1.11	0.21	0.09	0.14
AG	K15M + 1% PEOH	0.70	0.61	0.20	0.08	0.15
AH	K15M + PEOH + 0.5% PEOL	0.65	0.92	0.20	0.13	0.21
AI	K15M + PEOH + 0.5% PEG	0.65	1.14	0.20	0.09	0.14
AJ	K15M + PEOH + 0.5% KH17S	0.65	1.11	0.22	0.10	0.16
AK	K15M + PEOH + 2.0% PEOL	0.65	0.54	0.26	0.06	0.11
AL	K15M + PEOH + 2.0% PEG	0.65	0.58	0.20	0.07	0.11
AM	K15M + PEOH + 2.0% KH17S	0.65	0.77	0.15	0.08	0.11

5.3.3.1   Binder Effect on BB parameters

Figures 5.9 to 5.12 show the effect of varying the binder concentration on each of the BB parameters. Patterns in the data are very hard to discern due to the size of the error bars and the limited data set. Constraints on time and equipment access limited the number of experiments that could be performed. Later work was more rigorous and is discussed later in section 5.4.4.
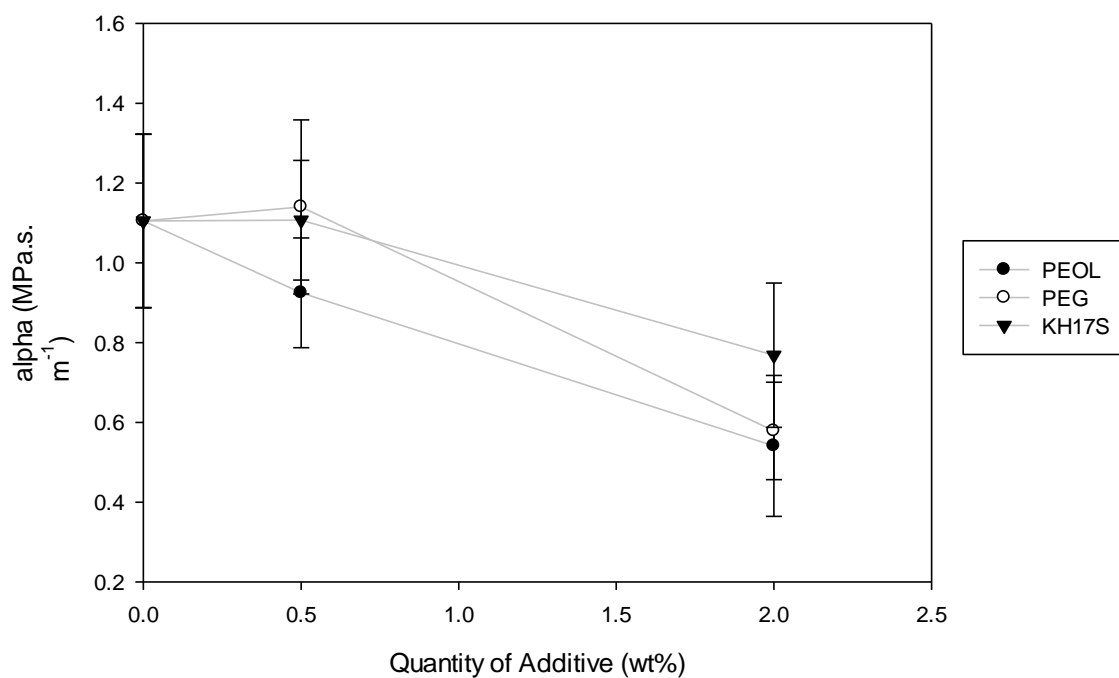
Figure 5.9 - Effect of PEOL, PEG, and KH17S on α
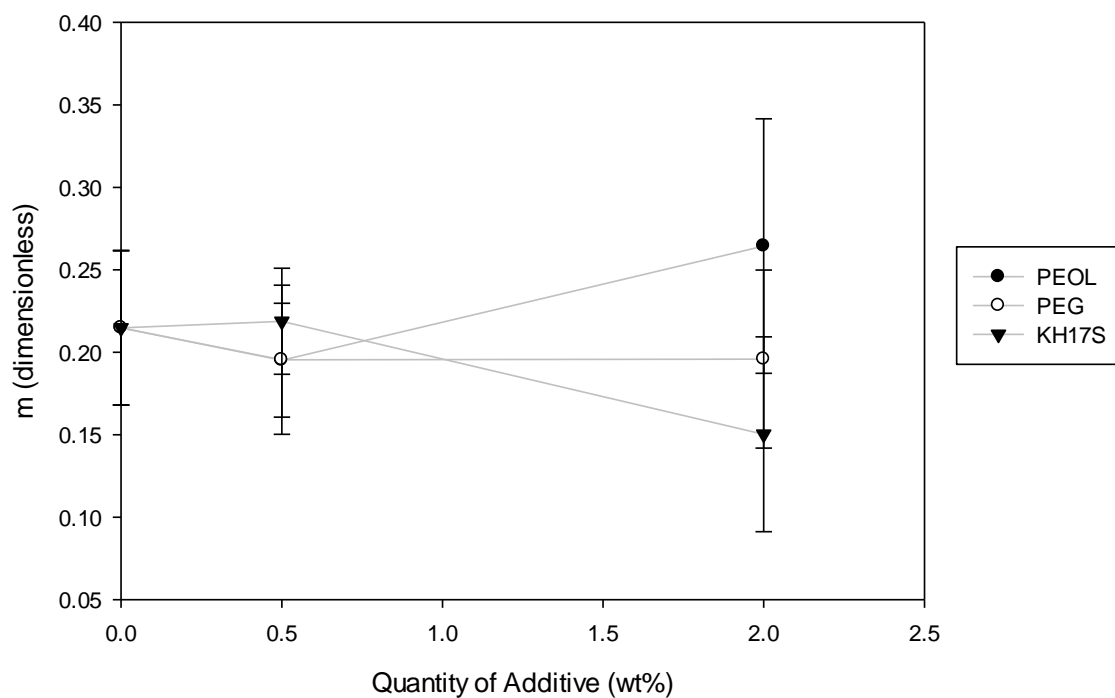
Figure 5.10 – Effect of PEOL, PEG, and KH17S on m
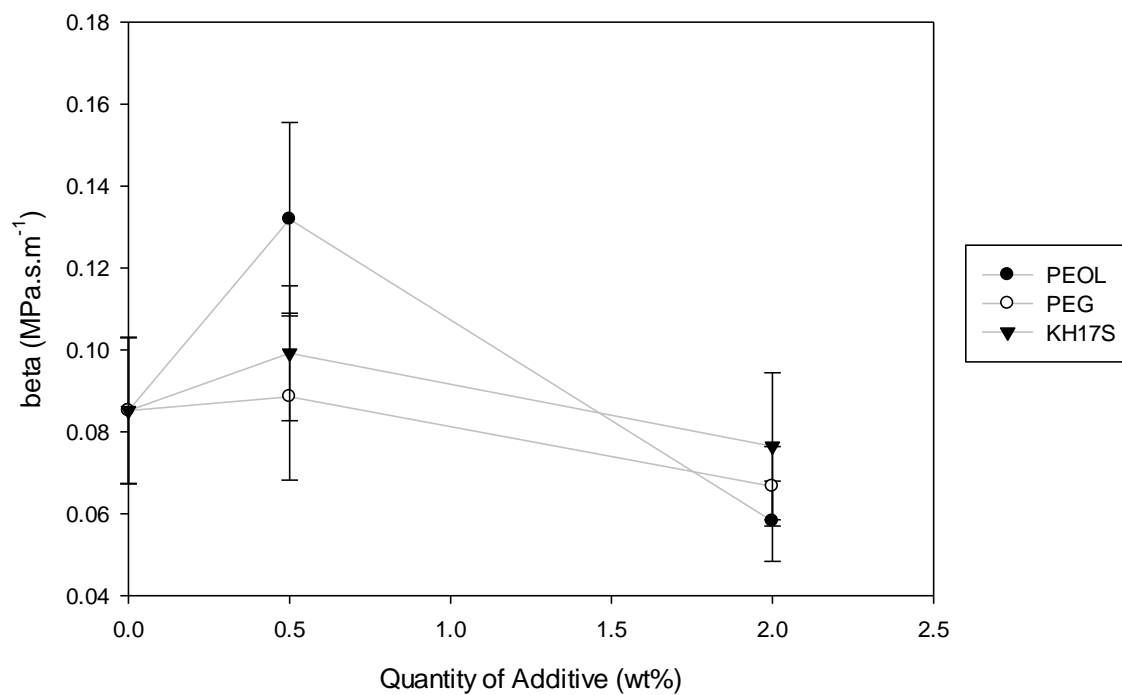
Figure 5.11 - Effect of PEOL, PEG, and KH17S on β
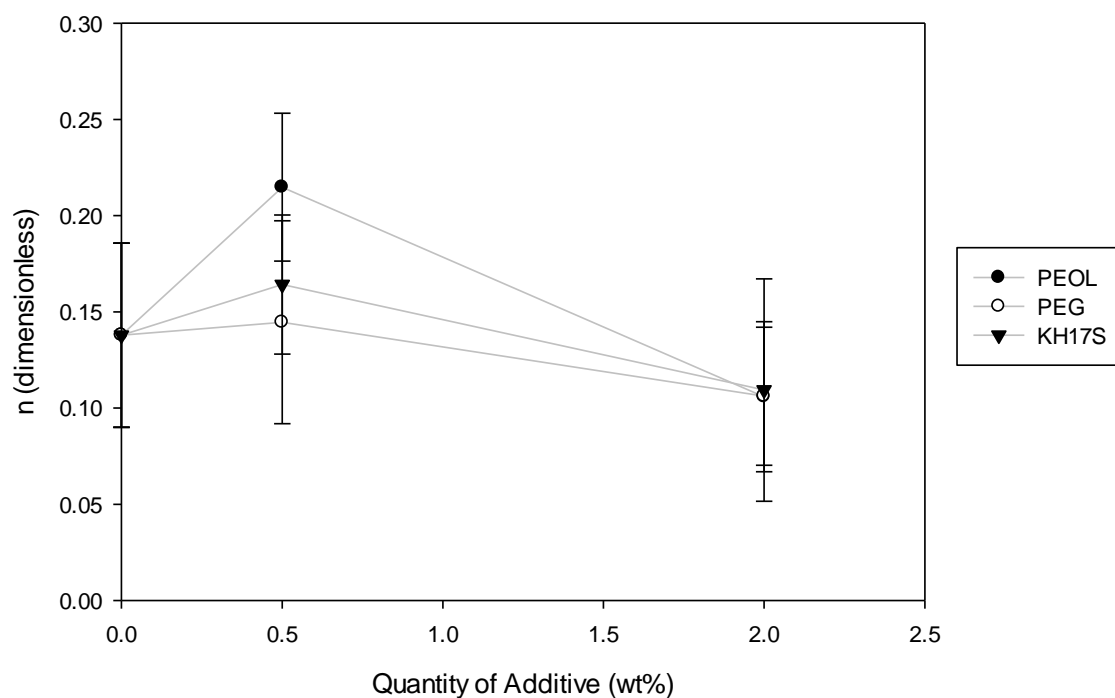
Figure 5.12 - Effect of PEOL, PEG, and KH17S on n

Figures 5.9 to 5.12 show the measured BB parameters for pastes AF and AH to AM. As all of these formulations have a solid to liquid ratio of 0.65, the figures show the effect of the additives, independent of the solid/liquid ratio. The size of the error bars are a consequence of there being no repeat results for any of the data.

From the data shown in Figure 5.9, it cannot be said that a low level of any of the additives reduce α. PEOL at a level of 2 wt% shows a reduction in α, whereas KH17S and PEG do not. A reduction in α suggests that the pressure drop in the convergent section of extrusion is less, making it easier to extrude through a die with a high ratio of barrel to die open areas.

As shown in Figure 5.10, there is no statistical difference in the values of m for any of the additives at any concentration. All that can be said for binder influence on this parameter is that any difference would be very small as the range is narrow. These results are suggestive that the parameter m, and therefore the velocity dependence of pressure drop in the convergent region, is not heavily influenced by liquid phase rheology. It may be that the solid phase plays a greater role in the relationship between velocity and pressure drop, however as the solid phase is fixed by MAST due to processing constraints, it is not practical to investigate this link further.

Similar to the results for α, Figure 5.11 does not show a statistically significant effect of binder concentration on β for any of the additives except PEOL, which shows a small effect at a low concentration. The parameter β describes the linear velocity component from friction at the wall. In honeycomb dies, the wall surface area is significantly higher than in the cylindrical test dies. Additionally, the amount of wall friction will increase dramatically as the cell geometry becomes finer. A paste with less resistance to wall friction should be more extrudable through a honeycomb die and be capable of producing finer cell geometry without suffering too high of an extrusion pressure.

Figure 5.12 shows the changes in n with binder concentration. The error bars are also too large here to allow any conclusions to be drawn with confidence. As with Figure 5.10, it can be said that the size of any effect of these parameters on n, if present, is only small. As with β, n is relates the pressure drop from friction at the wall to the velocity of the extrudate. As the term is an exponent, it has the potential to significantly change the sensitivity of the paste to velocity.

Missing from this data is the influence of PEOH on the BB parameters as this is kept constant in each of the formulations. The effect of PEOH could not be studied at this stage of the work, but is discussed in section 5.4.

As this data has not been repeated, the error bars are relatively large compared to the parameters however, the r-squared values for the fitting performed in SigmaPlot are all high (above 0.98). This suggests that it is possible to compare the BB parameters of a given paste to each other.

alpha vs m

beta vs n
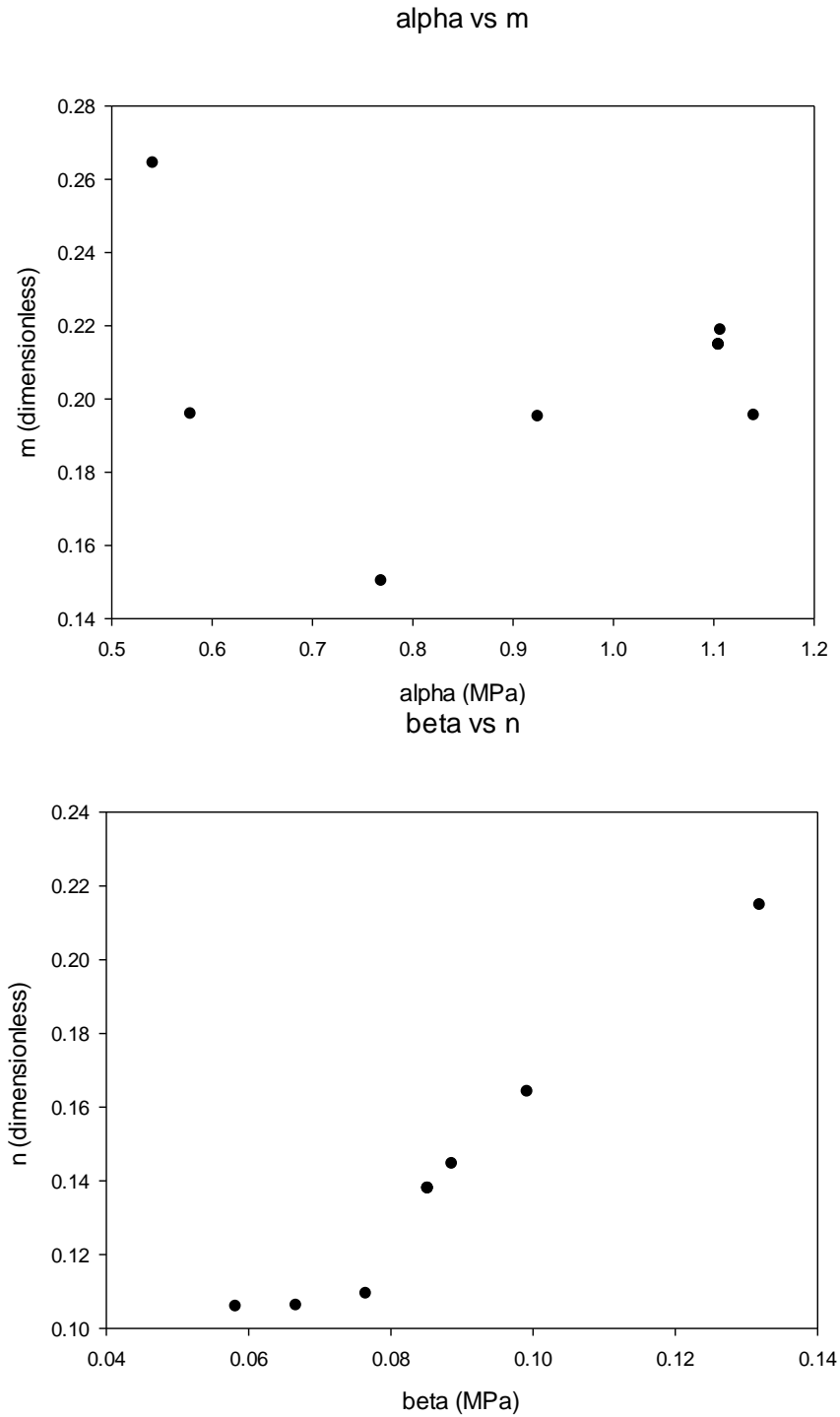
Figure 5.13 - Covariance in bulk and wall paste rheology

The relationship between β and n appears to be reasonably linear, as can be seen in Figure 5.13. It should be noted that in Chapter 4 it was discussed that this is not as a result of the BB model being ill-posed. These results mean that as the paste become more sensitive to changes

in velocity at the wall (characterised by a lower value of n), the paste also becomes less apt to develop wall friction (characterised by a low value of β). Figure 5.13 also shows the covariance in α and m but does not indicate any relationship between the two.

5.3.4 Comparison of Parameters to Monolith Quality

Monoliths were rated according to the single value monolith quality scale discussed in section 5.3.1.2. The multi-criteria rating scale was not used as there was too much room for interpretation to give consistent and reliable results. The results were then correlated with the Benbow Bridgwater parameters, shown in Figure 5.14.
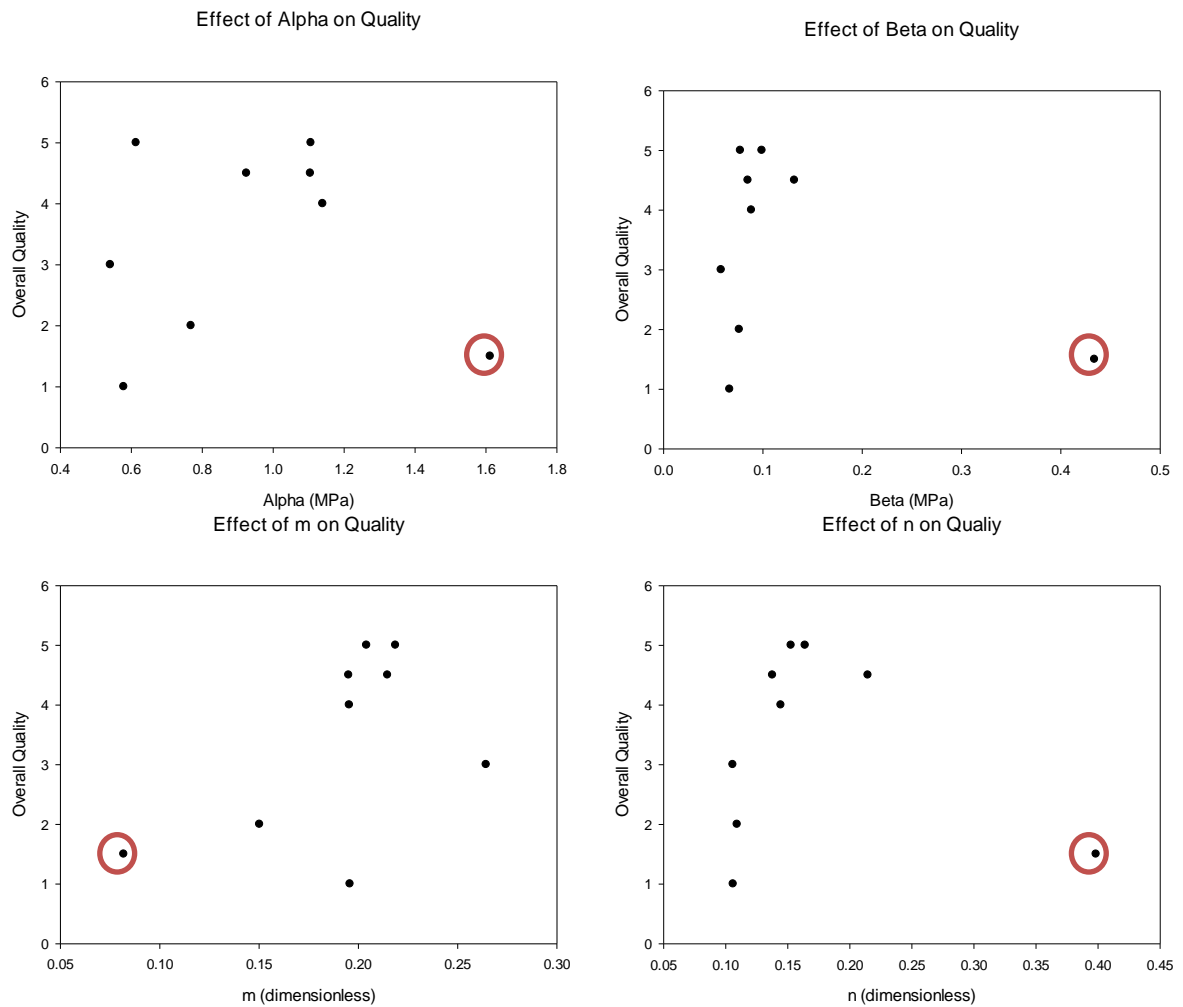
Figure 5.14 - Variation in Quality with BB Parameters

None of the results show any convincing evidence of any link between the characteristic BB parameters and the single monolith quality rating. There is one paste which appears to be anomalous, paste AE (circled in red). This paste had a smaller solid to liquid ratio than the other pastes, which may explain the reason for the difference. Figure 5.15 shows the data after the removal of paste AE from the results.
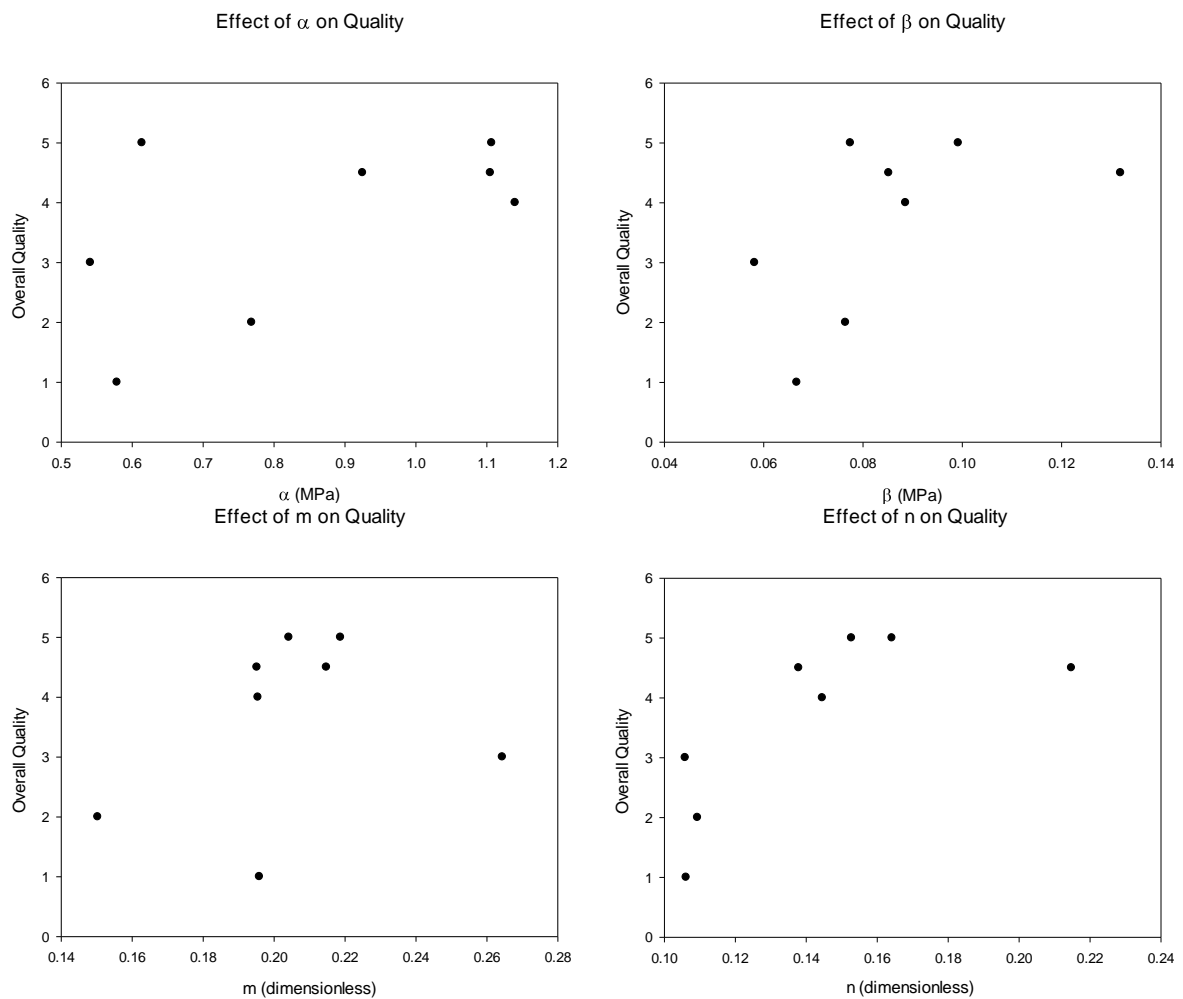
Figure 5.15 - Change in Quality with change in BB Parameters after removal of anomalous result

The results do not show very much convincing evidence of a link between the values of α and m parameters and extrusion quality. There is some suggestion, however, that there is some influence of n and perhaps β on extrusion quality. As both of these parameters are related to the conditions at the wall, this is plausible. The results appear to show that a paste formulation

with a higher value of n will likely resist the formation of defects, resulting in a better extrudate.
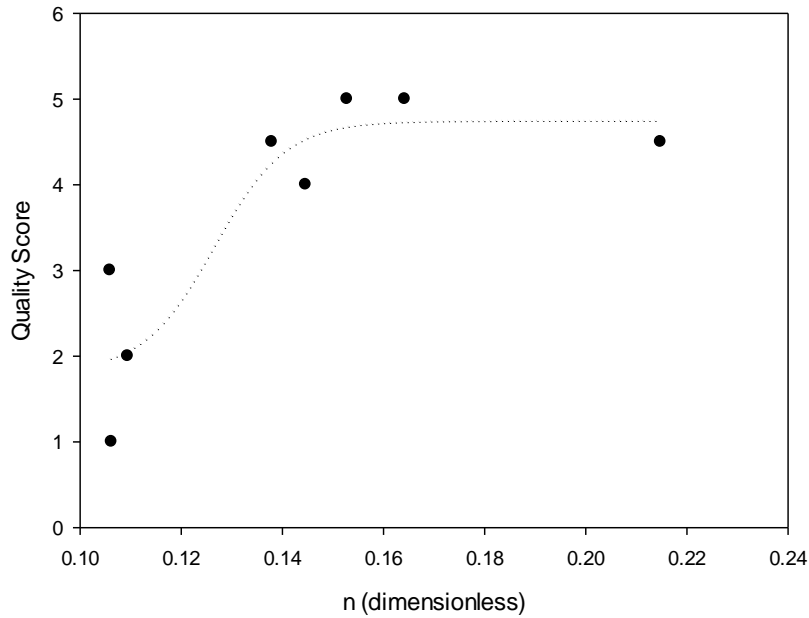
Figure 5.16 - Possible Relationship Between n and Overall Monolith Quality

Figure 5.16 shows a potential relationship between n and the quality score given by an operator. This data suggests that pastes characterised by a BB n value of more than approximately 0.15 will produce an acceptable monolith. There is a sharp decrease in quality between n values of 0.10 and 0.16 with quality dropping to 0 as n decreases further.

5.3.5 Discussion

Both methods of rating monolith quality subjectively were found to be wanting in several ways. A single monolith rating score does not provide the granularity of results required to determine whether different failure modes are caused by different BB parameters. This method is, however, more repeatable. Classifying the failure modes and awarding spate scores is a more comprehensive way of assessing monolith quality but is more prone to the failures

in subjective assessment described in 5.3.1.1. It was decided that for the sake of a reliable dataset, the single point rating scale would be used.

A base formulation was selected from a range of simple pastes to which two amounts of a tertiary binder were added. These pastes were characterised using the BB paste model. It was found that the three binders tested had effects on the rheology of the paste which could be measured directly using the BB paste model. Interestingly, the binders all appear to move the BB parameters in unique directions. If indeed a specific BB parameter may be linked directly to monolith quality it would be possible to influence the paste rheology using a blend of specific binders.

When the BB parameters are compared to the single point monolith quality score, the results do not show convincingly that there is any solid correlation. As the Benbow Bridgwater equation is a robust method for characterising pastes, it was surprising that the parameters did not correlate well. It is therefore very likely that the methodology for assessing monoliths is not suitable for this purpose. The rating system does not adequately characterise the defects in the system.

What little evidence these results provide suggest that the primary influence that the BB parameters have, if any, lies in the values of β and n. The behaviour of the paste at the interface between the die geometry and the paste itself is very likely a contributing factor in defect formation. This is especially so in honeycomb dies which have so many faces within the die land. As β and n describe the paste behaviour at the die/paste interface, this data may support this line of thinking. Referring back to Figure 5.12, the addition of a small amount of PEOL or KH17S may be helpful in reducing defect formation.

Without a robust understanding of the reason for defect formation, it is very difficult to categorise the types of defect. Without this understanding, monolith quality can only be defined using the kind of qualitative system outlined here. This severely limits our ability to draw a link between paste rheology (as characterised by the BB paste model) and by extension our ability to make any recommendations with respect to formulation.

It remains certain that paste rheology must influence the quality of extrusion to at least some degree. These results are suggestive of a link between the paste wall interaction but fall far short of proving a mechanism for defect formation.

5.4 Secondary Approach – Application of Benbow Bridgwater Model to Die Geometry

This secondary approach to understanding a link between paste rheology and defect formation is to apply the BB paste model to the honeycomb die geometry and use it to predict the flow profile of paste through the geometry.

5.4.1 Shared Cause of Defect Formation in Honeycomb Extrusion

The approach to predicting monolith quality from BB parameters is underpinned by the proposed mechanism of defect formation described here. The three most simple and perhaps most obvious causes of defect formation may be listed as follows:

- Die Blockage

A large or unusually shaped particle may become wedged in the die entry hole and restrict the flow of paste in a small area. This manifests itself as missing channels or warped internal structures. This has been a commonly encountered cause of defects encountered at MAST. When a die is blocked in one of the central channels, this defect will often go unnoticed.

Historically, when this occurs at one of the outer channels, it often misattributed to a failure of the paste rheology to fully fill the die. This cause of defects can be entirely avoided by carefully controlling the particle size distribution.

- Delamination

This is caused by elements of paste either not sufficiently bonding together after exiting the die or not cohering strong enough and becoming separated later under drying stresses. The ability of the paste to adhere to itself after passing through the die appears to be linked to the binder formulation and the ratio of solid to liquid in the paste. This type of defect is rarely seen at MAST.

- Phase Migration

This phenomenon is discussed in greater detail in Chapter 6. When this phenomenon occurs it results in the moisture in the paste becoming poorly distributed and drier overall as extrusion progresses. Drier pastes are more prone to brittle fracture and behave less like a viscoelastic fluid and more like a plastic. As the liquid content of the paste drops that required to lubricate the particles, extrusion may become very difficult and result in damage to equipment. Defects caused by this phenomenon are also seen rarely at MAST.

These three causes of defect account for some less common failure modes encountered at MAST. The cause of all of the other more common types of defect can be attributed to a single cause, poor flow distribution of the paste. Surface fracture, for instance, occurs when an area of the die face is flowing at a slower rate than the neighbouring paste elements. Slow paste elements are adhering to fast paste elements and this causes fracture along the slow paste elements. The fast paste pulls the slow paste apart. A simplified schematic is shown in Figure 5.17. The fast moving paste (shown in red) causes a tensile stress in the slower moving

paste (shown in orange). As extrusion continues, the slow paste yields to brittle fracture. The build of tension and subsequent fracture accounts for the regular appearance of sharks teeth in honeycomb extrusion.
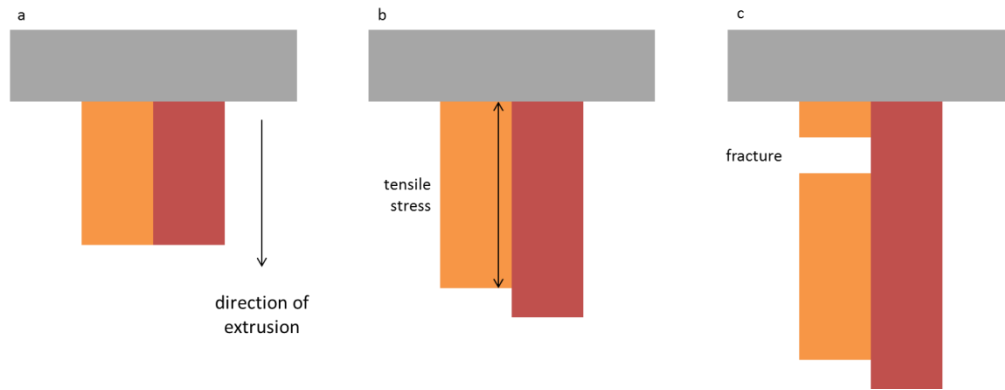
Figure 5.17 - Uneven flow causing paste fracture

In some cases, the slow moving paste is sufficiently ductile to avoid tearing. This poor flow distribution then manifests itself as a highly curved extrusion. In more extreme cases, the paste will both tear and become highly curved. The paste may also become completely static in one area of the die as paste flows preferentially to the 'fast' area of the die.

Monoliths have also been observed to develop a ripple or concertina type wall defect. This is caused when the bulk of the paste is moving slower than a small section of the wall. If the fast paste element is adhering to the bulk of the paste sufficiently, it will bunch up, creating the effect shown in Figure 5.1a. At a very small scale, the paste may appear bumpy, rather than smooth.

The reason for areas of paste to flow at different rates can be caused by a number of factors. A badly cleaned or badly worn die can lead to areas of local flow restriction. Misalignment of the washer can cause one side of the die to be restricted resulting in a one-sided extrusion. In a production environment, it is unreasonable to expect that the die will be perfectly aligned and unworn.

It is proposed that a paste which, as a result of its rheology, is *resistant* to variations in the conditions in the die land will result in a higher quality monolith. As argued here, an even flow profile in a honeycomb die will not allow the types of defects described in section 5.3.1.2 to form.

5.4.2   Application of Benbow Bridgwater Model to Die Geometry

In order to understand how paste is caused to flow unevenly, particularly at the wall, in honeycomb extrusion, the geometry of the die must be considered. Paste flows through the round feed holes on the barrel side of the die. Each of these holes has the same diameter and depth. The holes then feed the paste through a matrix of square pins. The vast majority of these pins are the same, however, around the outside of the die, the pins are partially cut away to fit within the circular washer. This configuration is shown in Figure 5.18.
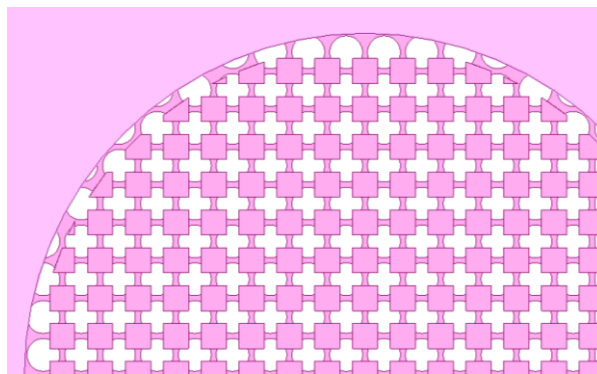
Figure 5.18 - Detail of Honeycomb Extrusion Die

If each of the feed holes is considered as an individual die being fed the same paste at the same pressure, the BB model can be applied and the extrudate velocity calculated. As each of the studied feed holes and the profile of the pins beyond them are different, we expect to see a variation in extrudate velocity given the same feed pressure. In this analysis, the standard deviation of the extrudate velocities was used an indirect indication of the paste's tendency to flow unevenly as a result of variation in die land conditions.

The form of the Benbow Bridgwater Model that is used is the general form of the equation for non-cylindrical dies (Equation 5.2).

$$P = \ln\left(\frac{A_0}{A}\right)(\sigma + \alpha V^m) + \frac{ML}{A}(\tau + \beta V^n)$$

Equation 5.2

As all the feed holes are identical, only the geometry of the pin profile on the opposite side needs to be considered. Additionally, the honeycomb die used in this analysis has a rotational symmetry of 4 with 2 mirror planes meaning that the total number of unique feed holes is only 10. The feed holes of interest are shown highlighted in Figure 5.19.
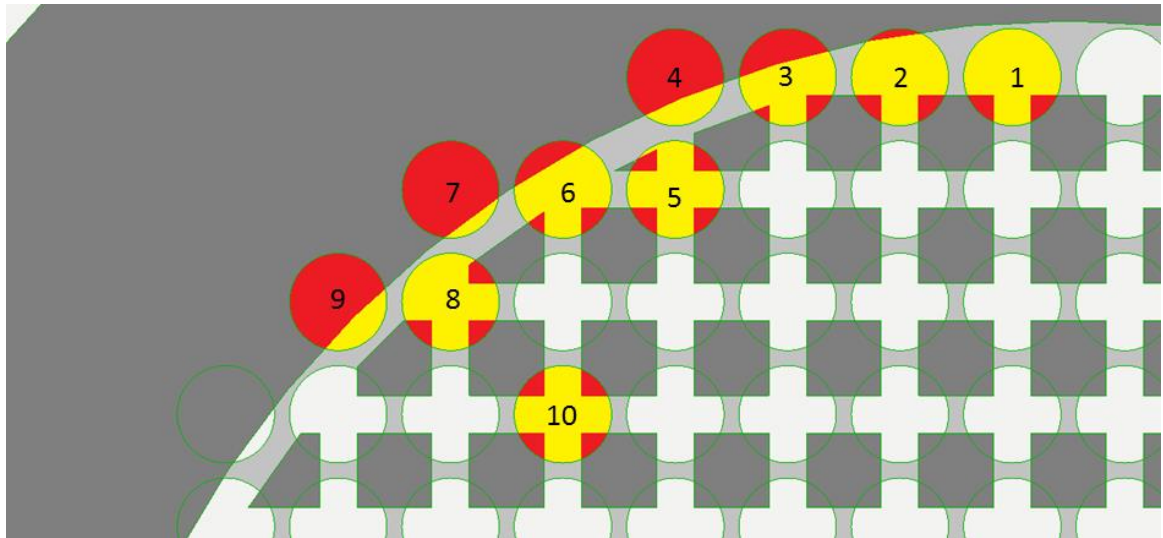
Figure 5.19 – Unique feed holes included in analysis

Regions highlighted in yellow indicate the open area of the feed hole. Red sections show the obstruction to paste flow caused by the overlap of the pins. The BB model is applied to the feed holes as though they are dies of the shape defined by the yellow section being fed from a barrel the diameter of the feed hole. In Equation 5.2, M is the perimeter of the red sections which meet the yellow region. A is the area of the red regions and A_0 is the total highlighted region. Feed hole 10 is representative of the majority of the feed holes covering the bulk of the die face. It is assumed that the paste will flow uniformly through these holes.

The 10 unique feed holes shown in Figure 5.19 were numbered and their open area and perimeter were measured. Dies were re-characterised for each of the different diameter washers.

Table 5.7 - Feed Hole Geometry for Ø27.0 mm washer

Hole	A_0	Pin Area	A	$\dfrac{A_0}{A}$	M	ML	$\dfrac{ML}{A}$
	mm^2	mm^2	mm^2	-	mm	m	-
1	1.33	1.02	0.31	4.30	1.13	7.89	25.59
2	1.33	0.23	1.10	1.21	2.06	14.43	13.15
3	1.33	1.18	0.14	9.26	0.88	6.15	42.93
4	1.33	0.33	1.00	1.33	2.29	16.02	16.02
5	1.33	0.30	1.03	1.29	3.02	21.11	20.54
6	1.33	1.02	0.31	4.32	1.11	7.74	25.19
7	1.33	0.51	0.82	1.62	2.37	16.59	20.27
8	1.33	0.21	1.12	1.19	2.12	14.86	13.30
9	1.33	0.16	1.17	1.14	1.39	9.76	8.35
10	1.33	0.31	1.02	1.31	2.79	19.52	19.22

Using Equation 5.2 and the geometries in Table 5.7, the extrusion pressure at an extrudate velocity of 20 mm.min^{-1} through feed hole 10 was calculated. As this pressure is applied equally over the face of the die, it was then possible to back-calculate the extrudate velocity through each of the other unique feed holes. Back calculation was performed using the DataSolver add-in for Microsoft Excel. A macro was created which could perform this operation for an arbitrarily large set of BB parameters. The method is given in Appendix D .
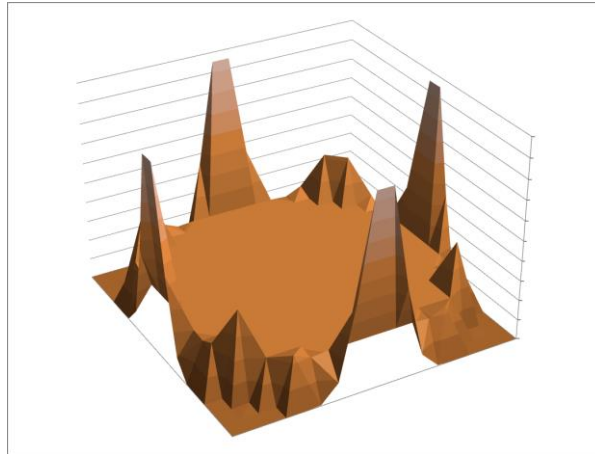
Figure 5.20 - Visualisation in Microsoft Excel of the initial velocity profile of paste exiting a honeycomb die. Height of the surface on the z-axis represents the relative speed of the paste exiting a hole at that location on the die face

5.4.2.1 **Limitations of this approach**

This approach does not account for a few factors which would improve its predictive power if included. If the cohesive force between pastes and the tensile strength were known and included in the calculation, fracture could more readily be predicted. If the influence of binder formulation on these factors was also known, paste reformulation would be even better informed. Additionally, the extrusion velocities of the paste elements are not independent of one another as has been implicitly assumed with this approach. Due to the shear forces present between paste elements, each one will either speed up or slow down its neighbours. In real terms, this causes a highly restricted feed hole to slow down the paste around it which is propagated through the face of the extrusion. If the shear forces between paste elements included in the analysis, the flow profile could be much more accurately be simulated.

This methodology is only applicable to complex die geometry such as the honeycomb dies described here. The assumption is made that paste does not fracture as it is extruded through the feed holes. Extrudate surface cracking when being extruded through cylindrical dies is reported in the literature by several authors. In the case of honeycomb dies, the diameter of

the feed holes and the geometry of the pins are small enough that defect formation of this type is unlikely.

5.4.3   Paste Characterisation

In the previous approach, the formulations all included PEOH, excluding it from the analysis. For this approach, a different range of formulations was analysed. In addition, Benbow Bridgwater parameters were obtained for three separate samples of each formulation and a high degree of repeatability was found. A base paste containing only K15M was used as a reference. To this, various quantities of the 4 binders of interest were added at levels of 0.5, 1, 2.5, 5 and 10 wt%. This is a much greater range of formulations than used in section 5.3. This makes 5 formulations for each binder and the reference paste for a total of 21 formulations.

Pastes were again characterised using the parameter non-linear Benbow Bridgwater model.

5.4.4 Effect of Binders on BB parameters

5.4.4.1 **PEOH**
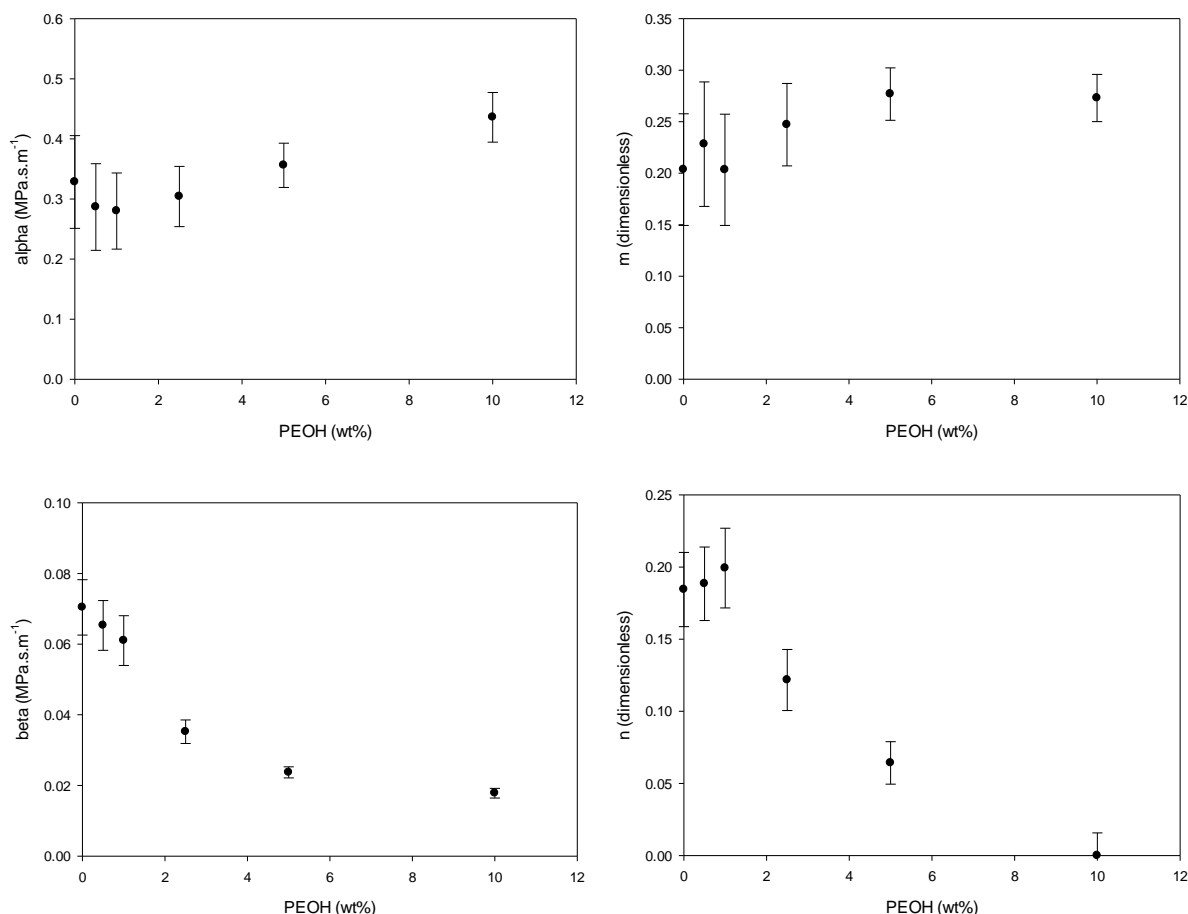
Figure 5.21 - Variation in BB parameters with wt% of PEOH

PEOH appears to have a profound effect on the paste rheology, particularly the value of n. The addition of 10 wt% of this additive reduces n to virtually zero, rendering extrusion pressure due to wall friction almost independent of extrusion velocity. A small addition of PEOH modestly increases n and significantly reduces α. Further addition of PEOH begins to increase α and significantly reduces n. PEOH increases m although the error bars on these results suggest that there is a large variability in this quantity. The value of β is also reduced dramatically with the addition of PEOH. This additive is known to possess interesting

extensional rheology [24]. PEOH forms an extremely 'stringy' fluid when mixed with water. High weight grades of PEO are even capable of forming an open siphon, i.e. may flow against gravity to flow into a container at a lower level. This interesting rheology may explain why this additive has such a large effect on the paste wall interaction when used in the binder package.

5.4.4.2 **PEOL**
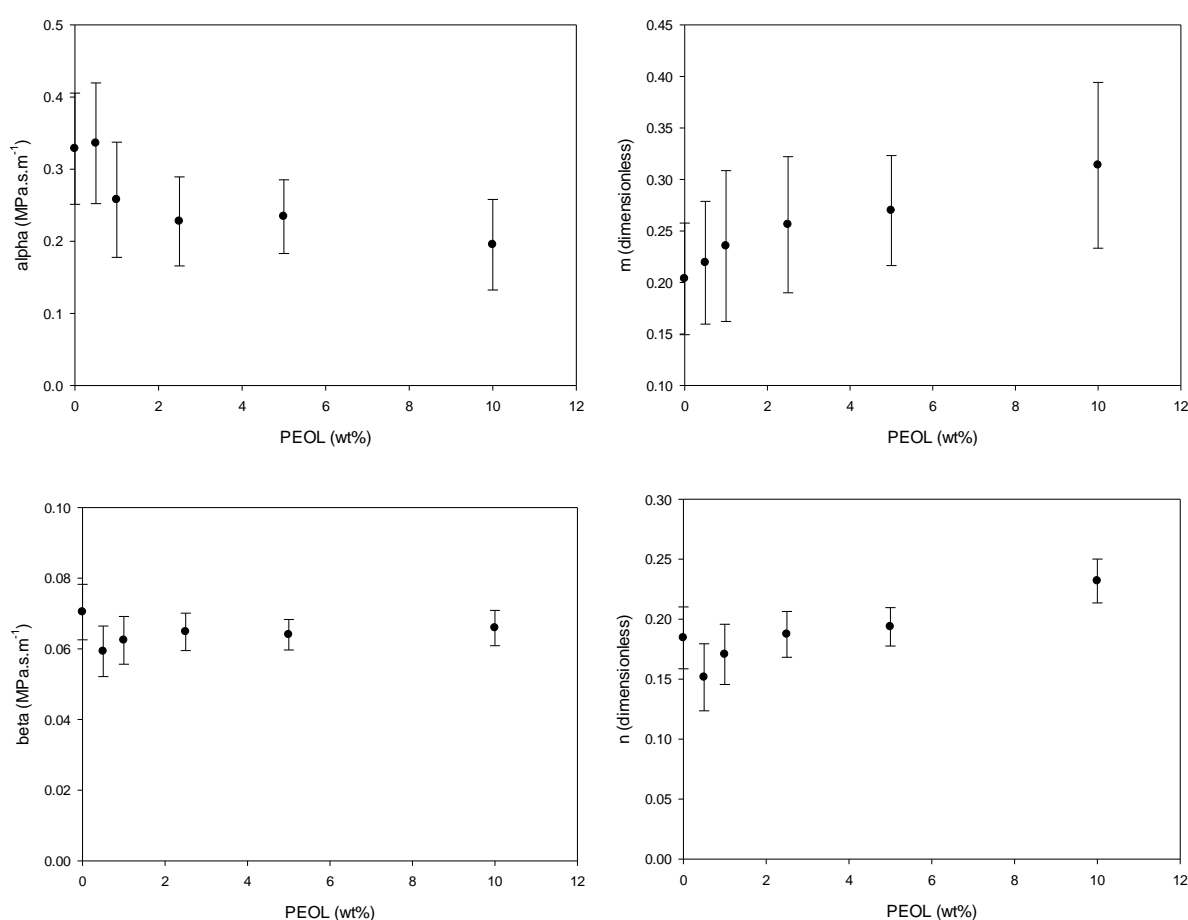
Figure 5.22 - Variation in BB parameters with wt% of PEOL

PEOL has a much smaller effect on the paste rheology that its higher molecular mass counterpart. In each of the plots in Figure 5.22, there is some uncertainty in the BB parameters, as indicated by the fairly large error bars. There is, however, some indication of

the overall trends. It appears that α and m may be lowered and increased respectively with the addition of PEOL. There is very little variation in the value of β. The value of n appears to increase roughly linearly with the addition of this additive.

5.4.4.3 **KH17S**
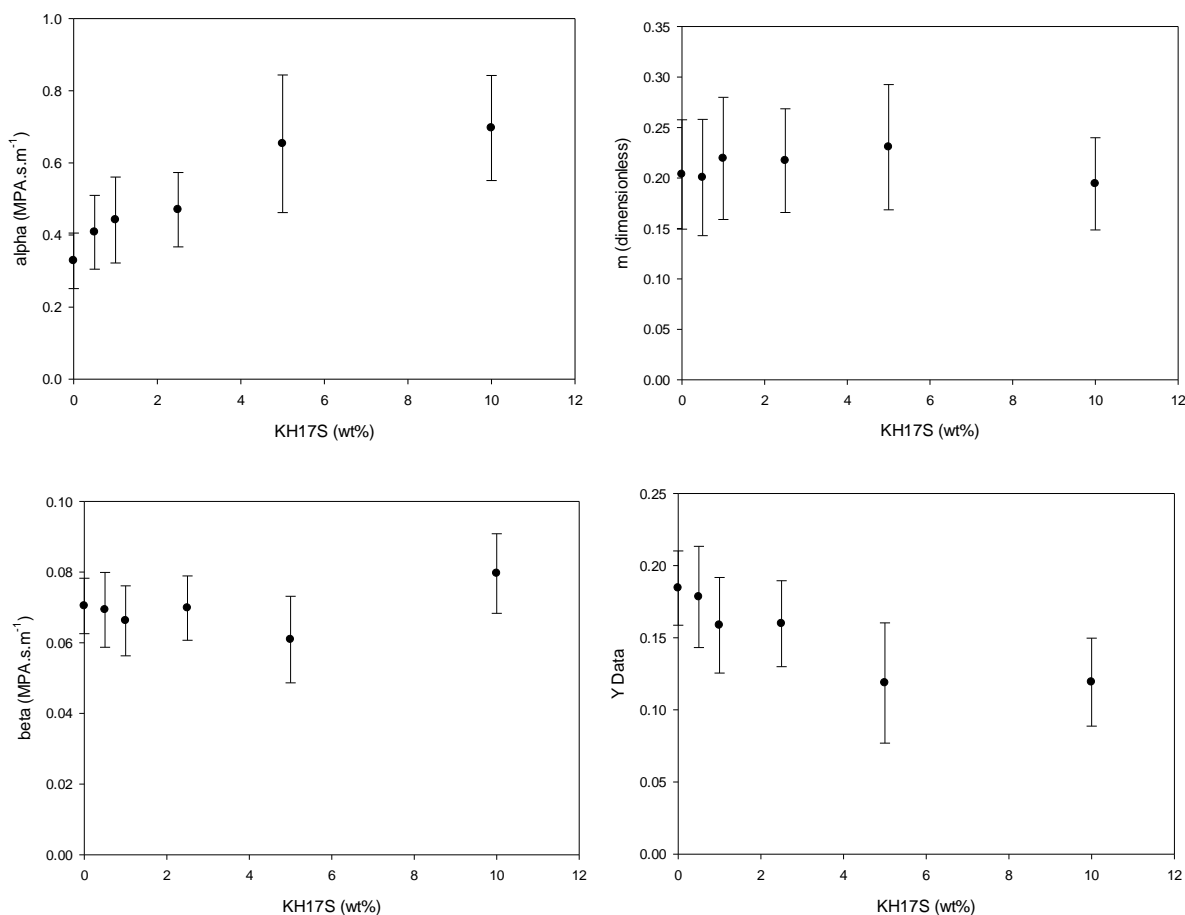
Figure 5.23 - Variation in BB parameters with wt% of KH17S

The effect of KH17S on the paste rheology is not very clear. The value of α appears to increase and n appears to decrease, but in both cases, the effect size is very small. The values of β and m appear to be largely unaffected.

5.4.4.4 **PEG**
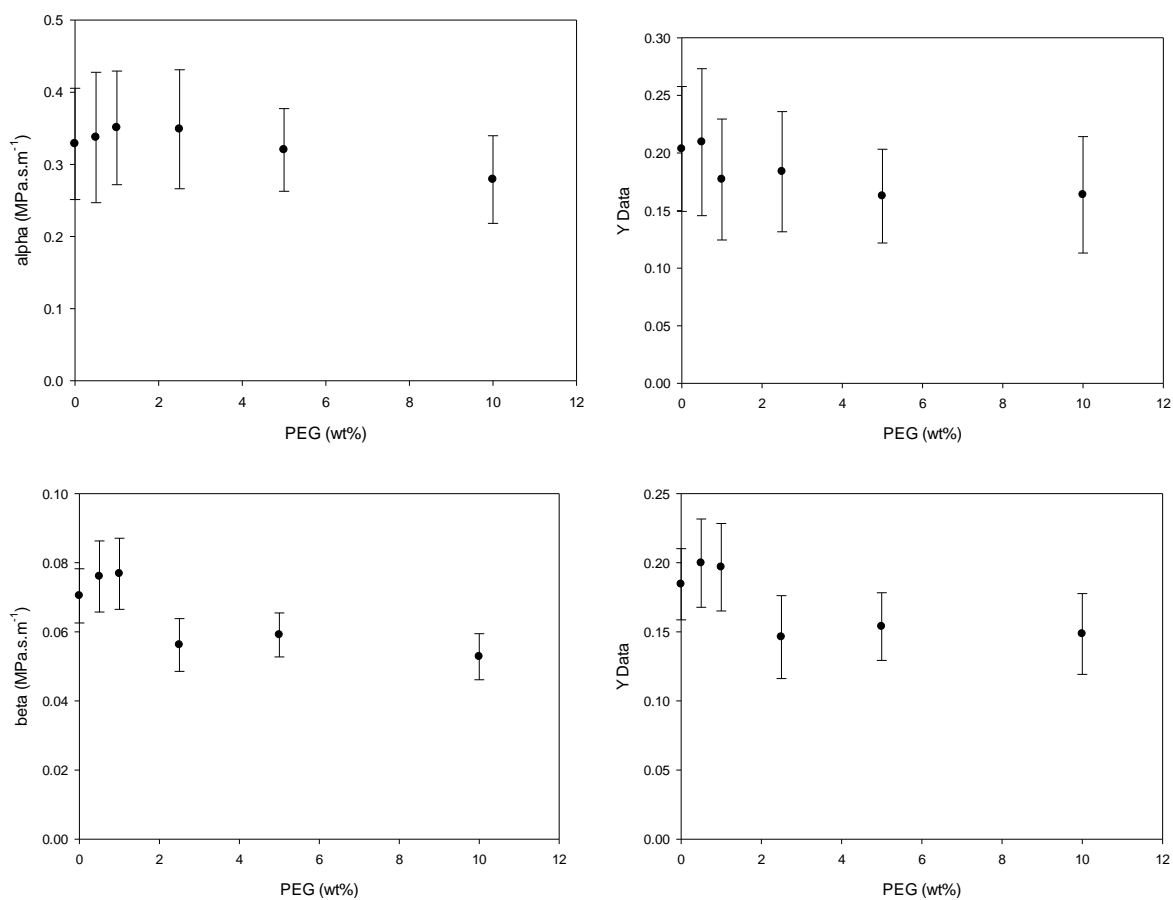
Figure 5.24 - Variation in BB parameters with wt% of PEG

The results show no influence on any of the BB parameters from PEG in the quantities it was incorporated into the pastes. Any effect that it might have is less than the uncertainty in the BB values themselves.

5.4.4.5 **Summary**

A summary of the effects of the four binders used is represented in the 'effects matrix' shown in Table 5.8.

<p align="center">**Table 5.8 - Summary of binder influence on paste rheology**</p>

Additive	α	m	β	n
PEOL	↓	↑	−	↑
PEOH	↑	↑	↓	↓
PEG	−	−	−	−
PVA	↑	−	−	↓

5.4.5   Effect of Benbow Bridgwater Parameters on Flow Profile

The effect of the four BB parameters on formulation variation was investigated using a design of experiments (DOE) approach. This approach involves assigning a high and low level for each of the input variables under investigation and performing a matrix of experiments designed to cover a full or partial range of possible combinations. The results of the experiments may then be collated to determine the influence of each of the input variables on an output variable.

In this work, the four BB parameters were assigned a high or low range and the velocity profile of the theoretical paste was calculated. The standard deviation of the velocities exiting the die was used as a proxy measurement for the evenness of the flow profile.

The 2 level full-factorial design is shown in Table 5.9. High and low ranges for the BB parameters were chosen as representative of the data gathered and presented in section 5.4.4.

Table 5.9 - 2-Level Full Factorial Design

Experiment Number	α	m	β	n
1	0.40	0.25	0.06	0.15
2				0.23
3			0.08	0.15
4				0.23
5		0.74	0.06	0.15
6				0.23
7			0.08	0.15
8				0.23
9	1.23	0.25	0.06	0.15
10				0.23
11			0.08	0.15
12				0.23
13		0.74	0.06	0.15
14				0.23
15			0.08	0.15
16				0.23
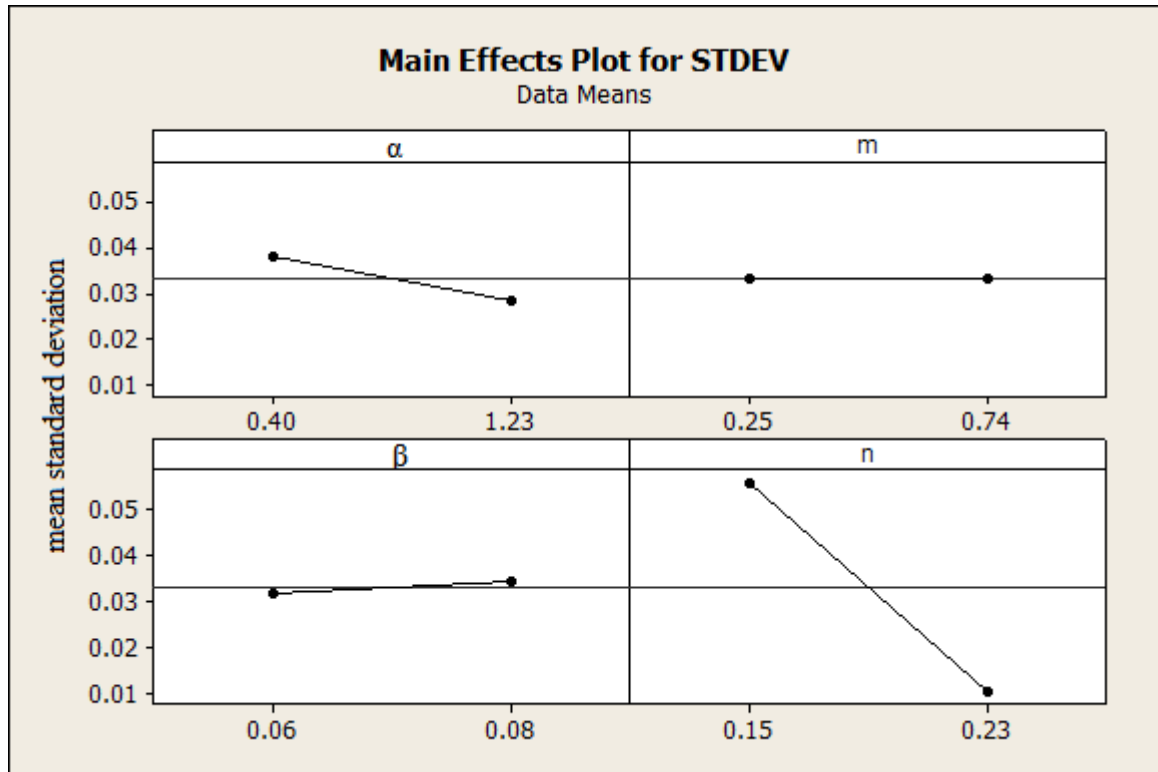
Figure 5.25 - DOE results

Figure 5.25 shows the results of the experiments listed in Table 5.9. The four individual figures represent the effect of each of the BB parameters on the standard deviation of the velocity profile over the face of the die. The x-axis shows the value of the parameter at the high and low levels and the y-axis shows the average standard deviation of the experiments where the parameter was at that level. The gradient of the line connecting the dots is indicative of the effect size of the parameter, with a steeper line indicating a greater influence. As only two levels of each parameter were used, these only serve as a guide to understanding how each of the parameters tends to influence extrusion quality. At this point, it should be again noted that the standard deviation of the βextrusion velocities through unique feed holes is used as a marker for evenness of flow and therefore extrusion quality. As such, a lower standard deviation is indicative of a more evenly flowing paste. As can be seen, β and m have no discernible influence on the flow profile, at least within the range of values encountered in

this work. The value of α has a small positive effect on extrusion quality as it increases. The value of n has by far the greatest influence on the extrusion quality. A low value of n is associated with a paste which is highly sensitive to changes in conditions in the die land. These results are consistent with the findings of the previous approach, discussed in section 5.3.4 and illustrated in Figure 5.14.

Pressure drop in the extrusion die is dominated by the friction at the wall. Changes in wall geometry (or indeed roughness) will lead to changes in extrusion velocity at a given pressure. The size of the change in extrusion velocity is governed by the second half of Equation 5.2 and more specifically the BB parameters β and n. Of these, n has the greatest potential to cause the most sensitivity in the relationship between pressure and velocity. It is for this reason that n has the greatest effect on the potential for variability in extrusion profile and, as is here argued, extrudate quality. The value of n has the potential to significantly affect the sensitivity of the relationship between extrudate velocity and the pressure drop from wall friction. As the honeycomb die geometry is dominated by wall effects, the relationship between extrusion speed and pressure drop in this region is critical.
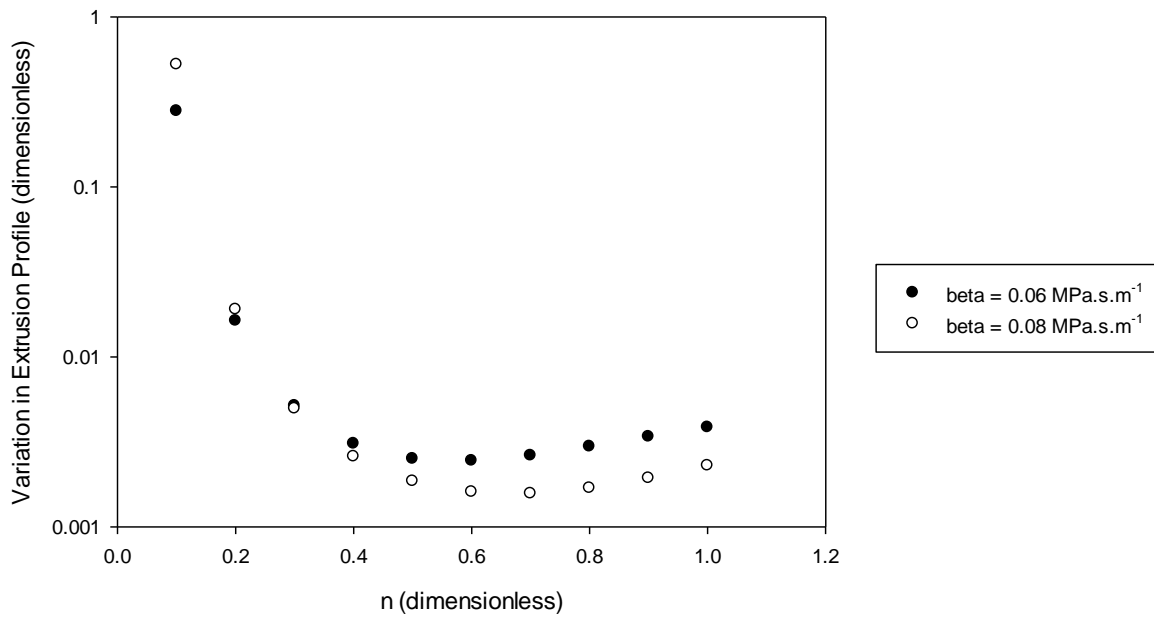
Figure 5.26 – Theoretical change in profile variation with value of n. α and m are constant.

Figure 5.26 shows the change in theoretical extrusion evenness over the full range of values (0.0 – 1.0). These results showed that the variation in flow is at its minimum at or around a value of 0.6. None of the formulations tested in this work had a value of n any larger than 0.23. The effect that n can have on extrusion quality is most significant over the region of 0.0 to around 0.3. Above this value, the potential effect on quality becomes much smaller.
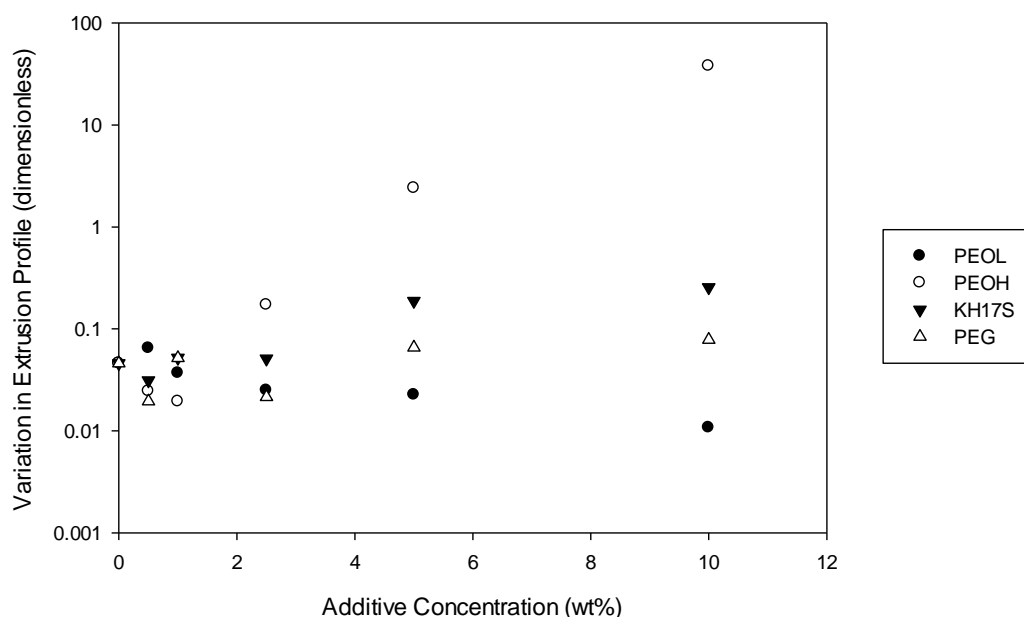
Figure 5.27 - Theoretical effect on extrusion sensitivity for all four binders

The BB parameters measured for the 21 pastes were used to simulate flow through the honeycomb die and the variation in velocity was calculated. The results are shown in Figure 5.27.

These results suggest, as a result of its influence on n, that when PEOH is added in high enough quantity it has the potential to cause pastes to become much more susceptible to any variation in die land conditions.

Conversely, these results indicate PEOL as being a positive influence on extrusion evenness due to the effect it has on n.

As a result of these findings, the standard formulation of pastes used in production at MAST was changed. At MAST Carbon's request, the precise formulation is not reported here, suffice to say that the binder package contained quantities of PEOL and PVA in addition to K15M. The extrusion profile is shown in Figure 5.28In the following trial period, monoliths were

produced on a regular basis on both small and large scale extruders through a range of different die designs. The rejection rate due to defects formed during extrusion was 0%.

Figure 5.28 – Extrusion profile of reformulated paste

5.4.6 Effect of Varying Die Geometry on Flow Profile

This method of applying the Benbow Bridgwater model to the die geometry allows the prediction of how changes in the geometry affect paste velocity. 3 different diameters of washer are available at MAST for their extrusion tools. The feed holes were characterised for each of the washer and the extrusion profiles of a selected paste were calculated.
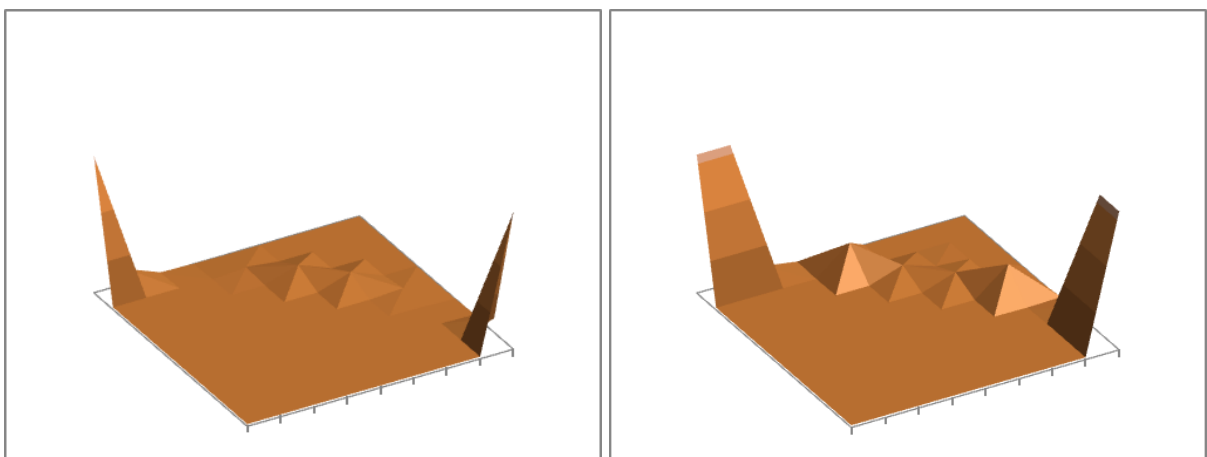
Figure 5.29 – Visualisation of extrusion profile with a Ø 27.0 mm (left) and Ø 27.4 mm (right) washer
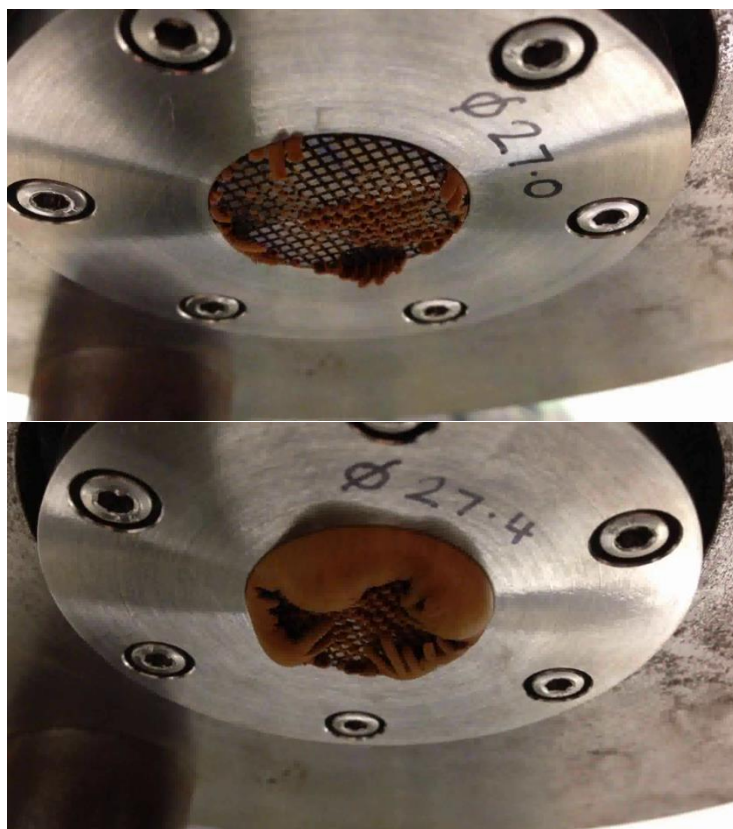
Figure 5.30 - Difference in extrusion profile between Ø 27.0 mm (top) and Ø 27.4 mm (bottom) washer

The Benbow Bridgwater model predicts that the wall velocity will increase compared to the central feed holes when the diameter of the washer is increased. These profiles match very well with monoliths which were extruded in these geometries.

5.5 Discussion

It was found to be extremely difficult to both define and measure monolith quality. Defects which form during extrusion may manifest themselves in a variety of different but overlapping ways. As a result, the subjective analysis was generally muddied and unreliable. Attempting to rate the defects separately led to a large difference in scores awarded between operators. By rating the monoliths on an overall basis, it was possible to get repeatable data, albeit with less specificity. Ultimately, this approach was not sufficient to draw any firm conclusions about the relationship between quality and paste rheology, therefore it was not

possible to gain any understanding of the formation of defects. That being said, there was some suggestion of an effect of the exponential wall friction term, n, on overall quality. This relationship was thought to be plausible as the extrusion die is dominated by pressure drop from wall friction.

A common cause of defects formed during honeycomb extrusion was proposed. It was hypothesised that the common defects such as surface tearing and curved extrusion were caused by a difference in the extrusion rates of paste streams exiting the die. By applying the Benbow Bridgwater model to each feed hole individually, it was possible to predict the initial extrusion velocity profile over the face of the die. It was then shown that the most significant effect on the variation of extrusion velocities comes from the BB parameter, n. This is supported by the qualitative results from the first approach. It was also demonstrated that the BB parameters could be controlled by varying the binder package in the paste. This made it possible to reformulate the paste according to which BB parameters were required to prevent uneven flow through the extrusion die. The reformulated paste was trialled during a production run at MAST and no extrusion defects were encountered.

This approach of applying the Benbow Bridgwater model has the potential to guide rheologists in two ways. First, it provides us with an ability to predict how a paste will behave in any given honeycomb type geometry, allowing one to design dies in such a way as to reduce the potential for defect formation. Secondly, by understanding how the additives in the binder package impact paste rheology as described by the BB model, it is possible to formulate a paste with the least potential to form extrusion defects. This latter approach has been adopted at MAST and reformulation has seen the rejection rate of production monoliths fall to 0.

It should be noted that the reduction in the formation of defects via the prevention of uneven flow, relies on the assumption that the paste being extruded remains stable and homogenous. If the paste becomes unstable, it may no longer behave as an elasto-viscoplastic and localised areas may fracture in the manner described. The following chapter deals with the problem of phase migration in pastes, a common cause of paste instability.

6 PHASE MIGRATION

In this chapter, the stability of phenolic resin pastes is shown to be linked to the viscoelasticity of the binder. Various concentrations and grades of Polyethylene Oxide (PEO) are characterised using the power-law fluid model. An empirical relationship between concentration and rheology is used to predict that two different grades of PEO can be dissolved at different concentrations and exhibit the same shear rheology, whilst having different viscoelastic properties. Unstable pastes were made from these binders and are made to undergo phase migration. It is shown that the rate of phase migration is different for each binder, despite having the same shear viscosity. The higher molecular mass PEO is shown to have a higher elastic component and is more resistant to dewatering.

6.1 Introduction

Phase migration had not previously been identified as a major source of problems for monolith production prior to the commencement of this work. MAST Carbon's typical formulation included a high concentration of K15M (in the region of 10 to 20 wt% in water) which reduced the occurrence of phase migration and prevented it from causing issues. During very early pilot work into adjusting the paste formulation, it was found that phase migration could very readily occur with the phenolic resin powder unless a high concentration of K15M was used.

6.1.1 Background

During a discussion regarding formulation adjustment at early stages of this work, two pastes, in particular, led to the idea that polymer chain length of the binder may have some significance with regard to phase migration. Both pastes consisted primarily of an aqueous solution of Polyethylene Oxide as a binder, one with a molecular mass of 6,000 g.mol^{-1} (PEG) and the other with a molecular mass of 5,000,000 g.mol^{-1}(PEOH). There was a marked difference between the stability of the two pastes. Both were extruded through a set of cylindrical dies at various ram speeds. A more detailed description of the procedure is given in Chapter 4. During these test extrusions, it was observed that the paste containing the lower molecular mass PEG suffered badly from phase migration while the paste containing the higher molecular mass PEOH, while still showing signs of phase migration, was much more stable. The two extrusion profiles are shown in Figure 6.1 and show the marked difference in stability.
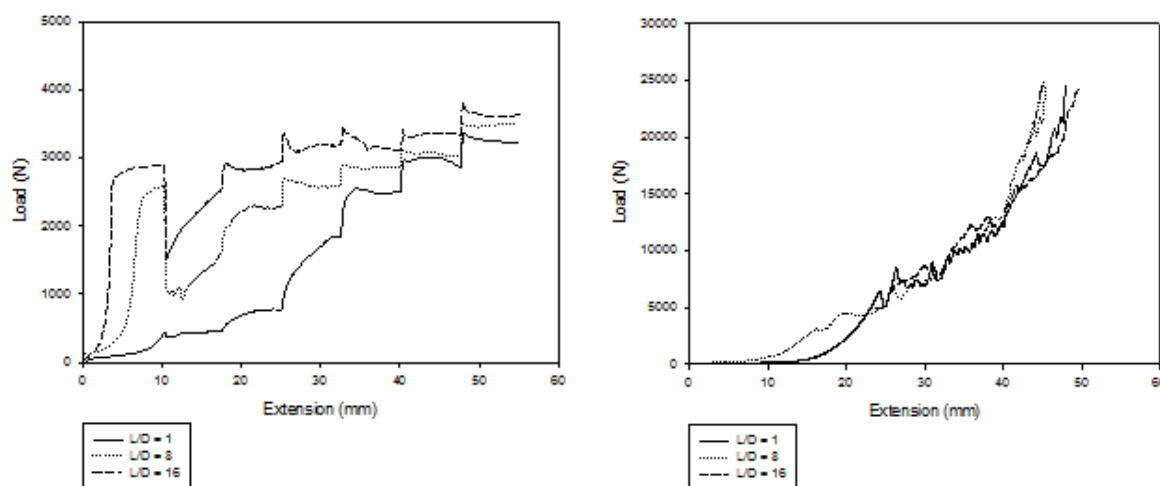
Figure 6.1 - Extrusion profiles for 2 different pastes containing PEOH (left) and PEG (right)

During extrusion, phase migration manifests as the initial paste being much wetter than the bulk. The extrusion pressure very quickly increases as the paste in the barrel dries out. This is shown clearly on the PEG extrusion profile.

6.1.2   Polyethylene Oxide

While reviewing these extrusion profiles, it was considered that the differences in the lengths of the two forms of PEG might be a contributing factor to the binder stability. PEO is a simple chain polymer; the monomer unit is shown in Figure 6.2. As the molecule features no side chains, the only difference between the high and low molecular mass forms of this molecule is the length of the chain.
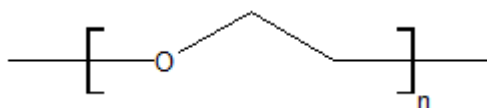
Figure 6.2 - Monomer unit of Polyethylene Oxide

It was thought that this simple difference might account for the difference in phase migration, particularly as the pastes behaved similarly when handled. One explanation considered for the

hypothetical effect of chain length on dewatering was that the heavier forms of PEO would entangle more and thereby reduce the rate of phase migration.

6.2 PEO Binder Characterisation

The viscosity of the binder is a significant contributor to the rate at which the paste will dewater. In order to isolate the effect of chain length, it was very important to eliminate rheological variation in shear viscosity as a variable. This was done by first determining the power law rheology models for each of the binders at various concentrations in water. It was then possible to use this information to create a set of binders which had the same shear rheology (and therefore viscosity at a given shear rate) but consisted of PEO of different molecular masses and chain lengths.

6.2.1 Sample Preparation

4 grades of PEO were selected and obtained from Sigma-Aldrich. The range of molecular masses chosen and the codes to which they are referred are shown in Table 6.1.

Table 6.1 - Grades of PEO used

Code	Molecular Mass $(g.mol^{-1})$
200kPEO	200,000
400kPEO	400,000
1MPEO	1,000,000
4MPEO	4,000,000

8 samples of each grade of PEO were prepared 24 hours before being tested at various concentrations equally distributed from 1.25 wt% to 10.00 wt%. Samples were prepared at specified concentrations and 100 ml of distilled water was used in each case. Figures are reported in weight percent with respect to the mass of water.

The mass of PEO powder was difficult to control and as a result, the concentrations varied slightly from those stated. Exact concentrations were recorded and used for all calculations in section 6.2.3.

Binder solutions were prepared by adding distilled water to powdered PEO in a beaker and worked with a spatula. Samples were then covered and left overnight to fully dissolve.

6.2.2 Sample Rheometry

Approximately 2 ml were removed from the 100 ml samples and tested on an AR-500 rheometer. Tests were conducted with a cone and plate geometry. The test was performed over a range of shear rates from 100 to 2000 s^{-1}, distributed logarithmically.
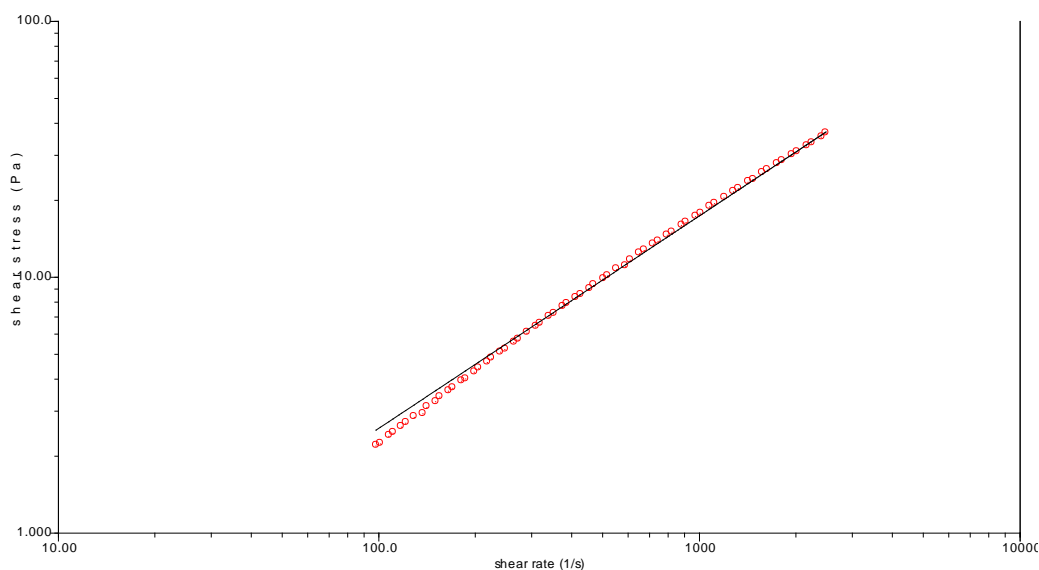
Figure 6.3 - Stress/Strain Curve for 1.25 wt% solution of 400k PEO

Figure 6.3 shows one set of rheometric results for a solution of 400kPEO. Results were analysed using TA Instruments Rheology Advantage Data Analysis suite. A power law model (Equation 7.1) is fitted to the data set from within the software. This was repeated up to 4 times for each sample and power law models fitted to each curve. Figure 6.4 shows the results

from 3 such repeats on 1.25 wt% solution of 400kPEO. The stress-strain curves overlap almost exactly between tests.

$$\tau = k\dot{\gamma}^n$$ **Equation 6.1**
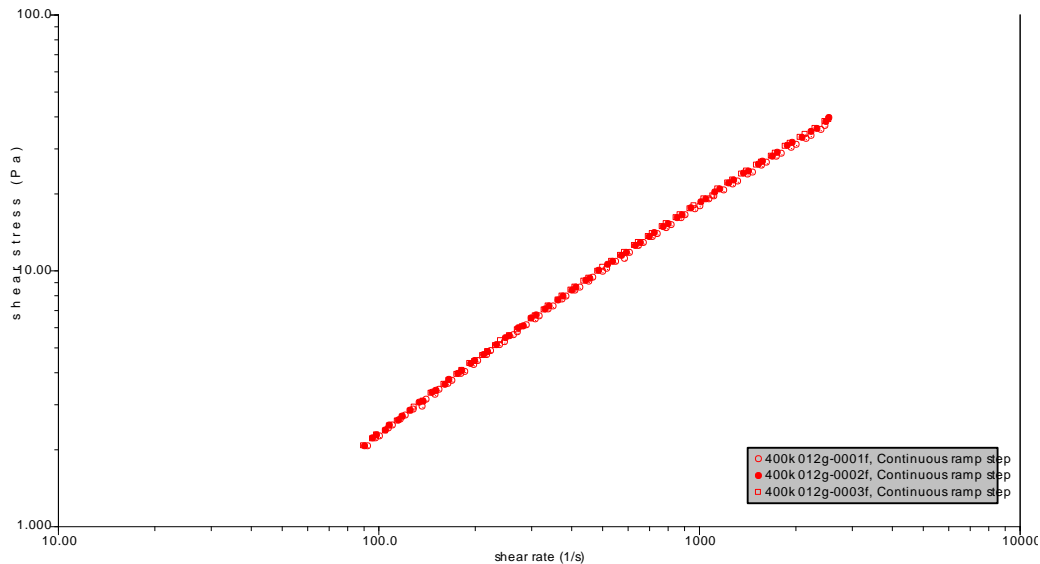
Figure 6.4 - Results for 3 different tests on 1.25 wt% solution of 400kPEO

The power law constants, k, and n, for each set of results were averaged and 95% confidence intervals calculated.

The results for all 4 grades are plotted in Figure 6.5 and Figure 6.6. Increasing the chain length and concentration increases the strength of the polymer network in solution by increasing the amount of chain entangling. The power law model contains 2 parameters, the consistency index (k) and the behaviour index (n). The consistency index may be generally considered to describe how 'stiff' or 'viscous' (the term being used here in a general sense) the fluid is. The behaviour index describes the degree of shear thinning the fluid will undergo as strain rate increases.

Table 6.2 - Power law constants for various concentrations of 400kPEO

Concentration (wt%)	k (Pa.s)	n (dimensionless)	Error in k (95% confidence)	Error in n (95% confidence)
0.00	0.00	1.00	0.00	0.00
1.29	0.05	0.84	0.00	0.00
2.50	0.08	0.83	0.02	0.01
3.07	1.47	0.63	0.03	0.00
3.75	3.10	0.59	0.22	0.00
5.00	8.56	0.56	1.51	0.03
6.20	27.16	0.47	8.68	0.06
7.48	40.60	0.45	4.02	0.03
8.70	70.59	0.41	5.57	0.02
10.00	75.12	0.50	7.98	0.02

As was expected, the consistency index (k) increases with both concentration and polymer chain length because the increased strength of the chain network contributes to the 'stiffness' of the fluid. Also as expected, the value of 'n' decreases with increasing concentration and molecular mass. Shear thinning is caused by the breakdown of the polymer network as shear is applied to the fluid. At rest, the polymer network is strongest and as shear is applied, the network is disrupted and the apparent viscosity of the fluid decreases. At higher concentrations and chain length, there are more entangled chains to become disrupted and therefore a higher degree of shear thinning is observed.
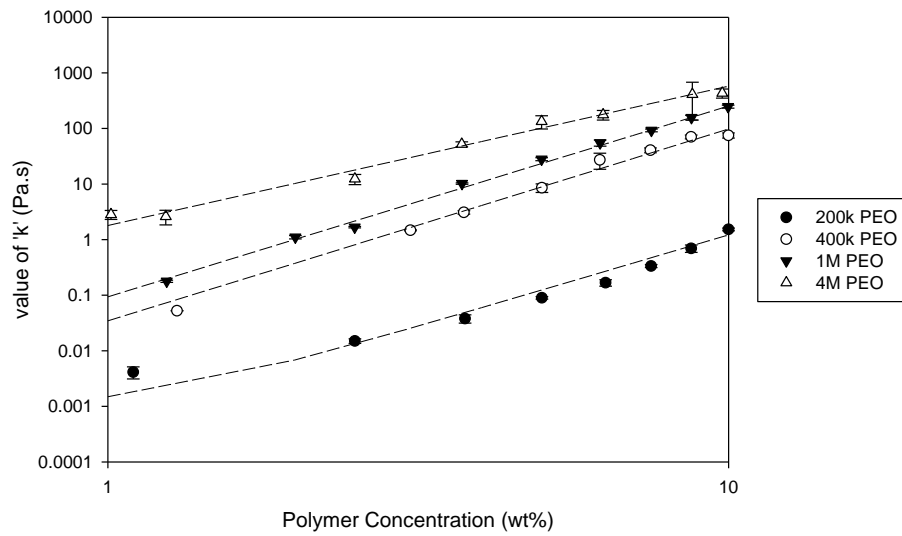
Figure 6.5 - Change in consistency index (k) with concentration for 4 PEO grades
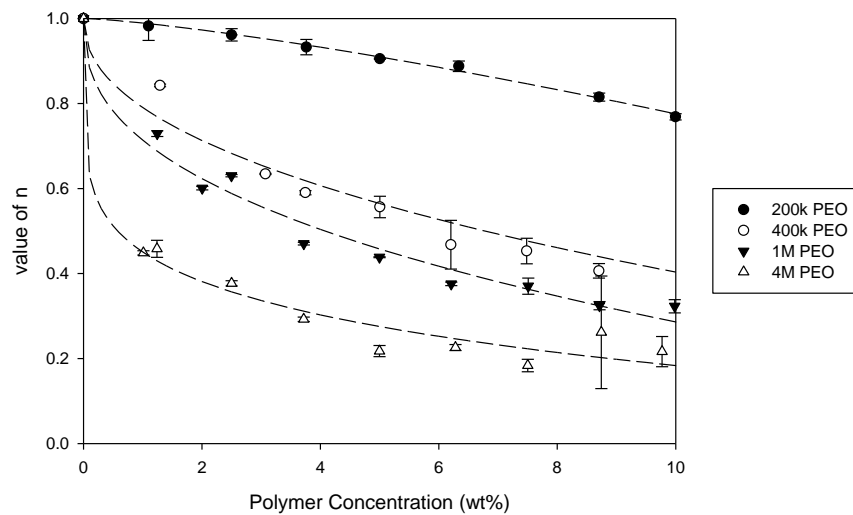
Figure 6.6 - Change in behaviour index (n) with concentration for 4 grades of PEO

6.2.3   Relationship between chain length, concentration and rheology

The data gathered allowed a relationship between concentration and rheology to be determined for each of the PEO grades studied. An empirical relationship was fitted to each of the data sets, shown in Figure 6.5 and Figure 6.6 by dashed lines. These curves primarily exist to allow prediction of rheology at intermediate concentrations rather than to reveal any intrinsic rheological property of PEO.

The equations describing the empirical relationship between concentration and the power law constants are given in Equation 6.2 and Equation 6.3. The equations were fitted to the data set using SigmaPlot's non-linear regression curve fitting feature and the resulting fitting parameters A – E are given in Table 6.3.

$$k = A + B \times conc^C$$

Equation 6.2

$$n = 1 - D \times conc^E$$

Equation 6.3

Table 6.3 - Fitting parameters for Equation 6.2 and Equation 6.3

PEO Grade	A	B	C	D	E
200k	8.90E-04	6.0E-04	3.31	0.01	1.31
400k	8.90E-04	0.03	3.46	0.21	0.45
1M	8.90E-04	0.09	3.44	0.29	0.40
4M	8.90E-04	1.79	2.51	0.55	0.17

The curves appear to fit the data very well and allowed determination of the rheology of intermediate concentrations.

The next step was to use this information to determine at which concentrations and polymer chain lengths the rheology of two fluids would overlap. To do this, first, the fitting parameters were plotted against polymer chain length. This showed that there is a dramatic change in the relationship between concentration and the value of 'k' between 1MPEO and 4MPEO. That is to say that the three lowest grades of PEO all have similar relationships between k and concentration whereas 4MPEO is quite different. This suggested that it would be more likely to find overlapping values of k using the three lowest weight grades of PEO.

Conversely, it was found that there was a dramatic change in the relationship between n and concentration between 200kPEO and 400kPEO. That is to say that the three *highest* weight grades of PEO all share a similar relationship with n and concentration. This result suggests that the three highest grades of PEO are more likely to have the potential for overlapping rheology.

Taking both of these results into account, it was decided that a comparison should be made between 400kPEO and 1MPEO.

In order to accomplish this, the rheology, defined by the power law constants (k and n), of concentrations of 400KPEO and 1MPEO at 0.5 wt% intervals up to 10 wt% were calculated. Then a simple error value was calculated for values of k and n were calculated using Equation 6.4. The results are shown in

Table 6.4.

$$'error' = \frac{k_{400kPEO} - k_{1MPEO}}{k_{400KPEO}}$$

Equation 6.4

Table 6.4 - Comparison of power law constants for 400KPEO and 1MPEO at the same concentrations

Concentration	k		n		'error'	
wt%	400kPEO	1MPEO	400kPEO	1MPEO	k	n
0.5	0.00	0.01	0.85	0.78	1.39	0.08
1.0	0.03	0.09	0.79	0.71	1.70	0.10
1.5	0.14	0.37	0.75	0.66	1.70	0.11
2.0	0.37	1.00	0.71	0.62	1.69	0.13
2.5	0.81	2.16	0.68	0.59	1.67	0.14
3.0	1.52	4.04	0.65	0.56	1.66	0.15
3.5	2.59	6.86	0.63	0.53	1.65	0.16
4.0	4.11	10.85	0.61	0.50	1.64	0.17
4.5	6.17	16.27	0.58	0.48	1.63	0.18
5.0	8.89	23.36	0.56	0.46	1.63	0.19
5.5	12.37	32.42	0.55	0.44	1.62	0.20
6.0	16.72	43.71	0.53	0.42	1.61	0.21
6.5	22.06	57.55	0.51	0.40	1.61	0.22
7.0	28.51	74.24	0.49	0.38	1.60	0.23
7.5	36.20	94.10	0.48	0.36	1.60	0.24
8.0	45.27	117.47	0.46	0.35	1.59	0.25
8.5	55.85	144.67	0.45	0.33	1.59	0.26
9.0	68.07	176.07	0.43	0.32	1.59	0.27
9.5	82.09	212.01	0.42	0.30	1.58	0.28
10.0	98.04	252.88	0.40	0.29	1.58	0.29

Using the solver tool in Microsoft Excel, the concentration of 1MPEO was varied until the combined 'error' in k and n was minimised. This was repeated for each 400kPEO concentration, resulting in a range of solutions with similar power law parameters.

Table 6.5 – Predicted concentrations of 1MPEO to match power law constants

Concentration		k		n		error	
400kPEO	1MPEO	400k	1M	400k	1M	k	n
0.500	0.371	0.00	0.00	0.85	0.81	0.000	0.040
1.000	0.746	0.03	0.03	0.79	0.75	0.000	0.045
1.500	1.122	0.14	0.14	0.75	0.70	0.000	0.048
2.000	1.499	0.37	0.37	0.71	0.66	0.000	0.049
2.500	1.877	0.81	0.81	0.68	0.63	0.000	0.050
3.000	2.256	1.52	1.52	0.65	0.60	0.000	0.050
3.500	2.635	2.59	2.59	0.63	0.58	0.000	0.050
4.000	3.014	4.11	4.11	0.61	0.56	0.000	0.050
4.500	3.394	6.17	6.17	0.58	0.54	0.000	0.050
5.000	3.775	8.89	8.89	0.56	0.52	0.000	0.050
5.500	4.155	12.37	12.37	0.55	0.50	0.000	0.049
6.000	4.536	16.72	16.72	0.53	0.48	0.000	0.049
6.500	4.917	22.06	22.06	0.51	0.46	0.000	0.048
7.000	5.298	28.51	28.51	0.49	0.45	0.000	0.047
7.500	5.680	36.20	36.20	0.48	0.43	0.000	0.047
8.000	6.062	45.27	45.27	0.46	0.41	0.000	0.046
8.500	6.443	55.85	55.85	0.45	0.40	0.000	0.045
9.000	6.825	68.07	68.07	0.43	0.39	0.000	0.045
9.500	7.208	82.09	82.09	0.42	0.37	0.000	0.044
10.000	7.590	98.04	98.04	0.40	0.36	0.000	0.043
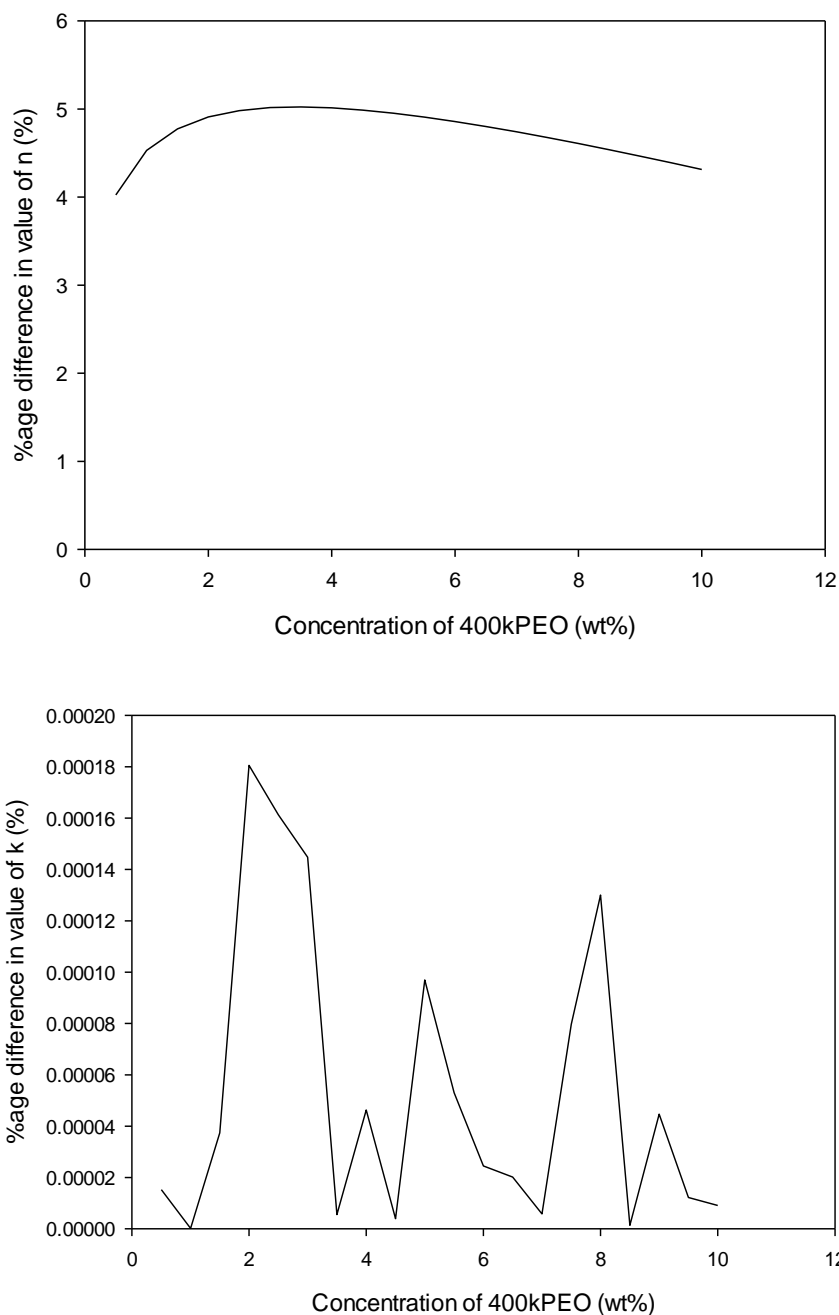
Figure 6.7 - Similarity of power law parameters for 400kPEO and 1MPEO solutions

In all cases, it was possible to get the error in the power law parameters down to 5% or less. Figure 6.7 shows the variation in the similarity in power law constants achieved at various concentrations. The constants become slightly easier to overlap as concentration increases, likely due to the increase in the magnitude of k.

It was important to select a pair of solutions which had a low enough value of k that phase migration would be observed, but not low enough that dewatering would occur too rapidly to be studied. To satisfy this, a concentration of 4.0 wt% 400kPEO and a corresponding 3.0 wt% of 1MPEO were selected, despite having close to the highest error in power law parameters. The error was still very low and increasing the concentrations would have increased the value of k without very much benefit with regard to the closeness of the power law constants.

6.2.4   Verification of Similarity

Solutions of 4.0 wt% 400kPEO and 3.0 wt% of 1MPEO were prepared and a continuous shear stress ramp test was performed. A shear stress range of .01 to 100 Pa was applied and the shear rate response was measured. Figure 6.8 shows the response curves of the two solutions.
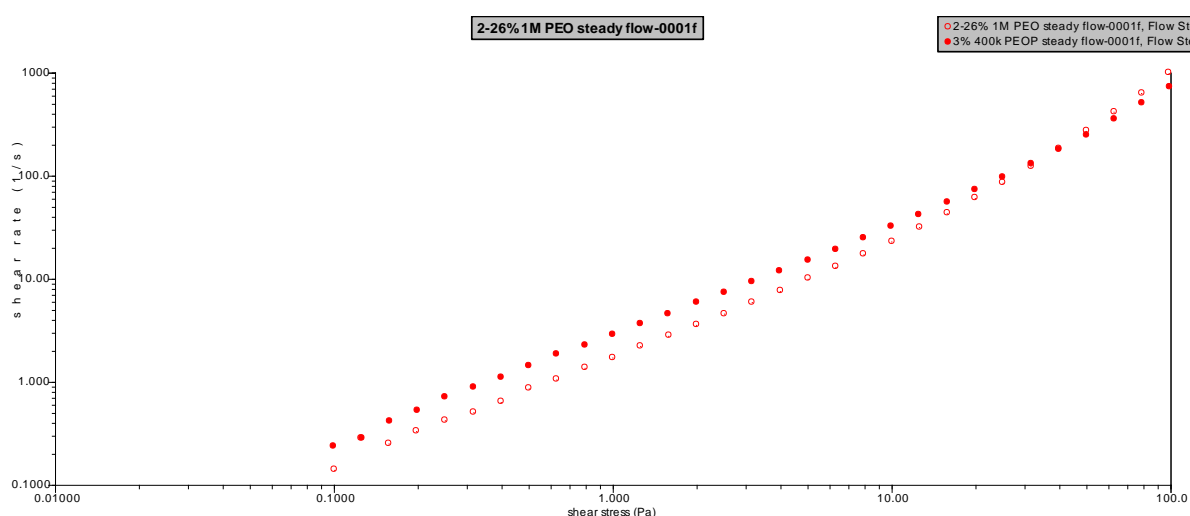
Figure 6.8 - Shear Rheology of two binder systems

These results show that the shear rheology of the two systems is very close, as predicted by the results in Table 6.5. The two systems most closely match over a shear range close to $100 - 1000 \text{ s}^{-1}$.

The shear rate in the die land can be estimated from Equation 6.5.

$$\dot{\gamma} = \frac{8V_e}{d}$$

Equation 6.5

The ram speed in the experiments was 5 mm.min^{-1}. Assuming that the paste is incompressible, the extrudate speed may be calculated from the ram speed using Equation 6.6.

$$V_e = \frac{A_0 \times V_r}{A}$$

Equation 6.6

With a barrel diameter is 35 mm, die diameter of 3 mm and ram speed of 15 mm.min^{-1}, the extrudate velocity is approximately 0.034 m.s^{-1}. Using the diameter of the die as the characteristic length in Equation 6.5, the shear rate experienced by the binder in the die land is calculated as follows:

$$\dot{\gamma} = \frac{8V_e}{d}$$
$$\dot{\gamma} = \frac{8 \times 0.034}{.003}$$
$$\dot{\gamma} = 90.7 \ s^{-1}$$

This places the environment in the die land very close to the region in which the two binder systems are closest in terms of simple rheology.

6.2.5 Viscoelasticity Measurements

In addition to having their shear rheology measured, oscillatory rheometry was performed to measure the viscoelastic properties of the systems. Figure 6.9 shows the results. From the figure, it is clearly shown that the 400kPEO binder has a higher value of $\tan(\delta)$ (defined in Equation 6.7) than the 1MPEO binder across all test conditions.

$$\tan(\delta) = \frac{G''}{G'} \qquad\qquad \textbf{Equation 6.7}$$

This shows that the lower molecular mass solution has a higher loss to storage modulus ratio and implies a greater tendency to behave in a 'liquid' manner when compared to the higher molecular mass solution.
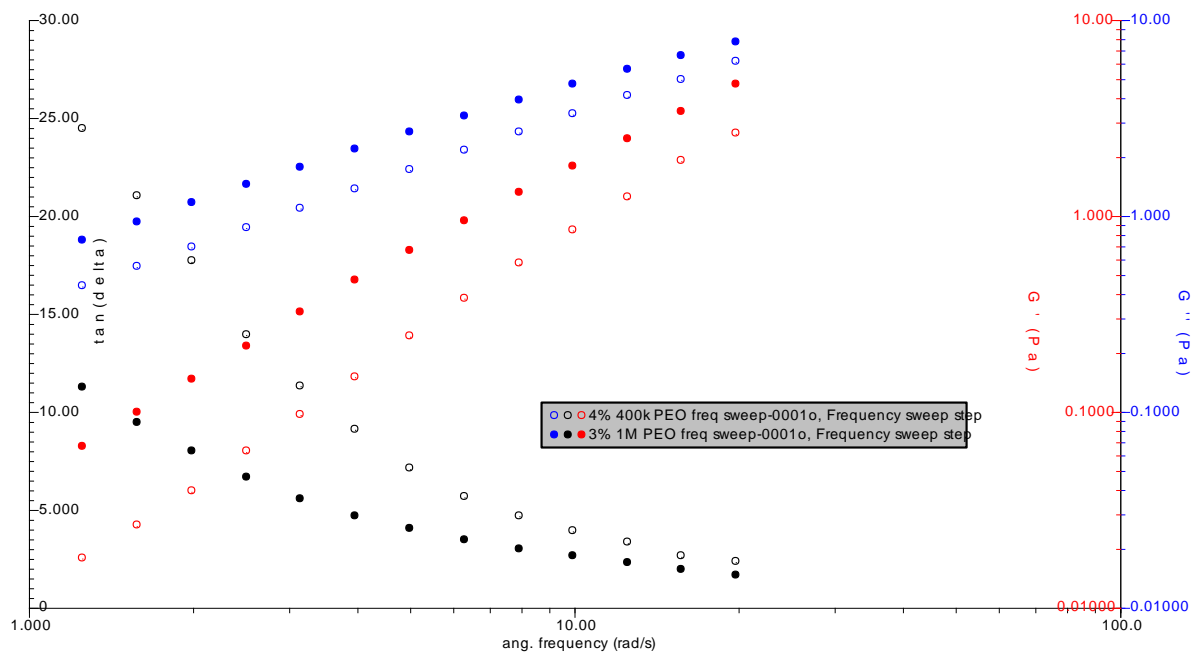
Figure 6.9 - Difference in viscoelasticity between binders

6.3 Phase Migration Measurements

6.3.1 Paste Preparation

MAST Carbon uses a specific blend of fine and coarse particles in normal production. The initial run of pastes used for this work was prepared using the same particle size blend in order to keep conditions as close to production as possible. The initial pastes showed many signs of general instability but no steady increase in extrusion pressure was observed. It was

quickly realised that the inclusion of the fine particle grade was decreasing the permeability of the solid matrix and preventing phase migration from occurring. In a production setting, this is a highly desirable result but for the purposes of investigating the phenomena, the fine particle fraction was removed.

The second run of pastes contained only coarse (~40 µm diameter) resin particles. The pastes contained only resin, water and wither 400kPEO or 1MPEO as a binder phase. Dry ingredients were mixed in a small z-blade mixer for 1 minute before water was added. The paste was allowed to mix for 20 minutes. Any paste which had adhered to the walls was occasionally reintroduced into the bulk of the mixer. Pastes were removed from the mixer and placed in a drawer overnight to equilibrate. The formulations are shown in Table 6.6.

Table 6.6 - 2nd Batch Paste Formulations

	400k Paste	1M Paste
Coarse Resin	60.0	60.0
Water	33.0	33.0
400kPEO	1.32	-
1MPEO	-	0.99

A third and final batch of pastes were prepared with slight modification to the formulation. The amount of water was increased to encourage more phase migration. 60 g of resin was not quite enough to fill the mixer and as a result, the paste was not mixing fully. The amount of resin was increased to 150 g. This better utilised the capacity of the mixer and also allowed for a longer extrusion run, allowing the experiment to run to completion. The revised formulation is shown in Table 6.7. In addition to the revised paste formulation, the extrusion and mixing facilities were moved to a different location. In the new laboratory, the temperature of the room could be controlled at 20℃ whereas the temperature in the previous

room varied with the prevailing weather conditions. Pastes were also kept in a refrigerator to equilibrate, rather than a bench drawer.

Table 6.7 – 3ʳᵈ Batch Paste Formulation

	400k Paste	1M Paste
Coarse Resin	150.0	150.0
Water	80.0	80.0
400kPEO	3.12	-
1MPEO	-	2.40

6.3.2 Extrusion Profiles

Extrusion profiles from the initial batch of pastes were extremely variable and did not show signs of phase migration. Figure 6.10 shows extrusion profiles for three pastes of the same formulation. An initial increase in pressure was followed by the onset of visible extrusion. The extrusion load quickly dropped and rise sharply to the instrument maximum load (10 kN). This is not shown in Figure 6.10 as the pressure increase happened faster than instruments sampling rate.
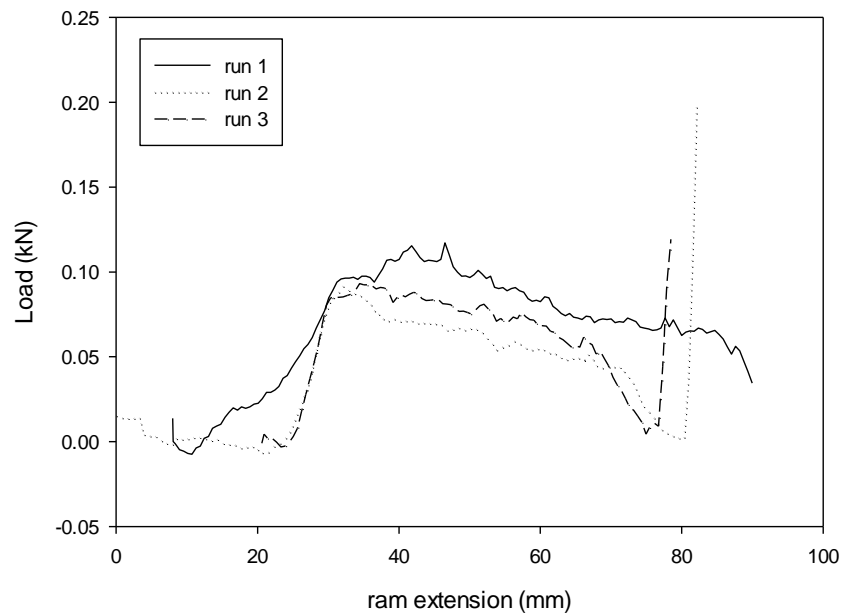
Figure 6.10 - Unstable extrusion profiles

Reformulation improved the paste stability. Fines had been removed from the formulation and mixing times were standardised.

The extrusion profiles obtained all follow the same general pattern. There is a steady increase in extrusion pressure as the ram coming into contact with the paste and is compacted. Visible extrusion occurs at or around a peak extrusion pressure, after which the extrusion pressure decreases. This is typical behaviour in a ceramic paste extrusion. In a stable paste, the extrusion pressure will then remain at a constant equilibrium extrusion pressure as long as the ram speed is not changed. In all of these extrusion profiles, the extrusion pressure increased, eventually reaching the maximum capacity of the load frame of 10 kN.
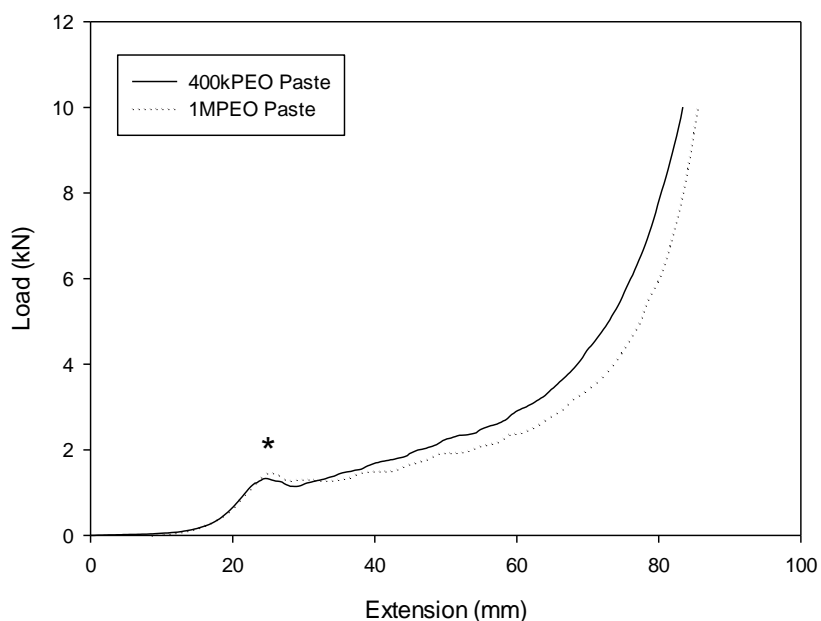
Figure 6.11 - Extrusion profiles for 400k and 1M PEO pastes. * indicates the onset of visible extrusion.

Figure 6.11 shows two typical extrusion profiles for the pastes containing 400k and 1MPEO as the binder phase. These profiles have been adjusted so that they overlap at the point of extrusion. These samples were prepared and tested in parallel to reduce the effect of ambient conditions on the results. These profiles track each other very closely up to the point of extrusion. After visible extrusion has begun, the extrusion profiles begin to diverge. The paste containing 400kPEO sees the extrusion pressure increasing at a higher rate than the paste containing 1MPEO as a binder. This appears to support the idea that low molecular mass binders are more prone to phase migration.
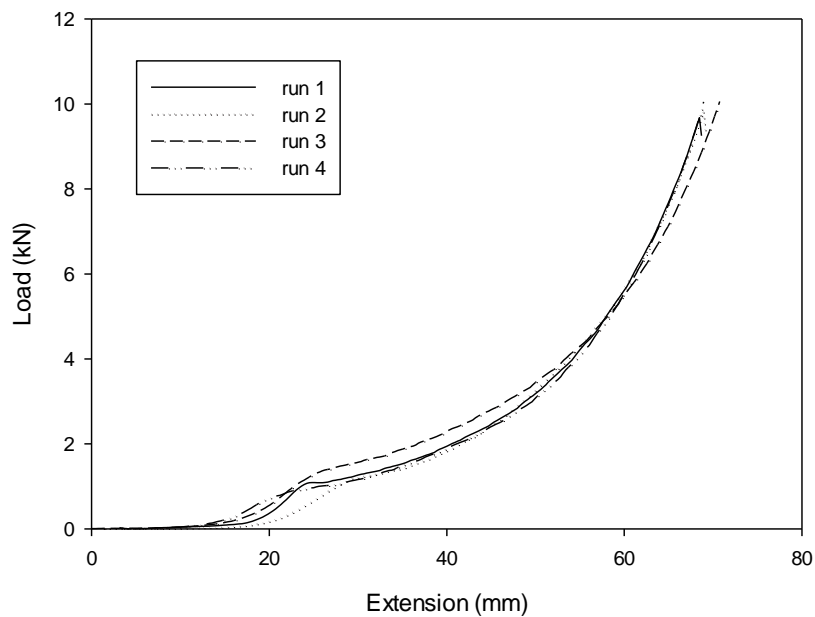
Figure 6.12 - Runs 1 to 4 of 400kPEO pastes

Figure 6.12 show the extrusion profiles of 4 tests done on 400kPEO pastes. All profiles have been aligned at the onset of extrusion. These results show that the paste behaviour is repeatable between samples. Figure 6.13 shows these plots averaged with 95% confidence intervals. This figure, in particular, shows that there is a very small variation in most of the extrusion profile with most of the variation found in the initial pressure increase as the paste is compressed. This is likely due to the differences in paste compression arising from slight variations in the way paste is packed into the barrel and is unrelated to the paste properties being studied.
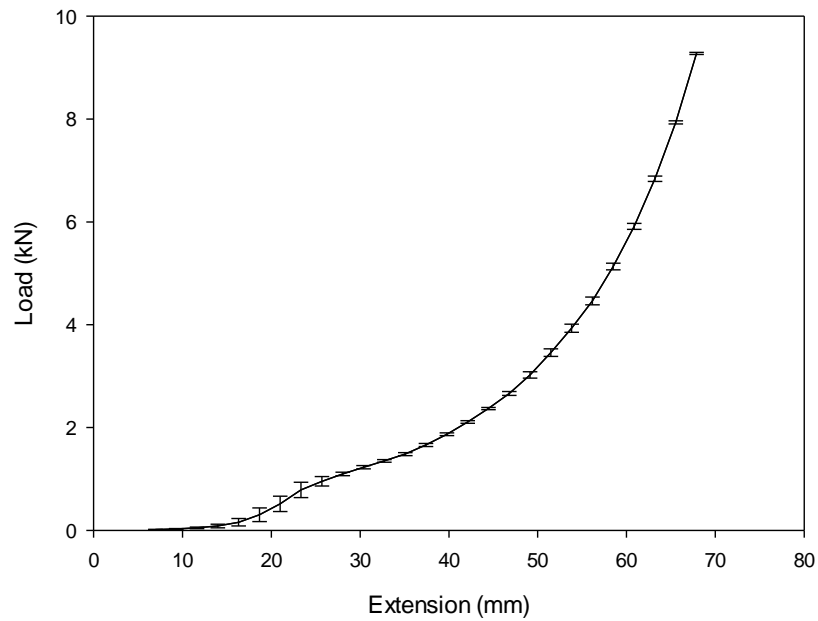
Figure 6.13 - Average of 400kPEO pastes extrusion profiles

The corresponding extrusion profiles from the 1MPEO pastes were also aligned at extrusion and average. The average extrusion profiles are compared in Figure 6.14.
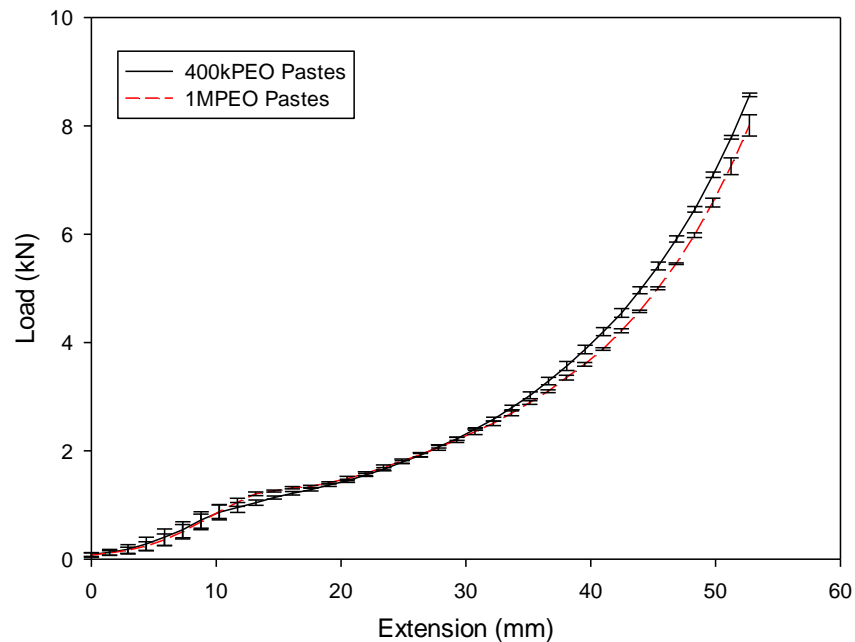
Figure 6.14 - Comparison of average extrusion profiles for both binder systems

This comparison shows that after extrusion there is a small yet statistically significant difference in the extrusion profiles in the two pastes, the only difference being the molecular mass of the binder phase. The difference is only observed after approximately 40mm of ram extension, before which the extrusion profiles track quite closely. When comparing individual pastes, prepared in parallel, the difference is observable much earlier in extrusion (see Figure 6.11). The variations between each run are enough to obscure this difference at smaller extensions but it is still apparent later in the extrusion.

In all of these tests, the load increases faster as extrusion progresses to the point that the pastes very quickly become too stiff for the equipment to safely extrude. This is because phase migration occurs more readily at lower moisture contents and for this reason, there is limited extrusion data to study. In order to have a longer extrusion run, the formulation was adjusted. Increasing the liquid component of the paste successfully increased the duration of the tests.
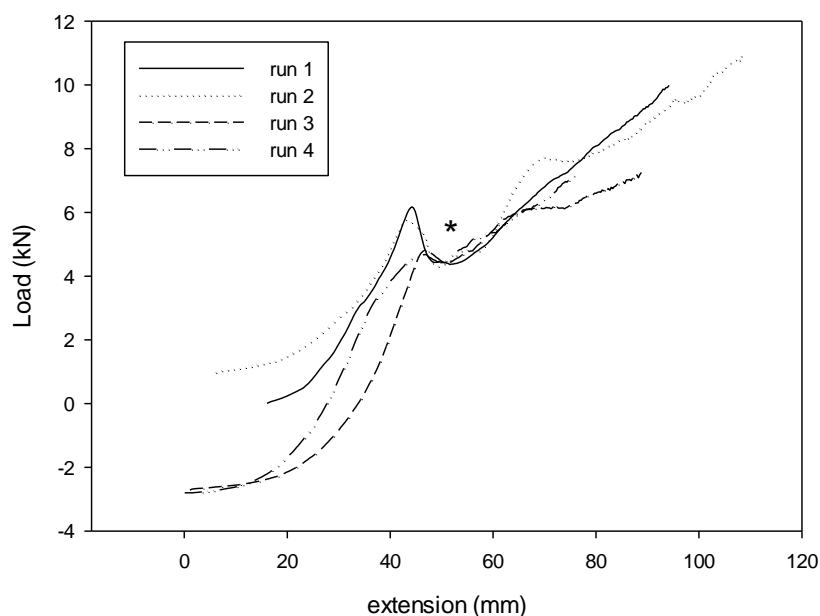
Figure 6.15 - 400kPEO extrusion aligned at point of extrusion

Figure 6.15 shows the extrusion profiles for the 400kPEO pastes, second formulation revision. These profiles have had both extension and load normalised at the onset of visible extrusion. These profiles show a much greater variation in the pre-compression phase before extrusion begins. As more liquid was added to the paste, this caused the paste to become more difficult to handle and as a result, pre-compression behaviour was found to be much more variable. For this reason, extrusion data prior to visible extrusion was omitted from analysis.
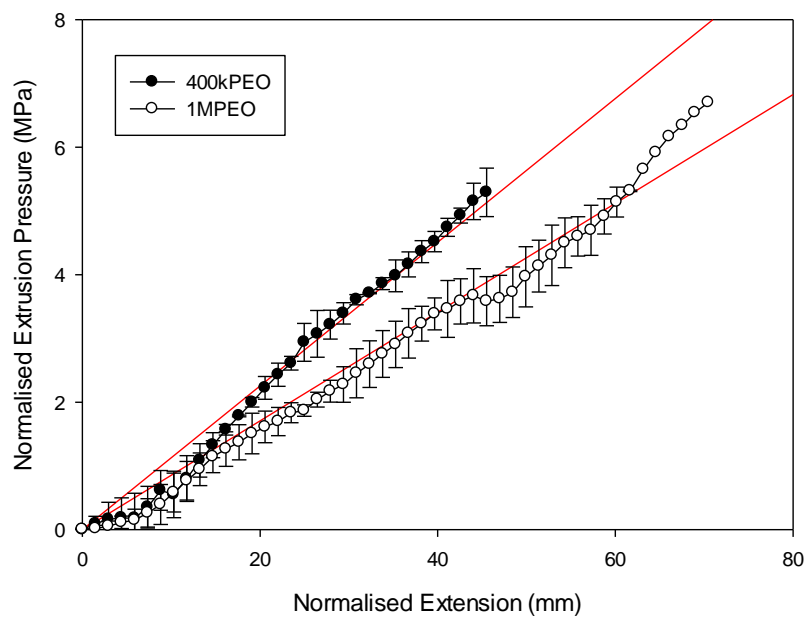
Figure 6.16 - Comparison of pressure increase in 400k and 1MPEO pastes

Figure 6.16 shows a comparison of the extrusion profiles of the two pastes after compression is complete. This figure clearly shows that phase migration is occurring to a much higher degree in the 400kPEO paste, with phase migration progressing at a rate of 0.13 MPa.mm^{-1} for the 400kPEO paste and 0.09 MPa.mm^{-1} for the 1MPEO paste. Regression lines are shown in red.

6.4   Discussion

The relationship between molecular mass and shear rheology was found, making it possible to prepare solutions of PEO such that different grades can be made to behave almost identically in terms of rheology, although this was only possible within a fairly narrow range of molecular masses and concentrations.

Pastes prepared with binders made of different PEO grades, but with the same shear rheological properties were extruded and made to undergo phase migration and it was observed that there was a repeatable and statistically significant difference in the rate of phase migration between the two different grades of PEO tested. It may be concluded that the phase migration behaviour of the binder is not a function of the shear rheology of the binder and paste formulation alone. It is possible that the difference in behaviour is related to the viscoelastic properties of the binder or some secondary permeability effect of the water in the polymer network. It is unlikely to be the latter as the concentration of polymer in solution is relatively low. The 1MPEO has a higher storage modulus than the 400kPEO. As the 1MPEO binder deformation is dominated by elastic forces while that of the 400kPEO is dominated by viscous forces, this will cause the two binders to respond differently to capillary forces and may explain why there is a difference in extents of dewatering.

It has been demonstrated by various authors that many factors can lead to undesirable dewatering in paste systems, such as extrusion speed, paste moisture content, and binder viscosity. It has been shown here that when all other factors suspected to affect the rate of phase migration are kept constant, there can still be seen a difference in paste stability during ram extrusion by changing the molecular mass of the binder, with a higher molecular mass resulting in a more stable paste. There is some evidence to suggest that another factor which can affect phase migration is binder viscoelasticity. Modification of the binder system to

increase the storage modulus of the binder may be a useful technique to alleviate problems caused by phase migration in practical contexts.

7 DRYING

The drying stage of the monolith production process presents a serious bottleneck and is unsustainable if the process is to be scaled up. In this chapter, a forced drying regime is applied to large diameter monolith and optimum conditions are suggested. A model describing the liquid content of the monolith during controlled drying is proposed and used to predict the shape of the stress field in the monolith as it dries.

7.1 Chapter Aims

The drying stage of the monolith production process presents a serious bottleneck and is unsustainable if the process is to be scaled up. This chapter aims to develop a forced drying regime that reduces the drying time to less than 24 hours without the introduction of any internal cracks. It also aims to investigate the causes of internal cracks that may form during drying.

7.2 Introduction

The current drying procedure is described in some detail in section 1.2.2.5, but a brief summary is provided here. The standard procedure at MAST Carbon has been to allow extrudate to dry in ambient conditions on a rolling table. For small production runs or experimental work, this has been more than sufficient. The rolling table used for larger diameter monoliths up to 2 m in length is shown in Figure 7.1.

Figure 7.1 - Large Roller Table

There are some concerns regarding the heretofore standard method of drying monoliths that must be addressed in this work.

7.2.1 Drying Time

The drying table in Figure 7.1 has a capacity of 22 full-length monoliths (2 interchangeable tables with 11 spaces each). It currently takes approximately 10 days for a full-length monolith to dry to an acceptable level. Monoliths feel dry to the touch after 2 or 3 days, but the remaining moisture evaporates during firing and causes the product to crack open. Over time, it was determined that monoliths which had been allowed to dry for at least 10 days contained little enough residual moisture that they would regularly survive firing. It is not known whether any studies were undertaken during early development to confirm the validity of this, but MAST Carbon have been using this rule of thumb for a number of years quite successfully.

At the start of the project, the drying stage was the most significant bottleneck in the entire monolith production process. In order to scale up the production capacity, it is necessary to either increase the capacity of the roller tables or to decrease the drying time. In order to increase drying capacity to 20 full sized monoliths a day, it would be necessary to purchase and make room for 18 additional roller tables. This is not the favoured solution. It is instead preferred to move to forced drying and reduce the drying time to under 24 hours including loading and unloading.

7.2.2 Failure During Drying

MAST Carbon has not had any problems with cracking during drying until comparatively recently. The overall formulation has not been changed very dramatically and it has been found to survive the gentle ambient drying adequately. Recently, however, MAST have been

experimenting with different carbon precursors and dramatically different binder formulations. In each case, cracks *have* formed during the drying process, even at ambient conditions, rendering the product unusable. It was thought that moving to forced drying would only exacerbate the problem.
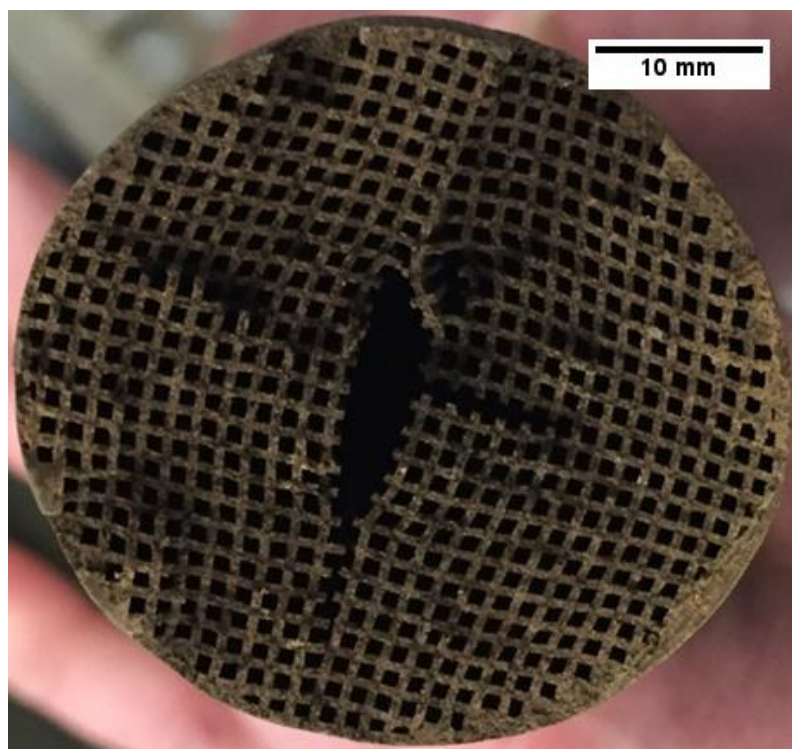
Figure 7.2 - Crack Formation in Honeycomb Monolith

The problem has been curtailed to a certain extent for small diameter monoliths by modification of the binder system but this is by no means certain to solve the cracking problem for larger pieces. In order to solve this problem, it is necessary to understand the reason for the formation of the cracks and study the effect of drying conditions and formulation in crack formation.

7.3 Study into forced drying

7.3.1 Experimental set up

MAST Carbon was involved in a project in late 2012 which required them to increase monolith production and demonstrate the feasibility of forced drying. This project offered the opportunity to perform some investigations into the effect of temperature and humidity on the rate of drying.

The purpose of this study was not to control the drying rate in order to reduce the formation of cracks, but rather to increase the drying rate without introducing cracks into the monolith.

A temperature and humidity controlled environmental cabinet was available for a period of approximately 2 months during which this work was undertaken. Because of the limited time that the equipment was available, there are a number of experiments that would have been performed but are missing from these results. These will be discussed at the end of this section.

A schematic of the experimental setup is shown in in Figure 7.3.
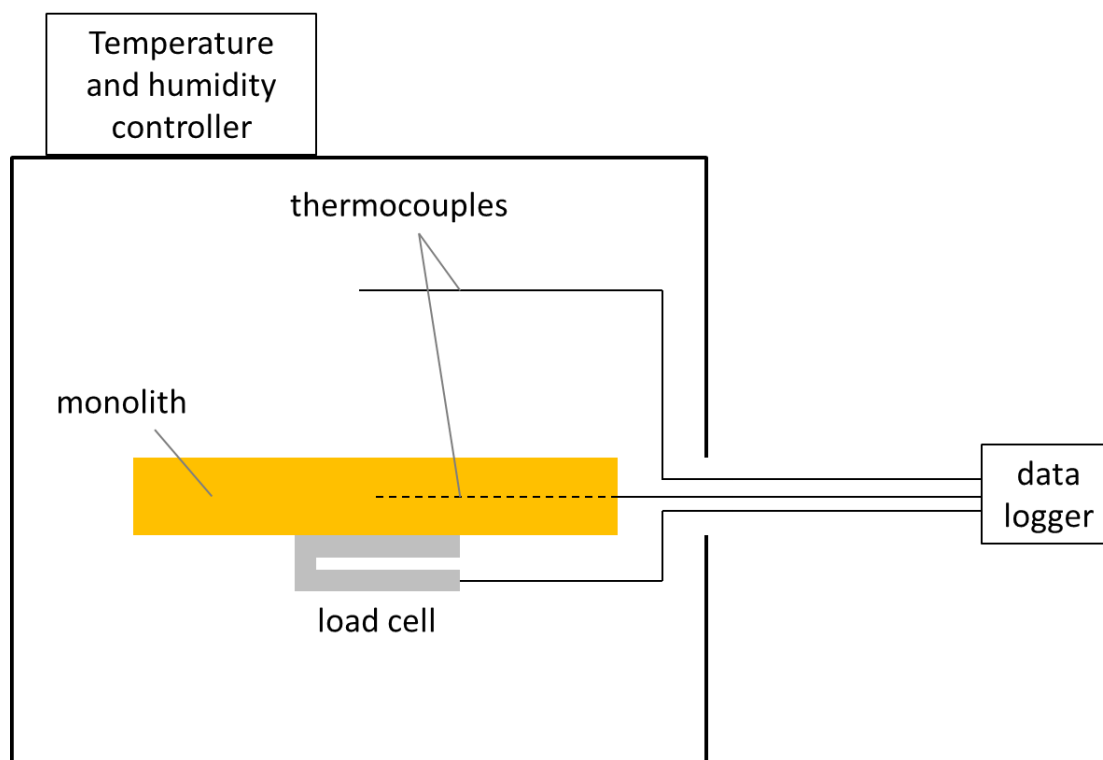
Figure 7.3 - Experimental Setup for Drying Trials

7.3.1.1 **Environmental Cabinet**

The environmental cabinet was hired, which could control both humidity (RH) and temperature independently, although its ability to do so at extremely low humidity and high temperature is fairly limited, due to the very low vapour pressure of water at high temperatures and that the air is cooled to condense moisture and reduce RH.

A thermocouple was placed inside the chamber to verify the read out on the cabinet. The temperature was found to be in very close agreement.

7.3.1.2 **Load Cell**

The load cell was purchased from RS Components. The load cell was connected to a Eurotherm 8150V data logger to measure the weight loss as drying progressed. It was calibrated before use with a set of calibration weights. A thermocouple was affixed to the side

of the load cell. A fixed weight was placed on the balance and the assembly heated to 100℃. No change in the output voltage was observed; therefore the effect of temperature was determined to be negligible.

7.3.1.3 **Monolith Test Piece**

During production on the Sulby ram extruder, a section of monolith of approximately 40 cm in length and 40 mm in diameter was cut from a full sized monolith. The monolith section was immediately placed onto the load cell assembly and tinfoil discs were fixed to the ends of the test piece. This was done in order to limit moisture loss from the ends and simulate the middle section of a much longer monolith. A thermocouple was then inserted into the central channel halfway into the length of the monolith.

The load cell assembly and monolith were then immediately placed into the environmental cabinet and a prepared drying program was started. Preparation of the monolith took no more than 5 minutes. Weight loss during this short period was unavoidable but considered to be negligible as the monolith was still at ambient temperature.

7.3.2 **Drying Programs**

Initially, it was intended that the drying procedure would be carried out in three stages; a fast temperature ramp, slow ramp, and a long dwell. This was done to reduce the stress in the monolith and the chances of cracks forming, as suggested by the literature[56].

It quickly became clear that the monoliths that were tested were not forming cracks under any conditions. Therefore, it was possible to simplify the experimental program. The temperature ramp was set to raise the temperature from ambient conditions to the final drying temperature over a period of 2 hours. Similarly, the humidity was reduced from ambient conditions to the final drying conditions over the same time period.

Table 7.1 - Drying programs

Run Number	RH %	Ramp 1 ℃.hr⁻¹	T1 ℃	Ramp 2 ℃.hr⁻¹	T2 ℃	Ramp 3 ℃.hr⁻¹	T3 ℃
1	10	9	29	30	50	120	60
2	10	9	29	30	50	120	70
3	0	9	29	30	50	120	70
4	0	9	29	30	50	120	80
5	60	9	29	30	50	120	70
6	80	9	29	30	50	120	70

7.3.3 Results

In all cases, the monoliths were fully dried without damage to the internal structure. An interesting observation is that the temperature at the centre of the monolith appears to reach a steady state just below the chamber temperature until the monolith reached its driest level, at which point the core temperature quickly rose to meet the external temperature. This was thought to be an effect of the remaining water at the core removing energy from the system in order to evaporate. At the point where the centre becomes fully dry, the thermocouple reaches equilibrium with the surrounding monolith. In a few cases, the jump in temperature occurred shortly before the monolith was fully dry, likely because the thermocouple was offset from the very centre of the monolith.

Figures 7.4 to 7.6 show the weight loss curves from the drying conditions in Table 7.1. Runs 1 and 2 both show a significant improvement in drying time over the air dried monoliths, see Figure 7.4. There is also an improvement in drying time at 70℃ compared with 60℃. In both cases, the monoliths were completely intact with no signs of internal or external cracking, which was very encouraging from a process optimisation point of view.
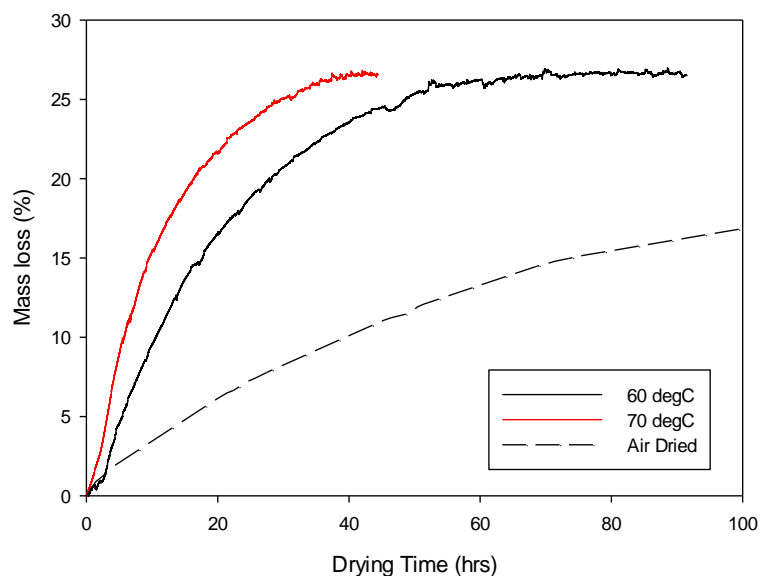
Figure 7.4 - Forced drying weight loss profiles at 10 %RH
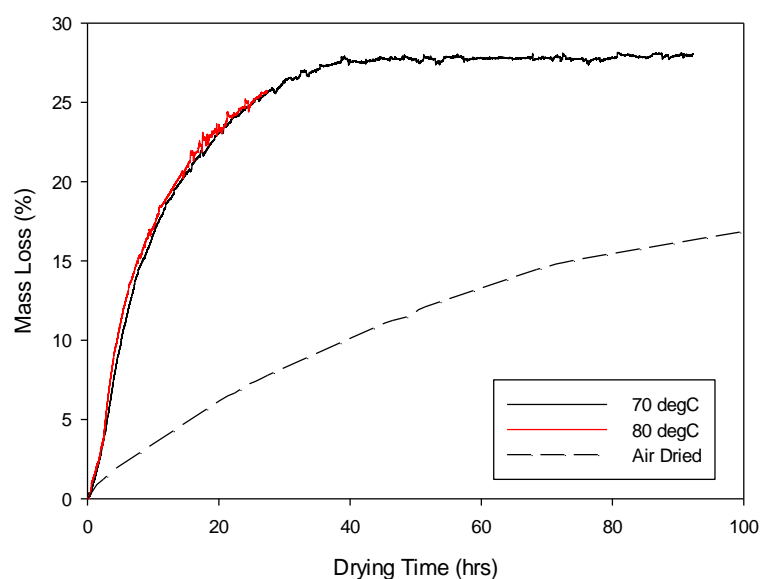
Figure 7.5 - Forced drying weight loss profiles at 0 %RH

Figure 7.5 shows the drying profiles of runs 3 and 4. In this case, there is no significant difference between the run at 80℃ and 70℃. Again, from a process optimisation point of view, this points very clearly to an optimal temperature of drying somewhere in the region of 70℃. It can also be seen that there is no constant rate drying period observable on these

results. This implies that the rate of evaporation at the surface is not rate limiting and the drying process can be modelled as a diffusion process.
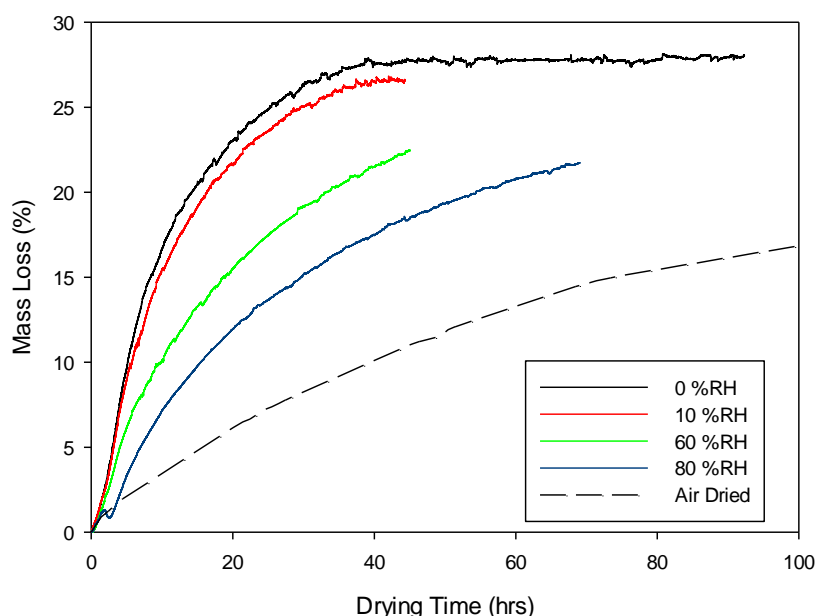
Figure 7.6 - Forced drying weight loss profiles at 70 ℃

Finally, Figure 7.6 shows drying runs performed at 70 ℃ and various levels of relative humidity. There is a clear trend showing that reducing the relative humidity in the chamber reduces the drying time. There is a modest decrease in drying time between an RH of 10 and 0 %. Once again, from an optimisation point of view, this is encouraging as it is significantly more difficult to reduce the chamber to 0 % RH, compared with 10 %.

The original intention of these forced drying trials was to find the most aggressive drying conditions which would not cause internal cracks to form. As none of the runs resulted in cracking, these results are not helpful in determining either the conditions required for or the mechanism of, internal cracking. The results, however, do indicate that a temperature of 70 ℃ and a relative humidity of around 10% would be optimal for force drying the monoliths.

Additionally, the weight loss data can be used to fit the model discussed in the following section.

7.4   Modelling of Drying Stage

7.4.1   Drying Mechanism and Assumptions

The monolith was modelled using a reaction engineering style approach with all transport mechanisms combined into a single effective mass transfer step. The monolith is supposed to be comprised a liquid and solid phase, denoted in the following text by the subscripts 1 and 2 respectively. The monolith is assumed to be a cylinder with three dimensions, longitudinal, radial and angular, denoted by z, r and θ respectively. The arrangement is shown in Figure 7.7.

$$\phi_1 = \text{volume fraction}$$

$$\phi_1 + \phi_2 = 1 \qquad\qquad \textbf{Equation 7.1}$$
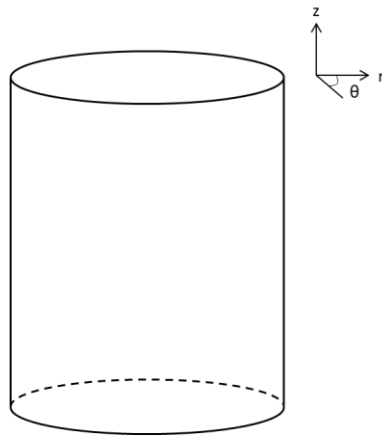
Figure 7.7 - Schematic representation of ideal monolith, showing dimensions

The liquid phase diffuses through the solid matrix and evaporates at the surface of the cylinder. The model does not take explicit account of the presence of organic extrusion aids

such as K15M and any influence they may have is included in the value of the diffusion coefficient. As the water phase leaves the solid phase, the volume of the solid matrix is reduced. Figure 7.8 shows a 'wet' and a 'dry' paste element. In the wet condition, the solid particles are separated by a film of liquid. Once the liquid phase has left the element the separation distance of the particles reduces, causing the shrinkage.
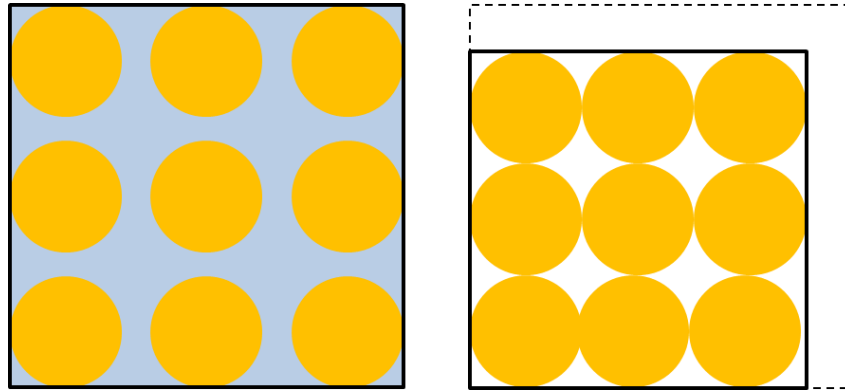
Figure 7.8 - Shrinkage of an element of paste due to drying

It is assumed that water does not diffuse longitudinally or angularly, meaning that the concentration profile of water only exists in the radial direction. This has been observed to be very close to reality over the majority of the length of monoliths with the exceptions of roughly 20 mm from either end.

Heat transfer was modelled using the heat equation, shown in Equation 7.3.

$$\text{Temperature} = T(r, t)$$

$$\text{concentration of } i = C_i(r, t) = \rho_i \phi_i(r, t) \qquad \textbf{Equation 7.2}$$

$$\frac{\partial T}{\partial t} + \alpha_H \frac{\partial^2 T}{\partial r^2} = 0 \qquad \textbf{Equation 7.3}$$

Boundary Condition 1

$$T(R,t) = T_{chamber}$$

Boundary Condition 2

$$\frac{d}{dr}T(0,t) = 0$$

Where $T_{chamber}$ is the temperature inside the oven and α_H is the heat transfer coefficient. In order to simplify the model, it was assumed that α_H is constant, i.e. does not change based on water concentration.

Mass transfer was modelled by radial diffusion according to Fick's Law and subject boundary conditions at the wall and at the core.

$$\frac{\partial \phi_1}{\partial t} + \frac{\partial j_1}{\partial r} = s_1 \qquad \textbf{Equation 7.4}$$

where

$$j_1 = -\frac{\partial}{\partial r}(\overline{D}\phi_1) \qquad \textbf{Equation 7.5}$$

and

$$\overline{D} = \overline{D}_0\, exp\left(-\frac{E_a}{R_{gc}T}\right) \qquad \textbf{Equation 7.6}$$

Boundary Condition 3

$$\phi_1(r = R, t) = \phi_{1,chamber}$$

Boundary Condition 4

$$\frac{\partial \theta_1(r = 0, t)}{\partial r} = 0$$

The quantity s_1 in Equation 7.4 is the accumulation term for the liquid phase and is set to zero. The total mass of the system with respect to time can be calculated from the integral of the local density and element volume.

$$M_T(t) = \int \rho(r,t)dV$$
$$= \int\int\int \rho(r,t)rdrd\theta dz$$
$$= L\int\int \rho(r,t)rdrd\theta$$

$$M_T(t) = 2\pi L \int \rho(r,t) r \, dr \qquad \textbf{Equation 7.7}$$

The average local density of the monolith can be expressed in terms of the volume fraction and density of the liquid and solid phases.

$$\rho(r,t) = \rho_1 \phi_1(r,t) + \rho_2 \phi_2(r,t)$$

Inserting Equation 7.1
$$\rho(r,t) = \rho_1 \phi_1(r,t) + \rho_2(1 - \phi_1(r,t))$$

$$\rho(r,t) = (\rho_1 - \rho_2)\phi_1 + \rho \qquad \textbf{Equation 7.8}$$

Equation 7.8 can be substituted into Equation 7.7 in order to express the total mass of the monolith in terms of the volume fraction of the liquid phase.

$$
\begin{aligned}
M_T(t) &= \int [(\rho_1 - \rho_2)\phi_1(r,t) + \rho_2] dV \\
&= \int (\rho_1 - \rho_2)\phi_1(r,t) dV + \int \rho_2 \, dV \\
&= (\rho_1 - \rho_2) \int \phi_1(r,t) dV + \rho_2 \pi R^2 L
\end{aligned}
$$

definition
$$\phi_1(r,t) = \frac{V_1(r,t)}{V}$$

$$
\begin{aligned}
\int \phi_1(r,t) dV &= \int \frac{V_1(r,t)}{V} dV \\
&= V_1(t)
\end{aligned}
$$

$$M_T(t) = (\rho_1 - \rho_2)V_1(t) + \pi R^2 L \rho_2$$

7.4.2 Model Solution

The above equations describe the concentration profile of the liquid phase, or 'dryness' over time. The model was discretised and solved in MatLab R2014a. The temperature and mass

transport coefficients were estimated and the resulting mass profile compared with real data from the earlier controlled drying trials.

MatLab contains a number of methods for solving a system of partial differential equations (PDEs), but to fit within the scope of this work, it was decided that a discretised system could be solved numerically as a system of ordinary differential equations (ODEs).

The single largest drawback of using this method of solving for the temperature profile is that it cannot be solved simultaneously with the concentration profile. The heat transfer coefficient is influenced by the moisture content of the paste and will certainly have an effect on the temperature profile.

Equations 7.3, 7.5 and 7.6 were approximated using a finite difference approach.

$$\frac{dT_i}{dt} = \alpha_H \frac{T_{i+1} - 2T_i + T_{i-1}}{\Delta r^2}$$

Equation 7.9

$$\frac{d\phi_i}{dt} = D \frac{\phi_{i+1} - 2\phi_i + \phi_{i-1}}{\Delta r^2}$$

Equation 7.10

```
% File: main_script.m

% Clear previous files
  clear all
  clc
```

The initial lines of the main MatLab script clear all previous saved variables and data from the current session to ensure that there are no errors from using old data.

```
% Parameters shared with the ODE routine
```

```matlab
global D0 phi1_chamb R alphaH pde_Tcall UGC Ea T T_chambprof tstep
pdeCcall T0

filename = 'dryingdata.mat';
m = matfile(filename);
Mreal = m.Mreal;
filename = 'coretempdata.mat';
m = matfile(filename);
Treal = m.Treal;
```

A number of global variables are declared to allow certain variables to be used in both the main script and from within the function files used by the ODE solvers while only having to define them once.

Next, two files containing the monolith mass and core temperature data are imported into the MatLab session and loaded into two arrays, Mreal and Treal.

```matlab
% Constants

pde_Tcall = 1;
pdeCcall = 1;
m1 = 895;              % initial mass of liquid phase (g)
m2 = 2258;             % initial mass of solid phase (g)
rho1 = 1.1;            % liquid density (g/cm3)
rho2 = 1.45;           % solid density (g/cm3)
v1 = m1/rho1;          % volume of liquid (cm3)
v2 = m2/rho2;          % volume of solid (cm3)
vt = v1+v2;            % total monolith volume (cm3)
phi1_chamb = 0;        % water fraction in chamber
phi1_init = v1/vt;     % initial water fraction
phi2 = v2/vt;          % solid fraction
phim = 0.57;           % monolith open area
shrinkage = .0255;     % shrinkage from wet to dry


L = 35;                % monolith length (cm)
```

```
R = 2.065;              % monolith radius (cm)


UGC = 8.314;            % universal gas constant (j/K/mol)


nx = 100;               % number of points in r mesh
xstep = R/nx;           % length of radius element (cm)


nt = 1000;              % number of time steps
t0 = 0.0;               % start time (s)
tf = 360000;            % end time (s)
tstep = tf/nt;          % duration of time step (s)


Ms = pi*R^2*...
    L*phi2*...
    rho2*phim;          % mass of solid (g)


T_init = 16+273;        % initial temperature (K)
```

All constants used in the script are defined in this section. Many are calculated from known

values.

```
% set up initial conditions
  for i=1:nx
    u0(i)=phi1_init;
    T0(i)=T_init;
  End
```

Two arrays are declared with the same size as the number of points in the space dimension.

T0 and u0 contain the initial (flat) temperature and water concentration profiles.

```
D0 = 4*10;              % maximum diffusion constant (cm2/sec)
  Ea = 40000;           % activation energy (j/mol)
  alphaH = .0008 ;       % heat coefficient
```

The three unknown variables from equations 7.3, 7.5 and 7.6 are estimated in this section of the script. They were later modified in order to better fit the simulated temperature and mass profiles to the recorded data. This is described in further detail below.

```matlab
tspan = linspace(t0,tf,nt);
  x = linspace(0,R,nx);

% ODE integration
  options=odeset('RelTol',1.0e-04,'AbsTol',1.0e-04);

  [t,T]=ode15s(@pde_T,tspan,T0,options);    % Temperature profile
  [t,u]=ode15s(@pde_c,tspan,u0,options);    % Concentration profile
```

The script then calls two instances of the ode15s function to numerically solve the temperature and concentration profiles in the monolith from the initial time to the specified final time.

The first function file, pde_T.m, codes for the heat transfer across the radius of the monolith. The function ode15s calls the time span, tspan, and the initial temperature profile, T0, as initial conditions.

```matlab
function [ Tt ] = pde_T(t,T)
%
% Problem parameters
  global alphaH R pde_Tcall T_chambprof

% PDE
n = length(T);
dx2 = (R/(n-1))^2;

 % set up chamber temperature profile
```

```
    if t==0
        T_chamb = 19;
    elseif t<1.11*3600
        T_chamb = 19+t*9/3600;
    elseif t<1.84*3600
        T_chamb = 29+(t-1.11*3600)*29/3600;
    elseif t<2*3600
        T_chamb = 50+(t-1.84*3600)*120/3600;
    else T_chamb=70;
    end
```

The temperature inside the test chamber ramped up over time. T_chamb contains the chamber temperature profile over time.

```
for i=1:n
  if(i==1)          Tt(i)=2.0*(T(i+1)-T(i))/dx2;
  elseif(i==n)      Tt(i)=alphaH*(T_chamb+273-2.0*T(i)+T(i-1))/dx2;
  else              Tt(i)=alphaH*(T(i+1)-2.0*T(i)+T(i-1))/dx2;
end
end


Tt=Tt';
```

The function file used the discretised approximation of the heat equation, shown in Equation 7.9.
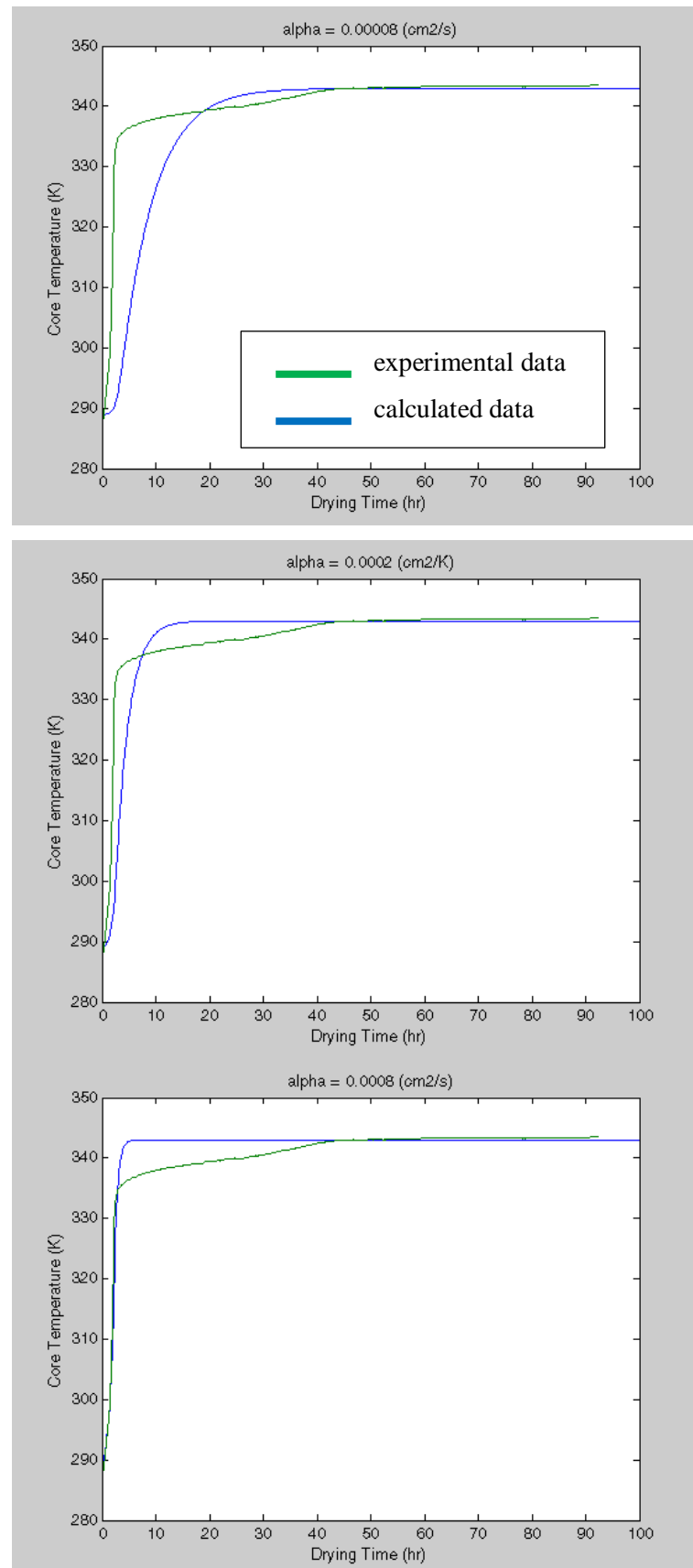
Figure 7.9 - Effect of varying α_H on predicted temperature profile at monolith core

Figure 7.9 shows the effect of varying the heat diffusivity constant. The green line represents the actual core temperature profile of a 40 mm diameter monolith. The blue lines represent the predicted temperature profile using the heat diffusivity shown. A heat diffusivity of 0.002 $cm^2.s^{-1}$ gave the closest approximation of the real temperature profile at the core. Due to the fact that the concentration profile could not be calculated simultaneously and subsequently, the effect of moisture content on the heat diffusivity constant could not be considered, the predicted core temperature diverges from the measured data. This was later found to have a negligible effect on simulating the overall monolith mass.

```
function [ ut ] = pde_c(t,u)
%
% Problem parameters
  global phi1_chamb R D0 UGC Ea T tstep T0

% PDE
n=length(u);
dx2=(R/(n-1))^2;

if floor(t/tstep) == 0
 for i=1:n
  D = D0*exp(-Ea/UGC/T0(i));
  if(i==1)        ut(i)=2.0*(u(i+1)-u(i))/dx2;
  elseif(i==n)    ut(i)=D*(phi1_chamb-2.0*u(i)+u(i-1))/dx2;
  else            ut(i)=D*(u(i+1)-2.0*u(i)+u(i-1))/dx2;
  end
 end
else
aprxtime = floor(t/tstep);
for i=1:n
  D = D0*exp(-Ea/UGC/T(aprxtime,i));
  if(i==1)        ut(i)=2.0*(u(i+1)-u(i))/dx2;
  elseif(i==n)    ut(i)=D*(phi1_chamb-2.0*u(i)+u(i-1))/dx2;
  else            ut(i)=D*(u(i+1)-2.0*u(i)+u(i-1))/dx2;
```

```
    end
end
end


ut=ut';
```

The output of the ode15s function as a number of mesh points in space and time dimensions equal to the number of points specified in the main script. The solver must actually calculate a number of values between the specified mesh points in order to solve the ode as accurately as possible. The number of intermediate values depends on the rate of change of the variables, with a higher rate of change requiring a larger number of intermediate values. As the mass transfer coefficient is dependent on temperature, the ode15s function to solve the moisture content profile must access the temperature profile, stored in T. As the matrix, T, only contains values for the specified mesh points, the function file, pde_c, must be able to approximate the local temperature when calculating intermediate points. This is achieved by dividing the time of the current iteration, dividing it by the time step and rounding down to find the most recent local temperature stored in the matrix, T.

The total monolith mass is calculated by summing the masses of the finite elements at each time step. The mass transfer constants in equations 7.5 and 7.6 can be adjusted such that the predicted weight loss curve matches the measured values.
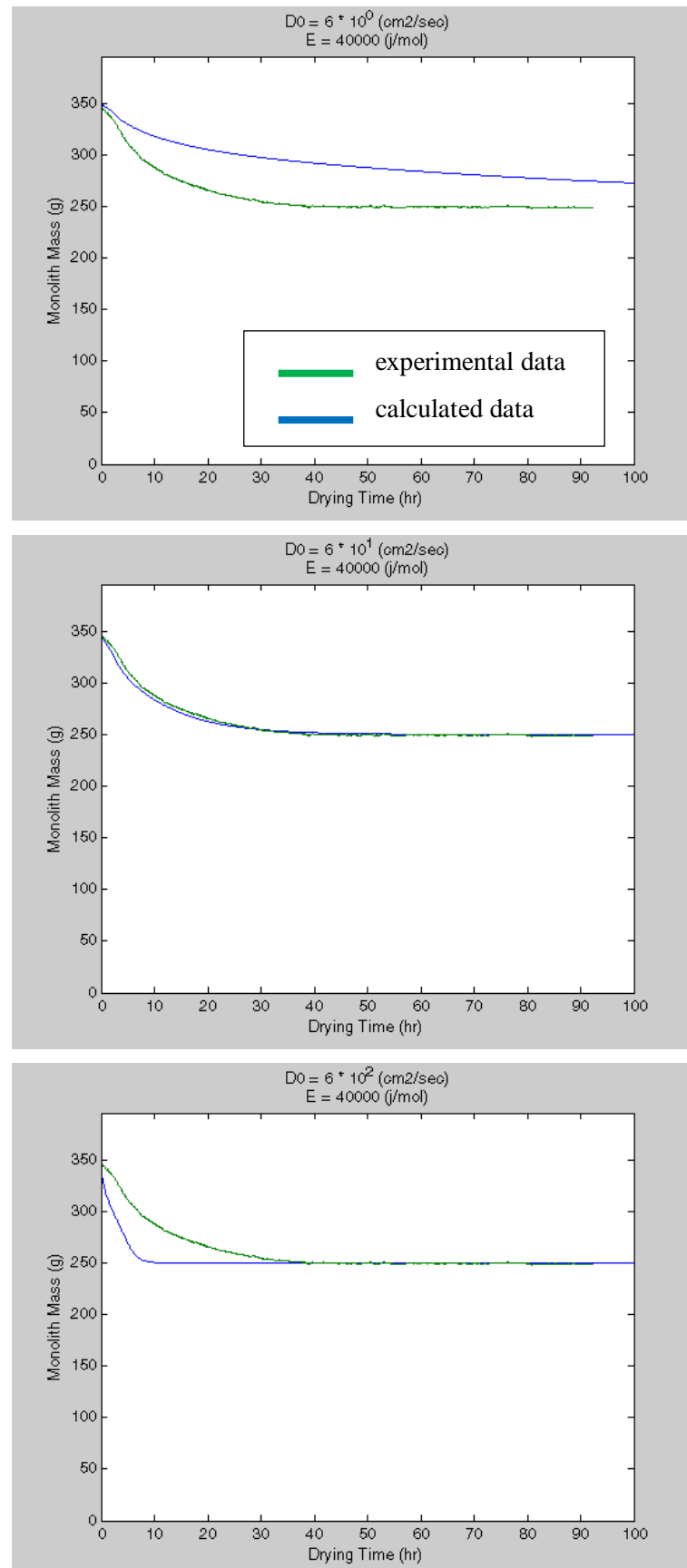
Figure 7.10 - Effect of varying maximum diffusion constant on weight loss profile
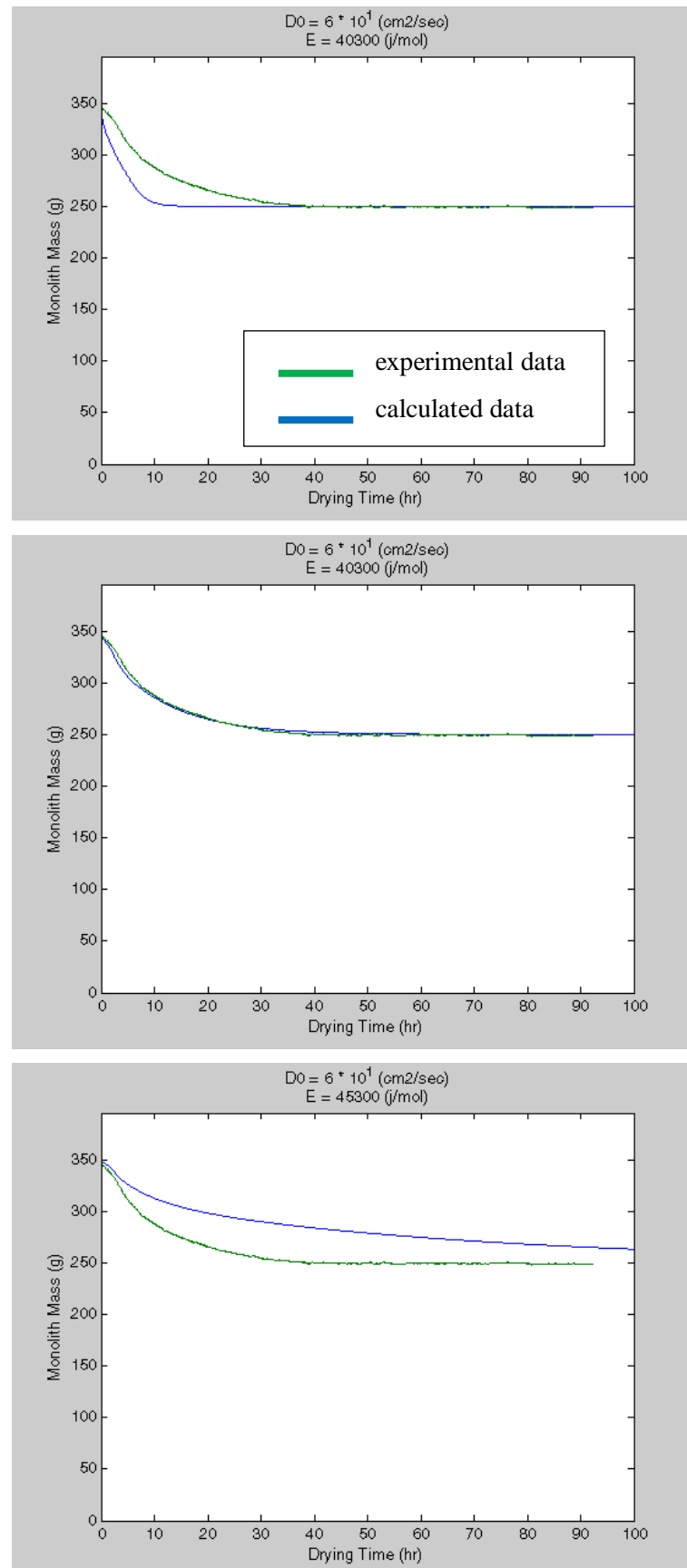
Figure 7.11 - Effect of varying activation energy on weight loss profile

Figures 7.10 and 7.11 show the predicted drying profile (shown in blue) of a monolith compared with real drying data (shown in green). Values of 60 cm^2.s^{-1} and 40300 J.mol^{-1} for the maximum diffusion coefficient and activation energy respectively, gave good agreement between the observed and predicted weight loss profile.

Figure 7.12 shows the change in the liquid content of the monolith with time. These results appear to be entirely typical of observations made when inspecting the monoliths during drying in terms of the size of the drying front.
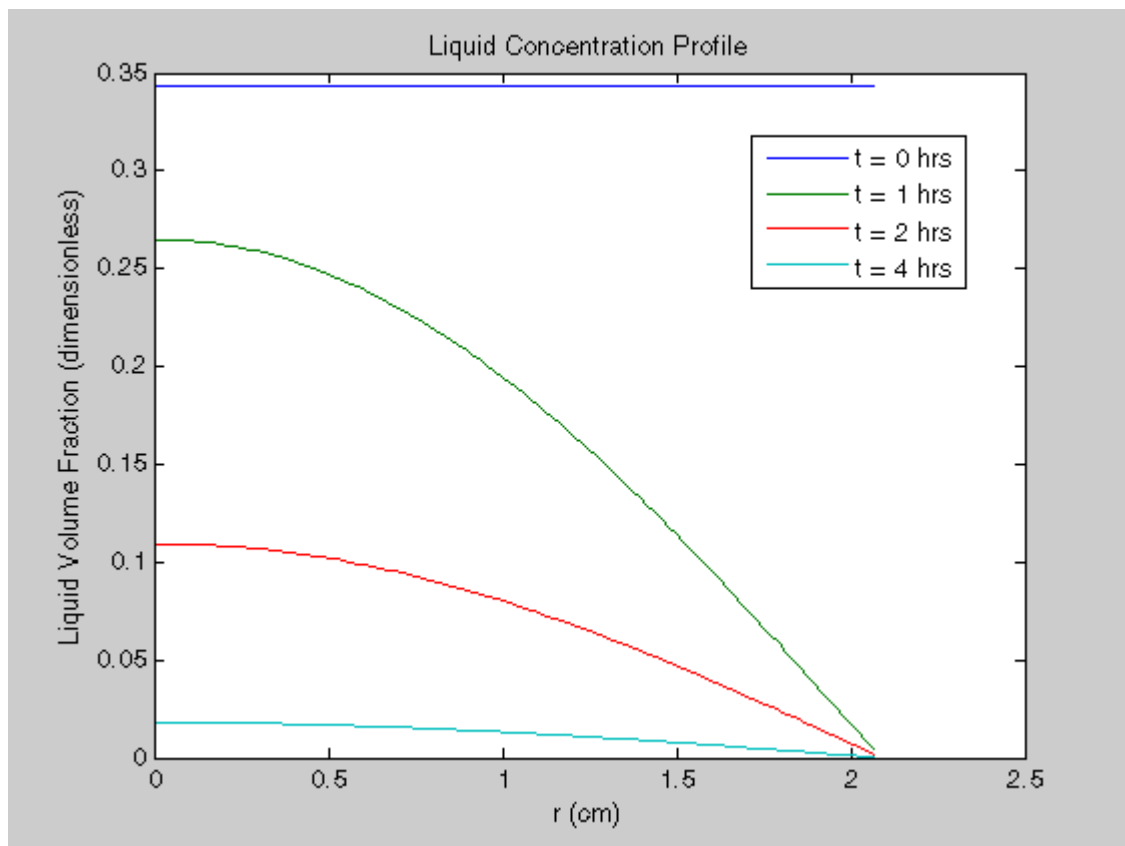
Figure 7.12 - Liquid concentration profile changing with time

7.4.3   Stress Profile

The linear shrinkage, ω, of a wet element of paste after complete drying was measured to be 2.55%. For simplicity, it was assumed that the shrinkage and Young's Modulus varies

linearly as the paste dries out. As the monolith dries out and begins to shrink, the differential shrinkage will necessarily lead to a stress profile within the monolith.

The moisture content and shrinkage data can be used to calculate the local strain. First, the current element length is calculated based on the level of dryness and therefore shrinkage. At t = 0, all element lengths are assumed to 1.

$$element\ length = l(r,t)\ = 1 - \omega$$

Equation 7.11

$$strain = \varepsilon(r,j) = \frac{l(r,j-1) - l(r,j)}{l(r,j-1)}$$

Equation 7.12

$$stress = \sigma(r,t) = E(r,t) \times \varepsilon(r,t)$$

Equation 7.13

Applying equations 7.11 to 7.13 the calculated dryness gradient shows a pronounced stress front which propagates from the wall to the core. This is illustrated in Figure 7.13.
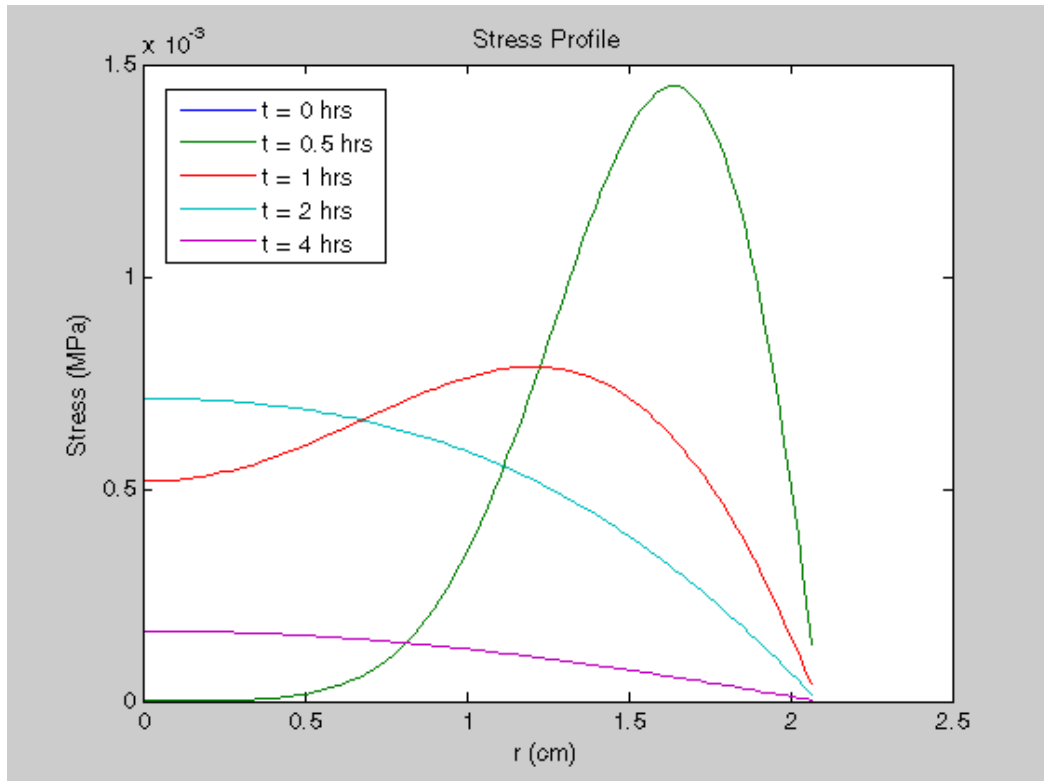
Figure 7.13 - Stress profile in monolith during drying

The stress front follows the drying front closely. The peak diminishes as it approaches the centre as a result of the flattening of the moisture (and by extension, the shrinkage) gradient. Also to be considered is the effect of the changing Young's modulus, which also follows the drying front.

Once the stress profile is known, it is, in principle, possible to compare the local stress with the local yield stress and predict the onset of brittle fracture. However, as Figure 7.14 illustrates, the cross section of the monolith is characterised by the square channels which are central to the monolith performance. The model as described in this section assumes that the monolith is homogenous in the angular dimension and the stress front is able to propagate through the radius of the monolith. The square channels, however, force the stress field to converge and concentrate through the narrow walls. It is, therefore, the case that while the general shape of the stress field can be estimated, its exact magnitude cannot be calculated.
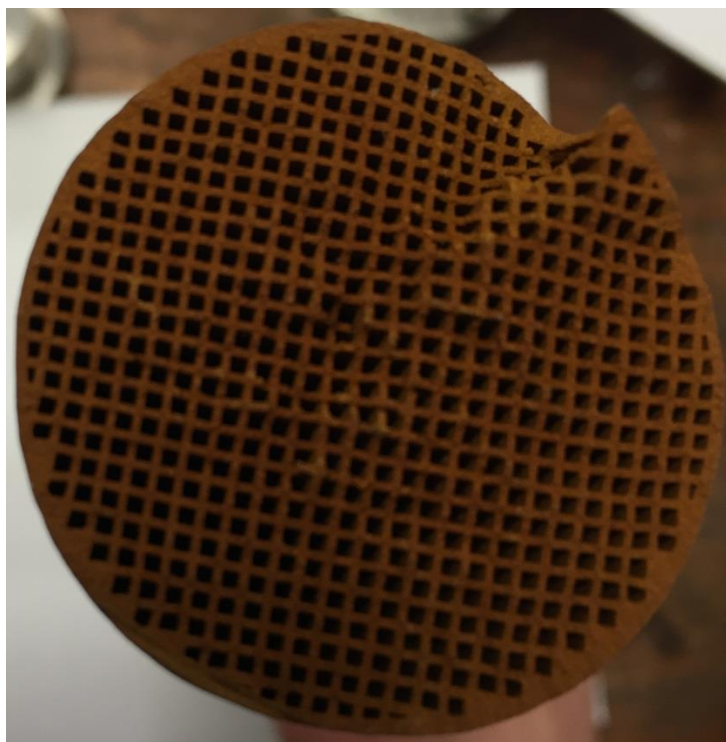
Figure 7.14 - End-on view of green monolith

In order for this analysis to be performed, a more sophisticated model would need to be developed. This would most likely be a finite element model in two spatial dimensions, the development of which is beyond the scope of this work.

7.4.4   Proposed Mechanisms of Fracture

Two mechanisms which could potentially lead to the internal cracking have been proposed. The first is illustrated in Figure 7.15.
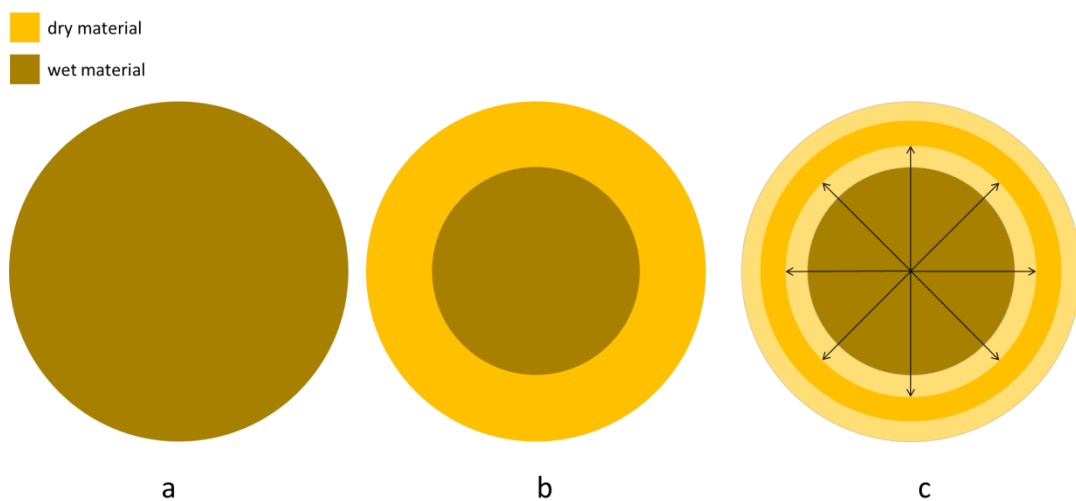
Figure 7.15 – Fracture mechanism 1

Figure 7.15(a) shows the cross section of a fully wet monolith. Figure 7.15(b) shows the progress of the drying front. For the purposes of this illustration, the front is shown as being very sharp, however, in reality, the drying front is far more diffuse. Figure 7.15(c) shows a heavily exaggerated representation of how the dry region of monolith may be expected to shrink. The inner boundary of the dry region moves away from the unchanged wet region, exerting a tensile stress on the centre of the monolith. If this stress is greater than the yield stress of the paste at that location, the monolith could split. Once the crack has begun, it will propagate through the monolith quite easily as the fine channel structure will concentrate the stress lines.

This mechanism, however, is unlikely to be the operative cause of the fractures seen in Figure 7.2. Work has been done on pyrolysis of phenolic resin tubes shows that as it shrinks, the internal and external diameter of a ring will both reduce by the same amount, as shown in Figure 7.16 and Table 7.2.
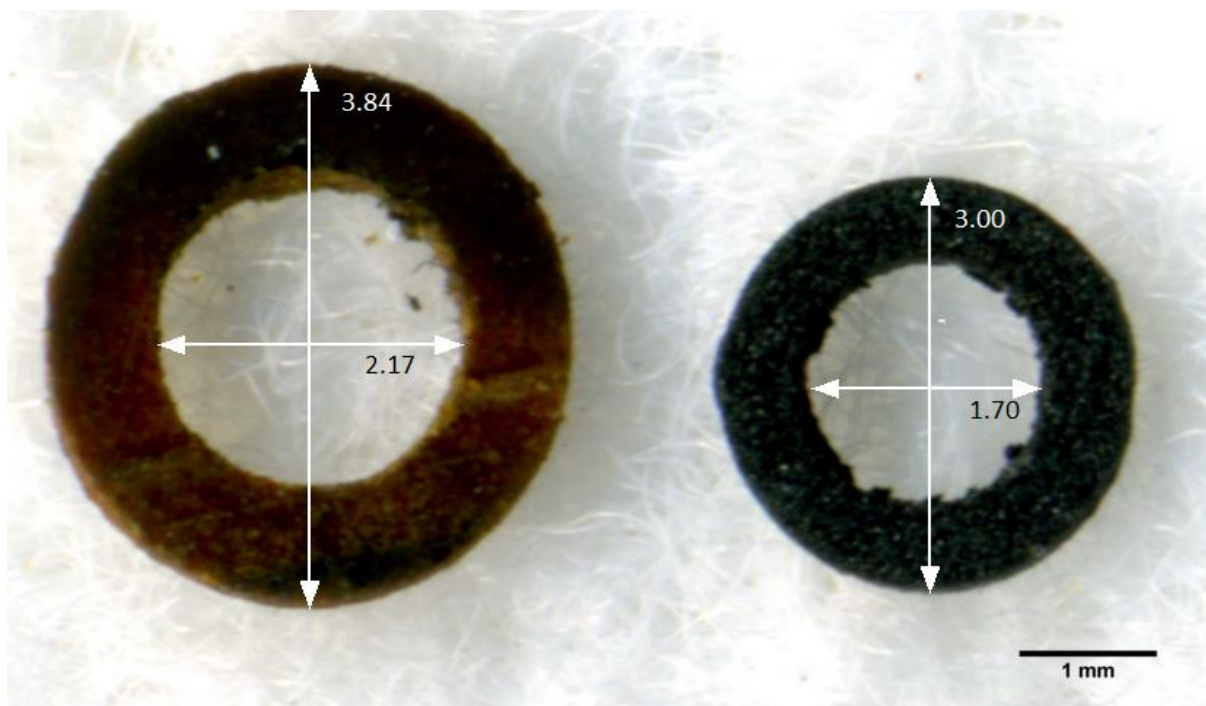
Figure 7.16 - Section of tubular extrudate before and after carbonisation

Table 7.2 - Shrinkage of Resin on Carbonisation

Outer Diameter (mm)	Inner Diameter (mm)	Shrinkage (%)
3.84	2.17	22
3.00	1.70	22

A second method of fracture was proposed which is consistent with the shape of the stress profile shown in Figure 7.13. The cracks are caused by the stress front propagating through the monolith to the core. The liquid content of the paste and the rate of drying directly influence the size of the stress field and the tensile stress of the paste. These competing factors will determine if and where a crack will form. Figure 7.13 shows a monolith undergoing fracture during drying. In Figure 7.13b, the outer edge of the monolith has begun

to dry and shrink. Although the stress is highest in this region, the speed of drying is matched by the rapid increase in tensile strength. In Figure 7.13c, the inner region of paste has fractures due to the prolonged, albeit lower, tensile stress. As this region shrinks, the centre is pulled apart due to the lower cohesive forces in the centre.
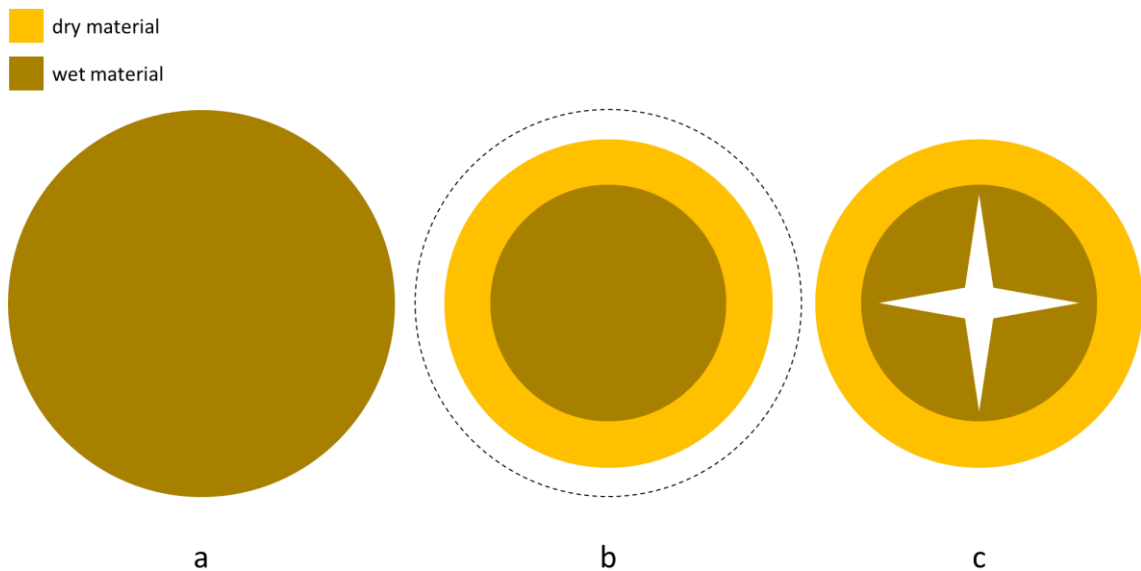
Figure 7.17 - Fracture mechanism 2

The competition between the stress front and the change in tensile strength should be more thoroughly investigated. A more sophisticated model will be required in order to properly account for the radial effects of shrinkage and the local geometry around the square channels.

7.4.5   Discussion of Model

The model described in this section, while not being developed enough to account fully for the effects of the square channels in the monolith, nonetheless was suitable for predicting the overall shape of the stress front during drying. The model predicts that the stress will be highest at the wall at the early stages of drying and the stress peak will decrease and move inwards towards the core of the monolith. A more sophisticated form of this model would be

able to take into account the complex honeycomb geometry of the monolith and would be able to predict where a fracture is most likely to occur.

It is, however, possible to use the shape of the stress profile to predict what mechanism might cause internal cracking. Two such mechanisms have been proposed. Both are consistent with the predicted stress profile, but only the second is consistent with observations made on the shrinkage of a tube of phenolic resin.

One disadvantage of the model presented here is that it does not account for effects of circumferential shrinkage on the stress field. It is highly likely that this will have a large effect on the mechanism of fracture, but not enough is known about how this causes the stress field to develop. Again, a two-dimensional finite element model would be able to take this into account and provide more insight into the fracture mechanism.

7.5 Summary

Forced drying of the monoliths has long been known to be necessary to reduce bottleneck in production that the drying stage introduces. It was thought that forced drying would lead to defect formation, so work was done to investigate the conditions necessary to dry the monolith quickly without breaking them. It was found that the standard resin monoliths are surprisingly robust during forced drying. Under all temperature and humidity conditions, the monoliths survived without any damage. It was found that there was little effect on drying time below about 10% RH and above about 70℃. This information is very useful from a process development point of view, but shed little light on the conditions that would lead to defect formation.

The drying data that was collected was used to determine the mass and heat transfer parameters in a simple drying model. A moisture content profile was generated using the

model which was used to predict the deformation profile of the monolith. This profile was then converted into a stress field. This predicted that there is a stress front which begins at the wall of the monolith and travels into the centre. This suggests that the cracking is caused by internal stresses brought on by the shrinkage of the monolith as it dries. There are many competing factors which will influence where the cracks occur. These include the yield strength of the material, the magnitude of the stress and the geometry of the monolith.

It has been suggested that, while beyond the scope of this project, a more robust model will be able to predict where fractures might occur and also include the effect of circumferential shrinkage. This model could then be used to simulate different materials and drying conditions to fully optimise the drying stage.

8 CONCLUSIONS

8.1 Overview

The objective of this project was to provide MAST Carbon with the knowledge required to scale up honeycomb monolith extrusion. The two largest barriers to scale up were the high rejection rate of monoliths during extrusion and the bottleneck in production caused by the very long drying time of the monoliths.

The most significant point of failure was defect formation during extrusion. The effect of paste formulation on extrusion quality was investigated. It was found paste rheology could be measured and used to predict the quality of extrusion. It was also found that paste rheology could be controlled by careful formulation of the paste and addition of certain 'extrusion aids'. This led to the development of a new formulation which is currently in use at MAST. Since the introduction of this new formulation, the rejection rate of monoliths during extrusion has dropped to zero. Additionally, it was shown that a cause of paste instability, known as phase migration, could be mitigated by increasing the 'elasticity' of the liquid phase in a paste.

A forced drying regime was shown to significantly reduce the time required to dry the green monoliths. For MAST's standard materials, no increase in failure rate was observed. However, MAST has increasingly been working with new materials which demonstrate a lower green strength and tendency to split while drying, even at ambient conditions. A model for predicting the stress profile in a drying monolith was developed. The model predicts that a stress front propagates from the outside wall to the core and is likely the cause of the fractures.

8.2 Paste Formulation

It has been shown that the addition of one or more additives to the 'extrusion package' added to the phenolic resin paste can influence the paste rheology which may be characterised using the Benbow Bridgwater paste model.

It has been argued that all failure modes during the extrusion of honeycomb monoliths can be traced back to a single mechanism, namely the variation of flow rates (also called the flow profile) of paste exiting the die. A difference in the flow rates of two adjacent paste elements, if large enough, can cause serious deformation of the extrudate. In cases where the variation is localised, perhaps due to a die blockage, this is sometimes manifest as the commonly encountered 'sharks teeth' defect. In some cases, the variation in flow may be more widespread across the die, perhaps due to variation in the die geometry. In these cases, the faster elements of past can be observed to 'pull' the adjacent paste elements with them causing one side of the die to extrude faster than the other and giving rise to an extremely bent monolith.

It has been shown that by applying the Benbow Bridgwater paste model to each of the channels in a honeycomb die individually, the extrusion velocity of each paste element can be calculated as a function of the extrusion pressure and channel geometry. By comparing paste rheology to the sensitivity of the paste to changes in die land conditions, it was found that pastes characterised by a low value of n, the non-linear velocity term for the die land in the Benbow Bridgwater model, were significantly less sensitive. The paste was then reformulated and shown to have an extremely even flow profile. This new formulation has been in use at MAST since the end of this work and has decreased the rate of rejection to zero.

Phase migration, a cause of instability of pastes, was found to be worsened when the liquid phase of the paste was more 'viscous' in terms of viscoelasticity. This was true even when the 'simple' rheological profile of the liquid phase was identical.

8.3   Drying Stage

Drying monolith at MAST carbon had previously be performed by leaving them to dry on rolling tables for upwards of 10 days. This presented a significant bottleneck in the production process. Sections of monoliths were force dried at various temperatures and levels of relative humidity. It was found that MAST's standard materials could be treated at 70℃ and 10 %RH and dried fully in less than 24 hours, without introducing defects into the monolith.

More recent work with natural materials has suggested that fractures during drying may soon become a significant problem. A model using the heat equation, Fick's diffusion law and Young's law was developed and used to predict stresses in the monolith due to shrinkage during drying. It was found that a stress front propagates from the outside of the monolith to the core and that this is likely the cause of the fractures seen in some monoliths.

8.4   Further Work

The application of the Benbow Bridgwater model to honeycomb dies has been shown to be successful for predicting the initial flow profile of paste as it exits the die. Once the paste has exited the die, however, the influence of adhesion of neighbouring pastes will have a significant effect on how the flow profile develops, which will be of significance when considering the formation of defects. It may be that variation in paste flow profile can be overcome by strong a strong cohesive force of the paste. This could be another vector for paste formulation design. Further work could also be done in investigating the effect of

interactions between the binders studied in this work. Combining binders may lead to interesting changes in

Only two binder packages could be found that were sufficiently alike in terms of simple shear rheology. Further work should be done to find other systems which share shear rheology but are different in terms of viscoelasticity.

The drying model proposed in this work was able to predict the general shape of the stress front as it travels through the monolith. It did not take into account the complex geometry of the honeycomb monolith, nor did it take into account any radial shrinkage that may occur and contribute to the stress field. For this reason, the model is insufficient to properly predict the time and location where cracks are most likely to initiate. A more sophisticated model which takes into account these properties of the honeycomb monolith is required before a more thorough design of drying regime can be achieved.

9 REFERENCES

1. Marsh, H. and F. Rodríguez-Reinoso, *Activated Carbon*. Activated Carbon2006, Oxford: Elsevier Science Ltd.

2. Tennison, S.R., *Phenolic-resin-derived activated carbons*. Applied Catalysis a-General, 1998. **173**(2): p. 289-311.

3. Bijmans, M.F.M., et al., *CAPMIX -Deploying Capacitors for Salt Gradient Power Extraction*. Energy Procedia, 2012. **20**: p. 108-115.

4. Lei, C., et al., *Activated carbon from phenolic resin with controlled mesoporosity for an electric double-layer capacitor (EDLC)*. Journal of Materials Chemistry A, 2013. **1**(19): p. 6037-6042.

5. Águeda, V.I., et al., *Effect of channel geometry, degree of activation, relative humidity and temperature on the performance of binderless activated carbon monoliths in the removal of dichloromethane from air*. Separation and Purification Technology, 2011. **78**(2): p. 154-163.

6. Barnes, L.-M., et al., *The cytotoxicity of highly porous medical carbon adsorbents*. Carbon, 2009. **47**(8): p. 1887-1895.

7. Crittenden, B.D., et al., *Nonuniform channels in adsorbent monoliths*. AIChE Journal, 2011. **57**(5): p. 1163-1172.

8. Bookbinder, D.C.C., NY), Deliso, Evelyn M. (Corning, NY), Johnson, Ronald E. (Tioga, PA), Streicher, Kevin P. (Bath, NY), *Activated Carbon Bodies Having Phenolic Resin Binder*, 1995, Corning Incorporated (Corning, NY): United States.

9. Grande, C.A., et al., *Electric swing adsorption as emerging CO2 capture technique*. Energy Procedia, 2009. **1**(1): p. 1219-1225.

10. Blackburn, S. and D.I. Wilson, *Shaping ceramics by plastic processing*. Journal of the European Ceramic Society, 2008. **28**(7): p. 1341-1351.

11. Händle, F., ed. *Extrusion in Ceramics* 2007, Springer: New York.

12. Bagley, R., *Extrusion method for forming thinwalled honeycomb structures*, 1974, Corning Glass Works: US.

13. Ishikawa, T. and T. Sumiya, *Extruding die for a honeycomb structure*, 1998, Ishikawa, T. Sumiya, T.

14. Frost, R.I., *Method for constructing a honeycomb extrusion die*, 2007, Corning Incorporated.

15. Byrne, N., J. Chen, and B. Fox, *Enhancing the carbon yield of cellulose based carbon fibres with ionic liquid impregnates*. Journal of Materials Chemistry A, 2014. **2**(38): p. 15758-15762.

16. Van Wesenbeeck, S., et al., *Biomass Pyrolysis in Sealed Vessels. Fixed-Carbon Yields from Avicel Cellulose That Realize the Theoretical Limit*. Energy & Fuels, 2016. **30**(1): p. 480-491.

17. Kim, D.-Y., et al., *High-yield Carbonization of Cellulose by Sulfuric Acid Impregnation.* Cellulose, 2001. **8**(1): p. 29-33.

18. Draper, O., et al., *A comparison of paste rheology and extrudate strength with respect to binder formulation and forming technique.* Journal of Materials Processing Technology, 1999. **92-93**: p. 141-146.

19. Powell, J. and S. Blackburn, *The unification of paste rheologies for the co-extrusion of solid oxide fuel cells.* Journal of the European Ceramic Society, 2009. **29**(5): p. 893-897.

20. Blackburn, S. and H. Böhm, *The influence of powder packing on the rheology of fibre-loaded pastes.* Journal of Materials Science, 1994. **29**(16): p. 4157-4166.

21. Benbow, J.J., et al. *The Causes and Prevention of Defects during Ceramic Forming*. in *Special Ceramics 9*. 1992. Shelton: Inst Ceramics.

22. Alfani, R. and G. Guerrini, *Rheological test methods for the characterization of extrudable cement-based materials—A review.* Materials and Structures, 2005. **38**(2): p. 239-247.

23. Malkin, A.Y., *Rheology Fundamentals*1994: ChemTec Publishing.

24. Barnes, H.A., *A Handbook of Elementary Rheology*. 1 ed2000, Aberystwyth: University of Wales Institute of Non-Newtonian Fluid Mechanics.

25. Malkin, A.Y. and A.I. Isayev, *Rheology - Concepts, Methods, & Applications*2006: ChemTec Publishing.

26. Cogswell, F.N., *Converging flow and stretching flow: A compilation.* Journal of Non-Newtonian Fluid Mechanics, 1978. **4**(1-2): p. 23-38.

27. Cogswell, F.N., *MEASURING EXTENSIONAL RHEOLOGY OF POLYMER MELTS.* Transactions of the Society of Rheology, 1972. **16**(3): p. 383-&.

28. Mezger, T.G., *The Rheology Handbook: for users of rotational and oscillatory rheometers*. 2 ed2006, Hannover: Vincentz Network.

29. Cosgrove, T., ed. *Colloid Science - Principles, Methods and Applications*. 2005, Blackwell Publishing.

30. Rahman, L., et al., *Ram Extrusion of Potato Starch Dough Through Multi-Holed Dies.* Food and Bioproducts Processing, 2002. **80**(1): p. 12-19.

31. Pruvost, K., et al., *Effect of Moisture Content on the Bulk and Wall Constitutive Behaviour of Starch Pastes.* Food and Bioproducts Processing, 1998. **76**(4): p. 188-192.

32. Halliday, P.J. and A.C. Smith, *Estimation of the wall slip velocity in the capillary flow of potato granule pastes.* Journal of Rheology, 1995. **39**(1): p. 139-149.

33. Benbow, J.J. and J. Bridgwater, *Paste Flow and Extrusion*. Oxford Series on Advance Manufacturing1993, New York: Oxford University Press Inc. 176.

34. Benbow, J.J., S.H. Jazayeri, and J. Bridgwater, *The Flow Of Pastes Through Dies Of Complicated Geometry.* Powder Technology, 1991. **65**(1-3): p. 393-401.

35. Benbow, J.J., E.W. Oxley, and J. Bridgwater, *The extrusion mechanics of pastes--the influence of paste formulation on extrusion parameters.* Chemical Engineering Science, 1987. **42**(9): p. 2151-2162.

36. Stitt, H., M. Marigo, and S. Wilkinson, *How Good is Your Model?* Johnson Matthey Technol. Rev., 2015. **59**(2).

37. Basterfield, R.A., C.J. Lawrence, and M.J. Adams, *On the interpretation of orifice extrusion data for viscoplastic materials.* Chemical Engineering Science, 2005. **60**(10): p. 2599-2607.

38. Adams, M.J., et al., *A finite element analysis of the squeeze flow of an elasto-viscoplastic paste material.* Journal of Non-Newtonian Fluid Mechanics, 1997. **71**(1-2): p. 41-57.

39. Domanti, A.T.J., D.J. Horrobin, and J. Bridgwater, *An investigation of fracture criteria for predicting surface fracture in paste extrusion.* International Journal of Mechanical Sciences, 2002. **44**(7): p. 1381-1410.

40. Horrobin, D.J. and R.M. Nedderman, *Die entry pressure drops in paste extrusion.* Chemical Engineering Science, 1998. **53**(18): p. 3215-3225.

41. Dettman, M.A., *Civil Engineering 410 Soil Mechanics*, 2005, Western Kentucky University.

42. Andrade, F.A., H.A. Al-Qureshi, and D. Hotza, *Measuring the plasticity of clays: A review.* Applied Clay Science, 2010. **In Press, Corrected Proof**.

43. Modesto, C.d.O. and A.M. Bernardin, *Determination of clay plasticity: Indentation method versus Pfefferkorn method.* Applied Clay Science, 2008. **40**(1-4): p. 15-19.

44. Blackburn, S., *Cone Penetration to Calculate Yield*, 2010, University of Birmingham.

45. Sun, A. and S. Gunasekaran, *Yield Stress in Foods: Measurements and Applications.* International Journal of Food Properties, 2009. **12**(1): p. 70-101.

46. Norton, F.H., *Elements of Ceramics* 1974, Reading, Massachusetts: Addison-Wesley.

47. Baran, B., et al., *Workability test method for metals applied to examine a workability measure (plastic limit) for clays.* Applied Clay Science, 2001. **20**(1-2): p. 53-63.

48. Domanti, A.T.J. and J. Bridgwater, *Surface Fracture in Axisymmetric Paste Extrusion: An Experimental Study.* Chemical Engineering Research and Design, 2000. **78**(1): p. 68-78.

49. Domanti, A.T.J. and J. Bridgwater, *On the Origins of Paste Fracture.* Industrial & Engineering Chemistry Research, 2004. **43**(14): p. 3750-3757.

50. Kulikov, O.L. and K. Hornung, *Wall detachment and high rate surface defects during extrusion of clay.* Journal of Non-Newtonian Fluid Mechanics, 2002. **107**(1–3): p. 133-144.

51. Azzolini, A., V.M. Sglavo, and J.A. Downs, *Novel method for the identification of the maximum solid loading suitable for optimal extrusion of ceramic pastes.* Journal of Advanced Ceramics, 2014. **3**(1): p. 7-16.

52. Bayfield, M., et al., *Liquid Phase Migration in the Extrusion of Icing Sugar Pastes.* Food and Bioproducts Processing, 1998. **76**(1): p. 39-46.

53.   Rough, S.L., D.I. Wilson, and J. Bridgwater, *A Model Describing Liquid Phase Migration Within an Extruding Microcrystalline Cellulose Paste.* Chemical Engineering Research and Design, 2002. **80**(7): p. 701-714.

54.   King, A.G., *Ceramic Technology and Processing*. Ceramic Technology and Processing2002, Norwich, NY: William Andrew Publishing.

55.   Misra, R., A.J. Barker, and J. East, *Controlled drying to enhance properties of technical ceramics.* Chemical Engineering Journal, 2002. **86**(1-2): p. 111-116.

56.   Aranzabal, A., et al., *Optimization of process parameters on the extrusion of honeycomb shaped monolith of H-ZSM-5 zeolite.* Chemical Engineering Journal, 2010. **162**(1): p. 415-423.

57.   Putranto, A. and X.D. Chen, *An assessment on modeling drying processes: Equilibrium multiphase model and the spatial reaction engineering approach (S-REA).* Chemical Engineering Research and Design, 2015. **94**: p. 660-672.

58.   Chou, S.K., et al., *On the Intermittent Drying of an Agricultural Product.* Food and Bioproducts Processing, 2000. **78**(4): p. 193-203.

59.   Batista, L.M., C.A. da Rosa, and L.A.A. Pinto, *Diffusive model with variable effective diffusivity considering shrinkage in thin layer drying of chitosan.* Journal of Food Engineering, 2007. **81**(1): p. 127-132.

60.   Corzo, O., N. Bracho, and C. Alvarez, *Water effective diffusion coefficient of mango slices at different maturity stages during air drying.* Journal of Food Engineering, 2008. **87**(4): p. 479-484.

61.   Mariani, V.C., A.G. Barbosa de Lima, and L. dos Santos Coelho, *Apparent thermal diffusivity estimation of the banana during drying using inverse method.* Journal of Food Engineering, 2008. **85**(4): p. 569-579.

62.   Sherwood, T.K., *The Drying of Solids—IV Application of Diffusion Equations.* Industrial & Engineering Chemistry, 1932. **24**(3): p. 307-310.

63.   Puyate, Y.T. and C.J. Lawrence, *Sherwood's models for the falling-rate period: A missing link at moderate drying intensity.* Chemical Engineering Science, 2006. **61**(21): p. 7177-7183.

64.   Hussain, S., C. Keary, and D.Q.M. Craig, *A thermorheological investigation into the gelation and phase separation of hydroxypropyl methylcellulose aqueous systems.* Polymer, 2002. **43**(21): p. 5623-5628.

65.   Anhui Wanwei Updated High-Tech Material Industry Company Ltd. *PVA Usage*. 2011; Available from: http://www.wanwei-pva.com/PVA-Usage.htm.

66.   Kim, J.-H., R.E. Robertson, and A.E. Naaman, *Structure and properties of poly(vinyl alcohol)-modified mortar and concrete.* Cement and Concrete Research, 1999. **29**(3): p. 407-415.

67.   Nath Das, R., C.D. Madhusoodana, and K. Okada, *Rheological studies on cordierite honeycomb extrusion.* Journal of the European Ceramic Society, 2002. **22**(16): p. 2893-2900.

68.	Su, B. and T.W. Button, *A comparative study of viscous polymer processed ceramics based on aqueous and non-aqueous binder systems.* Journal of Materials Processing Technology, 2009. **209**(1): p. 153-157.

Appendix A

Rheometry results for different grades of PEO

Polymer	water g	powder g	Concentration wt%	k (Pa.s)				n				kav	nav	kerr	nerr
				1	2	3	4	1	2	3	4				
200k	50.0	0.0	0.00	-	-	-	-	-	-	-	-	0.00	1.00	0.00	0.00
200k	56.9	0.6	1.10	0.00	0.01	0.00		1.00	0.95	1.00		0.00	0.98	0.00	0.03
200k	50.0	1.3	2.50	0.01	0.01	0.02		0.97	0.97	0.95		0.01	0.96	0.00	0.01
200k	50.0	1.9	3.76	0.04	0.03	0.04		0.92	0.95	0.92		0.04	0.93	0.01	0.02
200k	50.0	2.5	5.00	0.09	0.09	0.08		0.90	0.91	0.91		0.09	0.91	0.00	0.00
200k	50.0	3.2	6.34	0.18	0.17	0.15		0.88	0.89	0.90		0.17	0.89	0.02	0.01
200k	50.0	3.8	7.50	0.33	0.36	0.31	0.34	0.88	0.88	0.88	0.88	0.33	0.88	0.02	0.00
200k	49.9	4.3	8.71	0.75	0.74	0.59		0.81	0.81	0.82		0.69	0.82	0.11	0.01
200k	50.0	5.0	10.00	1.61	1.52	1.46		0.76	0.77	0.78		1.53	0.77	0.09	0.01
400k	50.0	0.0	0.00	-	-	-	-	-	-	-	-	0.00	1.00	0.00	0.00
400k	50.0	0.6	1.29	0.05	0.05	0.05		0.84	0.84	0.84		0.05	0.84	0.00	0.00
400k	50.0	1.3	2.50	0.07	0.08	0.10		0.84	0.83	0.81		0.08	0.83	0.02	0.01
400k	49.96	1.53	3.07	1.459	1.50	1.45		0.634	0.63	0.64		1.47	0.63	0.03	0.00
400k	50.2	1.9	3.75	3.32	2.98	2.99		0.59	0.59	0.59		3.10	0.59	0.22	0.00
400k	50.0	2.5	5.00	7.16	9.82	8.68		0.58	0.54	0.54		8.56	0.56	1.51	0.03
400k	50.6	3.1	6.20	15.77	27.02	28.48	37.35	0.55	0.46	0.46	0.40	27.16	0.47	8.68	0.06
400k	50.1	3.7	7.48	36.61	43.41	41.78		0.48	0.43	0.45		40.60	0.45	4.02	0.03
400k	50.2	4.4	8.70	69.35	66.41	76.01		0.42	0.41	0.39		70.59	0.41	5.57	0.02
400k	50.0	5.0	10.00	70.59	83.24	71.52		0.48	0.51	0.51		75.12	0.50	7.98	0.02

| Polymer	water	powder	Concentration	k (Pa.s)				n				kav	nav	kerr	nerr
	g	g	wt%	1	2	3	4	1	2	3	4				
1M	50.0	0.0	0.00	-	-	-	-	-	-	-	-	0.00	1.00	0.00	0.00
1M	49.9	0.6	1.24	0.17	0.19	0.18		0.74	0.72	0.73		0.18	0.73	0.01	0.01
1M	50.0	1.0	2.00	1.04	1.17	1.11		0.60	0.60	0.60		1.11	0.60	0.08	0.00
1M	50.0	1.2	2.50	1.63	1.68	1.72		0.63	0.63	0.63		1.68	0.63	0.05	0.00
1M	49.9	1.9	3.72	10.29	10.41	9.93		0.47	0.47	0.47		10.21	0.47	0.28	0.00
1M	50.0	2.5	5.00	26.72	27.62	29.70		0.44	0.44	0.44		28.01	0.44	1.73	0.00
1M	50.4	3.1	6.21	61.44	54.52	49.17		0.37	0.38	0.37		55.04	0.38	6.96	0.00
1M	50.0	3.8	7.51	85.06	92.67	94.66	97.06	0.39	0.34	0.37	0.38	92.36	0.37	5.08	0.02
1M	50.0	4.4	8.71	146.60	152.00	171.70		0.32	0.33	0.33		156.77	0.32	14.95	0.01
1M	52.3	5.2	9.98	261.00	233.60	246.50		0.33	0.33	0.31		247.03	0.32	15.51	0.02
4M	50.0	0.0	0.00	-	-	-	-	-	-	-	-	0.00	1.00	0.00	0.00
4M	50.1	0.6	1.24	3.27	2.65	1.91		0.45	0.45	0.48		2.61	0.46	0.77	0.02
4M	50.0	1.2	2.50	12.56	9.95	14.47		0.38	0.38	0.37		12.33	0.38	2.57	0.01
4M	50.0	1.9	3.72	48.97	49.85	57.61		0.30	0.29	0.29		52.14	0.29	5.38	0.01
4M	50.0	2.5	5.00	133.80	183.40	118.50	98.44	0.22	0.20	0.23	0.23	133.54	0.22	35.53	0.01
4M	50.0	3.1	6.28	162.10	155.50	211.70		0.22	0.23	0.22		176.43	0.23	34.76	0.01
4M	50.0	3.8	7.50	327.20	429.80	321.60		0.17	0.20	0.18		359.53	0.18	68.93	0.01
4M	50.0	4.4	8.74	259.60	287.00	683.80		0.20	0.19	0.40		410.13	0.26	268.64	0.13
4M	51.1	5.0	9.77	444.80	496.20	355.60		0.18	0.25	0.22		432.20	0.22	80.50	0.04
4M	50.2	0.5	1.01	3.21	2.53	2.74		0.44	0.45	0.45		2.83	0.45	0.52	0.01

Appendix B

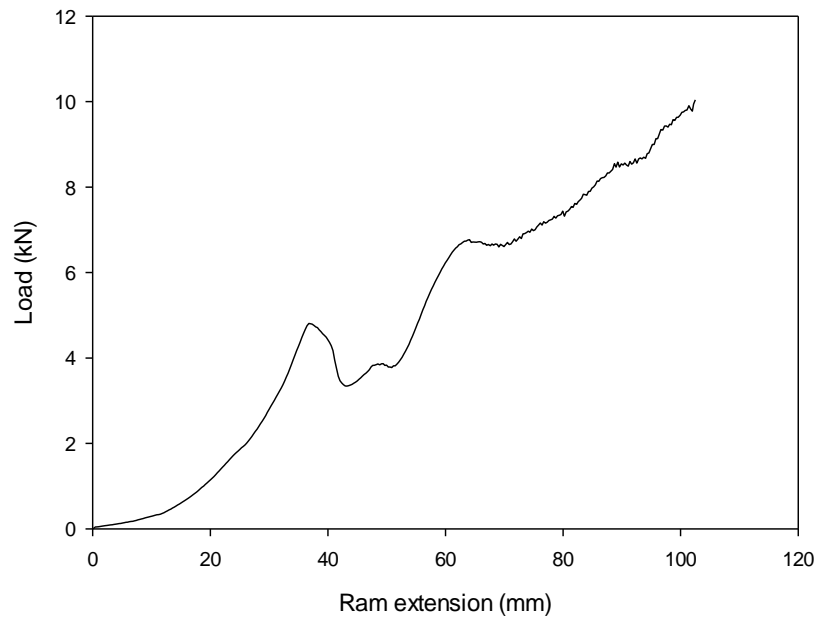Extrusion profiles of pastes in Table 6.7 at constant ram speed.
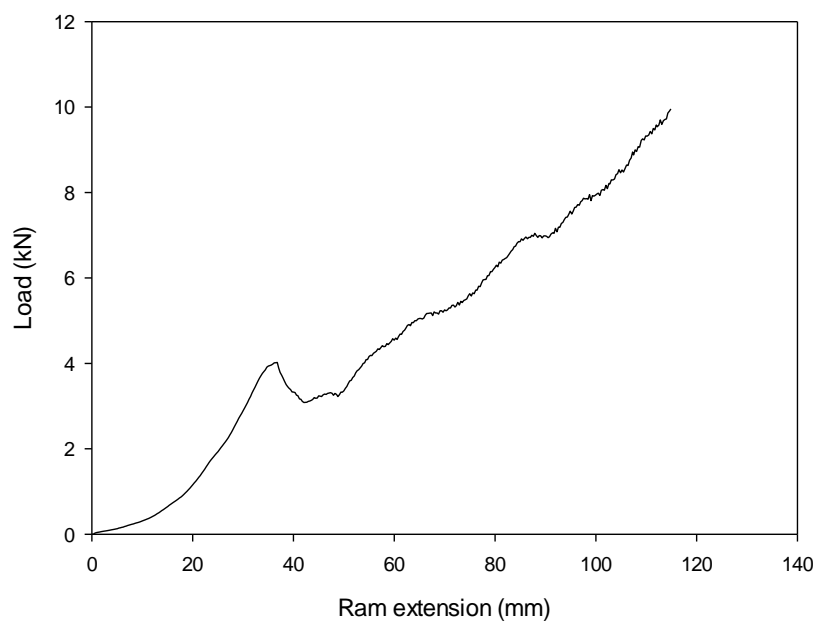
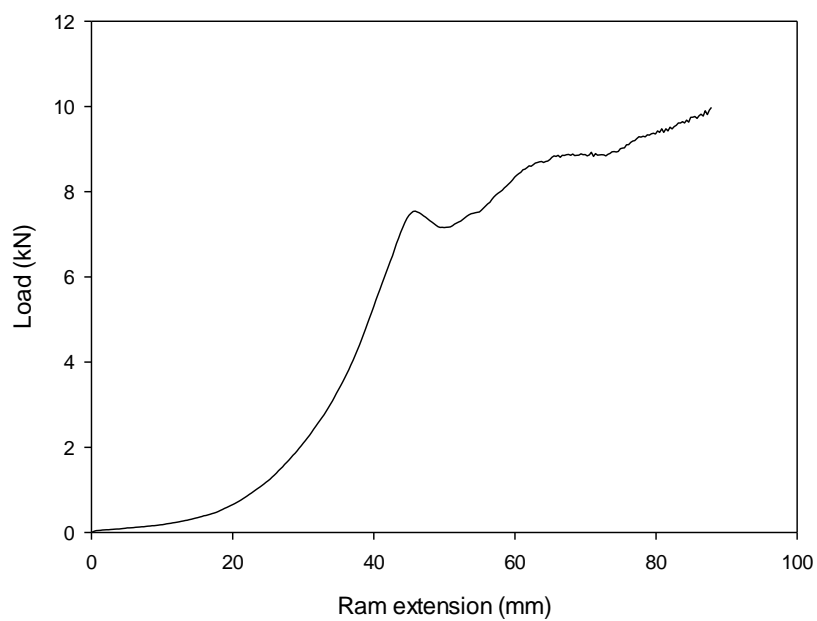### 400k PEO run 1
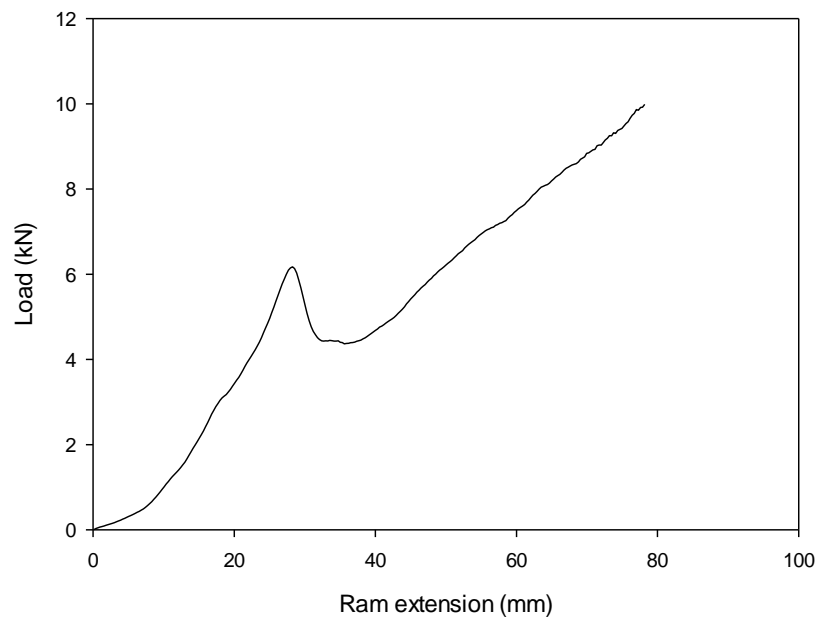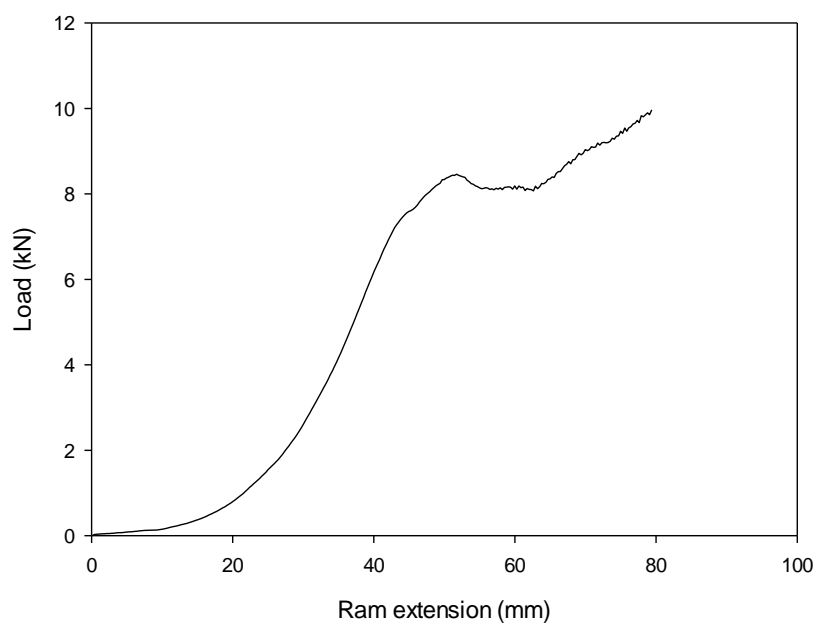

400k PEO run 2
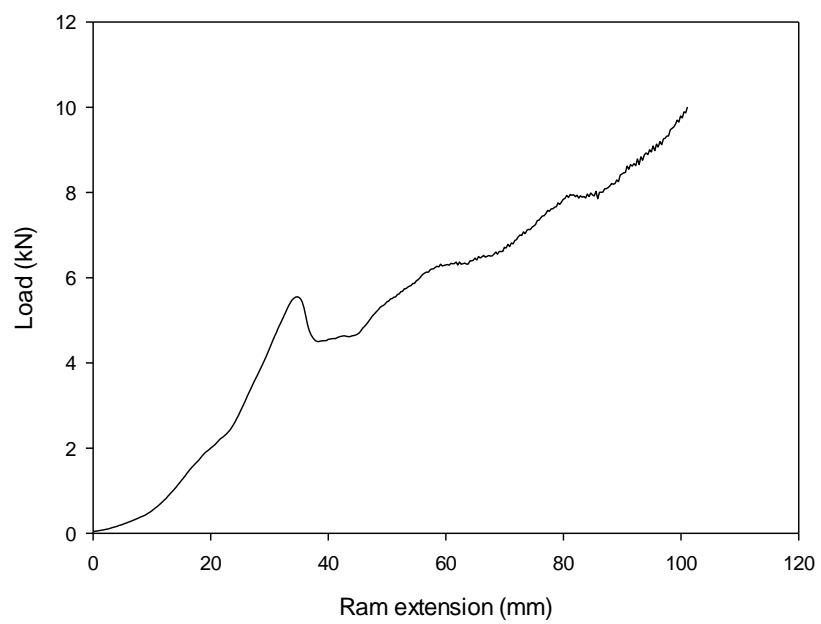
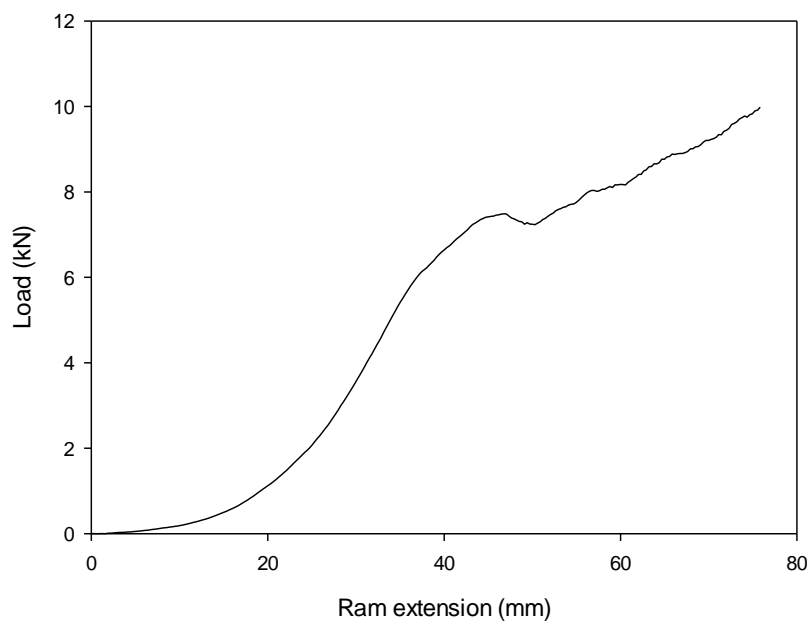400k PEO run 3

400k PEO run 4
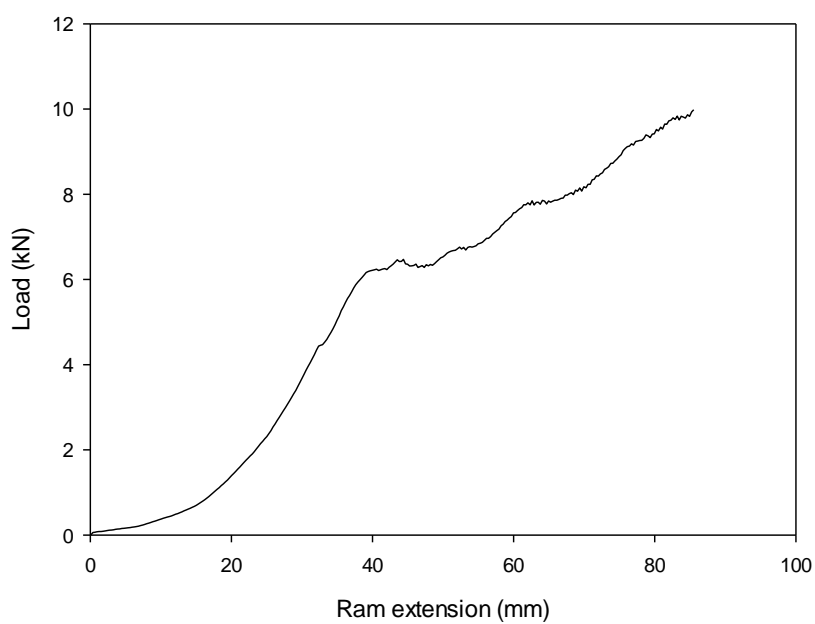
1M PEO run 1

1M PEO run 2

1M PEO run 3

1M PEO run 4

Appendix C

Full Benbow Bridgwater Results for pastes described in section 5.4

Additive	Additive concentration	α MPa.m.s^{-1}	β MPa.m.s^{-1}	m -	n -	α_{err} MPa.m.s^{-1}	β_{err} MPa.m.s^{-1}	merr -	nerr -
PEOL	0.0	0.33	0.07	0.20	0.18	0.077	0.008	0.054	0.026
	0.5	0.34	0.06	0.22	0.15	0.084	0.007	0.060	0.028
	1.0	0.26	0.06	0.24	0.17	0.080	0.007	0.073	0.025
	2.5	0.23	0.06	0.26	0.19	0.062	0.005	0.066	0.019
	5.0	0.23	0.06	0.27	0.19	0.051	0.004	0.053	0.016
	10.0	0.20	0.07	0.31	0.23	0.063	0.005	0.080	0.018
PEOH	0.5	0.29	0.07	0.23	0.19	0.072	0.007	0.060	0.025
	1.0	0.28	0.06	0.20	0.20	0.063	0.007	0.054	0.028
	2.5	0.30	0.04	0.25	0.12	0.050	0.003	0.040	0.021
	5.0	0.36	0.02	0.28	0.06	0.037	0.002	0.025	0.015
	10.0	0.44	0.02	0.27	0.00	0.041	0.001	0.023	0.016
KH17S	0.5	0.41	0.07	0.20	0.18	0.102	0.011	0.058	0.035
	1.0	0.44	0.07	0.22	0.16	0.119	0.010	0.060	0.033
	2.5	0.47	0.07	0.22	0.16	0.103	0.009	0.051	0.030
	5.0	0.65	0.06	0.23	0.12	0.191	0.012	0.062	0.042
	10.0	0.70	0.08	0.19	0.12	0.146	0.011	0.046	0.030
PEG	0.5	0.34	0.08	0.21	0.20	0.090	0.010	0.064	0.032
	1.0	0.35	0.08	0.18	0.20	0.079	0.010	0.053	0.032
	2.5	0.35	0.06	0.18	0.15	0.083	0.008	0.052	0.030
	5.0	0.32	0.06	0.16	0.15	0.057	0.006	0.041	0.025
	10.0	0.28	0.05	0.16	0.15	0.061	0.007	0.051	0.029